THE ASTROPHYSICAL JOURNAL SUPPLEMENT SERIES, 68:91–127, 1988 October

A CATALOG OF *IRAS* OBSERVATIONS OF LARGE OPTICAL GALAXIES

W. RICE,[1] CAROL J. LONSDALE,[1] B. T. SOIFER,[1,2] G. NEUGEBAUER,[2] E. L. KOPAN,[1]
LAWRENCE A. LLOYD,[1] T. DE JONG,[3] AND H. J. HABING[4]
Received 1987 June 22; accepted 1988 January 11

ABSTRACT

A catalog is presented of the *IRAS* observations of 85 galaxies listed in the *Second Reference Catalogue of Bright Galaxies* with blue-light isophotal diameters greater than 8′. "Total" flux densities at 12, 25, 60, and 100 μm, obtained from spatial maps constructed from co-added *IRAS* detector data, are reported.

Infrared brightness profiles of the detected galaxies and infrared surface brightness contour maps of the galaxies for which structural features were resolved are displayed in an atlas. A far-infrared classification scheme based on the degree of central concentration and spatial structure of the 60 μm emission of the best-resolved galaxies is proposed. The 60 μm and blue-light isophotal diameters of the largest galaxies are compared.

Subject headings: galaxies: photometry — galaxies: structure — infrared: sources

I. INTRODUCTION

Of the approximately 22,000 galaxies detected in the *Infrared Astronomical Satellite* (*IRAS*) all-sky survey (Chester 1985), about 100 of the nearest galaxies have large enough apparent optical extents to show spatial structure at the arcminute angular resolution of the *IRAS* beam. The *IRAS* observations of these optically large galaxies present unique data for comparing the spatial distribution of the mid- and far-infrared emission with the distributions of the stars and the gas within a variety of galactic disks. Such studies are important for determining the contribution of the various possible infrared emitting sources to the global infrared emission of external galaxies and for determining how the global infrared emission relates to stellar processes on a galactic scale. Clearly, these results are vital for interpreting the thousands of unresolved *IRAS* galaxy detections.

This catalog presents the *IRAS* observations of the optically large galaxies likely to show structural features at the *IRAS* resolution. The catalog sample consists of all galaxies observed by *IRAS*, which are listed in the *Second Reference Catalogue of Bright Galaxies* (de Vaucouleurs, de Vaucouleurs, and Corwin 1976, hereafter RC2) with apparent blue-light isophotal diameters greater than 8′. "Total" flux densities at 12, 25, 60, and 100 μm are reported, and an atlas of infrared brightness profile plots of the detected galaxies and infrared surface brightness contour maps of those galaxies for which structure was observed is presented. This catalog complements the existing *IRAS* catalogs, providing global flux densities, obtained from spatial maps constructed from co-added *IRAS* detector data, of the large galaxies for which the entries in the *IRAS Point Source Catalog* (1985, hereafter PSC) and the *IRAS Small Scale Structures Catalog* (1986, hereafter SSSC) underestimate the total flux density. [The PSC flux densities are total emission measurements for sources smaller than ~ 2′ (FWHM), while the SSSC flux densities represent the total emission for sources less than ~ 8′ (FWHM).]

The selection of the "large optical galaxy" sample is described in § II. In § III we describe the *IRAS* observations, the data processing, and data measurement techniques. Section IV reports the total *IRAS* flux densities and integrated infrared emission properties of the sample. The atlas, including maps of the best-resolved galaxies, is presented in § V. A brief preliminary analysis of the catalog is given in § VI. A detailed study of the spatial distribution of the infrared emission and colors of the large galaxies will be presented elsewhere (Rice 1988, hereafter Paper II). Additional galaxies with blue-light isophotal diameters greater than 8′ as listed in other catalogs are discussed in the Appendix.

II. THE LARGE OPTICAL GALAXY SAMPLE

Eighty-six galaxies in RC2 are listed with blue-light isophotal major diameters (D_{25}) greater than 8′. All but one of these galaxies, the dE5 pec galaxy A1110+22 (= Leo B), was observed by *IRAS*. The 85 observed galaxies are presented in Table 1. Column (1) is the galaxy RC2 identification—the NGC (N), IC (I), or anonymous coordinate (A) designation. An alternate designation—the Messier (M) catalog number, the traditional name, or the David Dunlap Observatory (D) designation (van den Bergh 1959, 1966) of unnamed dwarf systems—is given in column (2). Columns (3) and (4) are the optically determined equatorial coordinates of the galaxy (equinox 1950) as listed in RC2. The Galactic coordinates of the galaxy are given in columns (5) and (6). Column (7) gives the galaxy revised Hubble morphological type as listed in the catalog of Sandage and Tammann (1981, hereafter RSA) or, for galaxies not contained in RSA, the morphological type, in brackets, as reported in RC2. The morphological classification as coded in RC2 as a T index and bar parameter letter is listed in column (8). The RC2 apparent blue light major (D_{25})

[1]Infrared Processing and Analysis Center, California Institute of Technology.
[2]Division of Physics, Mathematics, and Astronomy, California Institute of Technology.
[3]Universiteit van Amsterdam.
[4]Sterrewacht, Leiden.

and minor (d_{25}) isophotal diameters in arcminutes are given in columns (9) and (10). Column (11) is the distance in megaparsecs based on RSA velocities and distance moduli (RSA, Table 2), or velocities listed in the sources cited and corrected, if necessary, using the precepts in RSA, and using a Hubble constant of $H_0 = 50$ km s^{-1} Mpc^{-1}.

III. *IRAS* OBSERVATIONS AND DATA REDUCTION

The *IRAS* data used to construct spatial maps of the sample galaxies have been taken from the high-sensitivity pointed observations (Neugebauer *et al.* 1984) whenever possible. The pointed observations were multi-leg raster pattern

TABLE 1

LARGE OPTICAL GALAXIES OBSERVED[a] IN THE *IRAS* MISSION

RC2 Name (1)	Other Name (2)	R.A. (1950) (3)	Dec. (4)	l (5)	b (6)	Type (7)	T (8)	D_{25} (9)	d_{25} (10)	Distance[b] (Mpc) (11)
N45	D223	$0^h11^m31^s.8$	$-23°27'36''$	55°.9	−80°.7	Scd(s)	8A	8'.1	5'.7	10.66
N55		0 12 24.0	−39 28 00	332.9	−75.7	Sc	9B	32.3	6.4	3.16
N134		0 27 54.0	−33 32 00	338.2	−82.4	Sbc(s)	4X	8.1	2.6	31.88
N147	D3	0 30 27.6	48 13 48	119.8	−14.3	dE5	−5	12.9	8.1	0.73
N185		0 36 11.4	48 03 42	120.8	−14.5	dE3 pec	−5	11.5	9.8	0.73
N205		0 37 38.4	41 24 54	120.7	−21.1	S0/E5 pec	−5	17.4	9.8	0.73
N224	M31	0 40 00.0	40 59 42	121.2	−21.6	Sb	3A	177.8	63.1	0.73
N247		0 44 39.6	−21 02 00	113.9	−83.6	Sc(s)	7X	19.9	7.4	3.16
N253		0 45 07.8	−25 33 42	97.6	−88.0	Sc(s)	5X	25.1	7.4	4.17
A0051−73	SMC	0 51 00.0	−73 06 00	302.8	−44.3	Im	9B	281.8	158.5	0.078
N300		0 52 31.2	−37 57 24	299.2	−79.4	Sc	7A	19.9	14.8	2.40
I1613	D8	1 02 13.2	1 51 00	129.7	−60.6	[Im(s)]	10X	12.0	11.2	0.85(1)
N598	M33	1 31 03.0	30 23 54	133.6	−31.3	Sc(s)	5A	61.6	38.9	0.90
N628	M74	1 34 00.6	15 31 36	138.6	−45.7	Sc(s)	5A	10.2	9.5	17.22
N660		1 40 21.0	13 23 18	141.6	−47.4	[Sa]	1B	9.1	4.1	19.64(2)
N891		2 19 24.6	42 07 12	140.4	−17.4	Sb	5A	13.5	2.8	15.58
N925		2 24 16.8	33 21 24	144.9	−25.2	SBc(s)	7X	9.8	6.0	15.84
N1023		2 37 16.2	38 50 54	145.0	−19.1	$SB0_1(5)$	−2B	8.7	3.3	17.90
A0237−34	Fornax Sys.	2 37 50.4	−34 44 24	237.3	−65.7	[E0p]	−5	19.9	13.8	0.16(1)
N1097		2 44 11.4	−30 29 06	226.9	−64.7	RSBbc(rs)	3B	9.3	6.6	25.68
N1291		3 15 28.8	−41 18 30	247.6	−57.0	SBa	0B	10.5	9.1	14.76
N1313		3 17 38.9	−66 40 42	283.4	−44.6	SBc(s)	7B	8.5	6.6	5.22
N1365		3 31 42.0	−36 18 18	238.0	−54.6	SBb(s)	3B	9.8	5.5	31.24
I342		3 41 57.6	67 56 24	138.2	10.6	[S(rs)cd]	6X	17.8	17.4	4.68(1)
N1448		3 42 52.8	−44 48 00	251.5	−51.4	Sc:	6A	8.1	1.8	20.76
N1560		4 27 03.6	71 46 12	138.4	16.0	[Sd(s)]	7A	9.8	2.0	4.68(1)
A0524−69	LMC	5 24 00.0	−69 48 00	280.5	−32.9	SBm	9B	645.6	549.5	0.057
N2403		7 32 03.0	65 42 42	150.6	29.2	Sc(s)	6X	17.8	11.0	3.57
N2683		8 49 34.8	33 36 30	190.5	38.8	Sb	3A	9.3	2.5	7.98
N2841		9 18 34.8	51 11 18	166.9	44.1	Sb	3A	8.1	3.8	14.28
N2903		9 29 20.4	21 43 12	208.7	44.5	Sc(s)	4X	12.6	6.6	9.44
N2997		9 43 27.6	−30 57 36	262.6	16.8	Sc(s)	5X	8.1	6.4	15.98
N3031	M81	9 51 30.0	69 18 18	142.1	40.9	Sb(r)	2A	25.7	14.1	3.57
N3034	M82	9 51 40.8	69 54 54	141.4	40.6	Amorphous	0:	11.2	4.6	3.57
N3109	D236	10 00 46.8	−25 54 48	262.1	23.1	Sm	9B	14.4	3.5	2.58
N3115		10 02 44.4	−07 28 30	247.8	36.8	$S0_1(7)$	−3	8.3	3.2	8.74
A1005+12	Leo I	10 05 46.2	12 33 12	226.0	49.1	[E3]	−4	10.7	8.3	0.12(1)
N3198		10 16 52.2	45 48 00	171.2	54.8	Sc(rs)	5B	8.3	3.7	14.04
I2574	D81	10 24 40.2	68 40 06	140.2	43.6	[Sm(s)]	9X	12.3	5.9	3.50(1)
N3521		11 03 15.6	0 14 12	255.5	52.8	Sb(s)	4X	9.5	5.0	12.54
N3556		11 08 36.6	55 56 42	148.3	56.3	Sc(s)	6B	8.3	2.5	15.80
N3621		11 15 50.4	−32 32 24	281.2	26.1	Sc(s)	7A	10.0	6.5	8.70
N3623	M65	11 16 18.6	13 21 54	241.3	64.2	Sa(s)	1X	10.0	3.3	13.50
N3627	M66	11 17 38.4	13 15 48	242.0	64.4	Sb(s)	3X	8.7	4.4	11.86
N3628		11 17 39.6	13 52 06	240.8	64.8	Sbc	3	14.8	3.6	14.38

TABLE 1—*Continued*

RC2 Name (1)	Other Name (2)	R.A. (1950) (3)	Dec. (4)	l (5)	b (6)	Type (7)	T (8)	D_{25} (9)	d_{25} (10)	Distance (Mpc) (11)
N3718		$11^h29^m49^s.8$	53°20′42″	147°.0	60°.2	Sa pec?	1	8′.7	4′.5	21.64
N4192	M98	12 11 15.6	15 10 48	265.4	75.0	Sb:	2X	9.5	3.1	21.88
N4216		12 13 21.0	13 25 24	270.5	73.7	Sb(s)	3X	8.3	2.2	21.88
N4236		12 14 19.2	69 45 00	127.4	47.4	SBd	8B	18.6	6.9	3.14
N4244		12 14 59.4	38 05 12	154.6	77.2	Scd	6A	16.2	2.5	4.98
N4258		12 16 29.4	47 35 00	138.3	68.8	Sb(s)	4X	18.2	5.0	10.40
N4395		12 23 19.8	33 49 30	162.1	81.5	Sd	9A	12.9	11.0	6.08
N4438		12 25 13.8	13 17 06	280.3	74.8	Sb	0A	9.3	3.9	21.88
N4472	M49	12 27 14.4	8 16 42	286.9	70.2	E1/S0$_1$(1)	−5	8.9	7.4	21.88
N4517		12 30 12.0	0 23 18	292.7	62.6	Sc	6A	10.2	1.9	15.93
N4559		12 33 29.4	28 14 06	198.4	86.5	Sc(s)	6X	10.5	4.9	15.42
N4565		12 33 51.6	26 15 36	230.8	86.4	Sb	3A	16.2	2.8	23.42
N4569	M90	12 34 18.6	13 26 24	288.5	75.6	Sab(s)	2X	9.5	4.7	21.88
N4594	M104	12 37 22.8	−11 21 00	298.5	51.1	Sa^+/Sb^-	1A	8.9	4.1	17.46
N4631		12 39 40.8	32 48 48	142.8	84.2	Sc	7B	15.1	3.3	12.12
N4656		12 41 31.8	32 26 30	140.3	84.7	Im	9B	13.8	3.3	12.48
N4725		12 48 00.0	25 46 30	295.1	88.4	Sb/SBb(r)	2X	10.9	7.9	23.34
N4736	M94	12 48 31.8	41 23 36	123.4	76.0	RSab(s)	2A	10.9	9.1	6.90
N4762		12 50 25.2	11 30 06	304.3	74.1	S0$_1$(10)	−2B	8.7	1.6	21.88
N4826	M64	12 54 16.8	21 57 06	315.7	84.4	Sab(s)	2A	9.3	5.4	7.00
N4945		13 02 31.8	−49 12 00	305.3	13.3	Sc	6B	19.9	4.4	6.92
N5033		13 11 08.4	36 51 48	98.1	79.4	Sbc(s)	5A	10.5	5.6	17.94
N5055	M63	13 13 35.4	42 17 48	106.0	74.3	Sbc(s)	4A	12.3	7.6	11.00
N5102		13 19 07.2	−36 22 06	309.7	25.8	S0$_1$(5)	−3A	9.3	3.5	6.92
N5128	Cen A	13 22 31.8	−42 45 30	309.5	19.4	S0+S pec	−2	18.2	14.5	6.92
N5170		13 27 07.2	−17 42 24	315.7	44.0	Sb:	5A	8.1	1.3	25.70
N5194	M51	13 27 45.6	47 27 18	104.9	68.6	Sbc(s)	4A	10.9	7.7	10.82
N5236	M83	13 34 10.2	−29 36 48	314.6	32.0	SBc(s)	5X	11.2	10.2	9.92
N5457	M101	14 01 27.6	54 35 36	102.0	59.8	Sc(s)	6X	26.9	26.3	7.59
A1508+67	U Mi	15 08 12.0	67 23 00	105.0	44.8	[E4]	−5	32.3	20.9	0.090(1)
N5907		15 14 36.6	56 30 24	91.6	51.1	Sc	5A	12.3	1.8	15.58
A1719+57	Draco Sys.	17 19 15.2	57 57 30	86.4	34.7	[E0p]	−5	39.8	24.5	0.095(1)
N6744		19 05 01.7	−63 56 18	332.2	−26.1	Sbc(r)	4X	15.5	10.2	13.26
N6822	D209	19 42 07.1	−14 55 42	25.3	−18.4	Im	10B	10.2	9.5	0.68
N6946		20 33 47.9	59 59 00	95.7	11.7	Sc(s)	6X	10.9	9.7	6.72
I5201[c]		22 17 55.0	−46 17 00	350.2	−54.9	SBcd	6B	8.5	4.3	14.56
N7331		22 34 47.2	34 09 30	93.7	−20.7	Sb(rs)	4A	10.7	4.0	22.28
N7640		23 19 43.1	40 34 12	105.2	−18.9	Sbc(s):	5B	10.7	2.5	13.38
N7793		23 55 15.5	−32 52 06	4.5	−77.2	Sd(s)	8A	9.1	6.6	6.62
A2359−15	WLM	23 59 23.9	−15 44 36	75.8	−73.6	[Im(s)]	10B	10.2	4.2	1.60(1)

[a] A1110+22 (= Leo B), a dE5 pec galaxy with an RC2 diameter of 14′.4, was not observed in the *IRAS* mission.
[b] Distance sources: RSA; (1) Kraan-Korteweg and Tammann 1979; (2) Huchra *et al.* 1983.
[c] Optical position from RSA.

scans of the *IRAS* survey detector array covering small areas of the sky (typically 1°.5×0°.5) centered on the targeted objects.

For the 36 galaxies of the sample for which pointed observations were not performed, maps were constructed from co-added all-sky survey data. The coverage of these fields was a minimum of four survey scans (or 2 hours confirming scans). These data were processed in the same way as the pointed observation data.

In the following, the in-scan direction refers to the scanning direction of the *IRAS* telescope and the cross-scan direction refers to the direction orthogonal to the scanning direction.

a) *Data Processing*

The various processing steps involved in constructing total flux surface brightness maps and point-source filtered maps from the detector data streams are described in detail in the *IRAS Explanatory Supplement* (1985, hereafter *IRAS* Supple-

ment) and the *Pointed Observation Products Guide* (Young *et al.* 1985, hereafter POG). Here, we describe the techniques used to remove residual photometric artifacts (intensity stripes) and background emission from the surface brightness maps.

i) *Detector Baseline Corrections*

Baseline variations in the detector data on the order of 10–15 times the data noise level resulted in discontinuities in the apparent intensity of the surface brightness maps orthogonal to the telescope scanning direction (e.g., Habing *et al.* 1984). This striping was corrected by comparing the data streams of adjacent wavelength band detectors of the detector array. The differences between adjacent spatial data samples of the paired detectors were histogrammed and the mode, or, if that failed, the median, of the differences was identified and used as an estimate of the offset between the detectors. This process was continued across the focal-plane detector array, producing a cross-scan offset profile for each band. The profiles were adjusted to zero mean and subtracted from the data. This technique also removed gross cross-scan field gradients in the data, along with the baseline offsets.

ii) *Background Removal*

A first estimate of the underlying background level in the surface brightness maps due to diffuse zodiacal and Galactic emission was taken to be the median of the map pixel values. This value was subtracted from the maps. Residual field gradients as large as 20 times the noise level remained in the maps. These were removed using one of two techniques. The first technique was similar to the de-stripping algorithm described above. The median differences of the pixel values in adjacent columns across the map were calculated, adjusted to zero mean, and removed. The process was then applied to the pixel rows of the map.

For maps with complicated backgrounds an alternate technique produced better results. A linear least-squares fit was computed for each pixel column of the map. The fits excluded the pixels of source emission with intensity values above a specified threshold. The parameters of the fitted lines, smoothed over the entire map, defined a surface that was removed.

The background removal processing resulted in maps in which the variation of the remaining background emission was typically less than ~ 3 times the map noise level over the entire field covered by the map. A few of the galaxies were embedded in patches of Galactic infrared "cirrus" emission (Low *et al.* 1984), and for these an estimate of the local background, taken to be the mean intensity within an outlying annular aperture centered on the galaxy image, was subtracted from the galaxy aperture measurements.

b) *Point-Source Filtered Maps*

The data were also processed to produce point-source filtered maps. In this processing, described in detail in the POG, a digital zero-sum bandpass filter centered on the *IRAS* point-source spatial frequency was applied to the spatially binned co-added detector data. This processing, which suppressed extended structure, resulted in a more sensitive measurement of the flux densities of unresolved sources.

c) *Total Flux Density Measurements*

The final maps were produced by co-adding the individual pointed observation or all-sky survey scan maps of the galaxy fields. The mean noise levels (1 σ) of the 12, 25, 60, and 100 μm surface brightness maps constructed from pointed observations are 4.6, 6.6, 3.8, and 7.2 mJy arcmin^{-2} (or 18, 26, 30, and 110 mJy per beam), respectively. The mean noise levels of the maps constructed from survey data are 11, 16, 8.5, and 11 mJy arcmin^{-2} (45, 64, 68, and 160 mJy per beam), respectively.

Total flux densities were obtained from either the point-source filtered maps or the surface brightness maps, depending on the spatial extent observed for the galaxy sources. For the sources for which a large infrared extent was not obvious, radial profiles of the galaxy surface brightness images along the *IRAS* in-scan and cross-scan directions were compared with the profiles of the star IRC +10011, a representative *IRAS* point source. The mean half-power width of the point-source in-scan profile, measured from both co-added pointed observation and co-added survey data maps, is approximately 0'.8 for the 12 and 25 μm maps, 1'.6 for the 60 μm maps, and 3' for the 100 μm maps. The cross-scan resolution (FWHM) is approximately 5' for each wavelength map. (Note that in co-added maps composed of observations with a large range of scanning angles, unique in-scan and cross-scan directions do not exist. For these maps, the orientation of the profile cuts was based on the dominant scanning direction as determined by the shape of the sources. Typically, the component observations of a co-added map had scanning angles that coincided to within $\sim 20°$.)

While the point-source filtered maps provide the best flux density measurements of unresolved sources, the point-source filtering can result in a significant underestimation of the integrated flux density of slightly extended sources. For this reason, the point-source filtered map measurements were taken as total flux densities only for sources with a pointlike surface brightness image *at all detected wavelengths*. If a source appeared extended *in any one* of the surface brightness wavelength maps, the total flux density *at all detected wavelengths* was obtained from the surface brightness maps. An exception was for faint 12 and 25 μm detections with marginal surface brightness map flux density measurements (< 0.2 Jy). For these, the flux densities extracted from the more sensitive point-source filtered maps are reported.

Total flux densities were obtained from the surface brightness maps by summing the map pixel intensity values within the 25 mJy arcmin^{-2} (~ 3–6 σ) brightness level contour of the galaxy image. If 3 times the map noise level was brighter than 25 mJy arcmin^{-2}, the brighter 3 σ threshold was used. The selection of 25 mJy arcmin^{-2} as the brightness limit for determining the galaxy total infrared emission is somewhat arbitrary, since it is based on the overall sensitivity of the *IRAS* data, along with the adequate removal of background emission from the maps using the techniques described above. However, the agreement between the optical size and the infrared 60 μm size of the largest infrared extended galaxies to this brightness level (see § VI*b*) implies that the bulk of the emission is contained within the selected brightness limit. Furthermore, the small contribution to the total emission of the low-level infrared emission observed in the outer regions

of the galaxies is consistent with the adopted surface brightness cutoff.

d) *Upper Limits and Uncertainties*

For galaxies not detected in a wavelength band, the reported upper limit is 3 times the noise level of the point-source filtered wavelength map for pointlike sources, or 3 times the noise level of the surface brightness wavelength map, integrated over the *IRAS* wavelength band beam, for extended sources. The surface brightness map 3 σ limits are reported for galaxies not detected in any band.

A more appropriate limit for a nondetection of an extended source may be the sum of the noise pixels of the surface brightness wavelength map over the observed infrared extent of the galaxy. Similarly, the nondetection of low-level diffuse emission at 12 and 25 μm for a galaxy observed as more extended at 60 and 100 μm could result in an underestimation of the "total" emission at the shorter wavelengths. Both possible underestimations assume an extended infrared emission model of galaxies in which the distribution of the diffuse emission at the various *IRAS* wavelengths is similar. The data analysis to determine the validity of this model has been deferred to Paper II, and the faint 12 and 25 μm total flux density measurements and upper limits reported in this catalog for extended galaxies should be viewed with caution.

The photometric accuracy of these measurements is compromised by uncertainties in the frequency response of the detectors as a function of source strength and undersampling due to dead and noisy detectors. While the undersampling can cause large integrated flux density errors (~ 25% or more) in the surface brightness maps for pointlike sources observed along tracks of the detector array containing the aberrant detectors, the uncertainties improve to 15% or better for sources observed either along the detector array prime track (i.e., targeted objects of pointed observations) or along a mixture of detector tracks (i.e., co-added survey data). For extended sources with half-power widths of 4′ or more (i.e., on the order of the cross-scan detector size) the estimated uncertainties are ~15% (POG). The flux density uncertainties of point sources extracted from co-added pointed observation and survey data point-source filtered maps, determined by comparing the flux densities of standard stars to PSC values, are ~10%.

Co-added survey data surface brightness maps were constructed for a subset of the galaxies with pointed observations, including the LMC and the SMC. Except for the faintest 12 and 25 μm sources (< 2 Jy), the flux densities obtained from the lower sensitivity survey data maps were in agreement, within the uncertainties, with the values obtained from the pointed observation maps. The survey data map flux densities of the fainter sources were as much as 50% lower than the pointed observation map measurements, depending on the depth of the survey coverage.

IV. THE CATALOG

a) *Total Flux Densities*

Table 2 lists the "total" *IRAS* flux densities of the sample galaxies obtained from co-added maps and the "point-source" flux densities of these galaxies reported in the PSC. The column entries are described below.

Column (1).—Galaxy name.

Column (2).—Observation type. "PO" denotes that the galaxy maps were constructed from pointed observation data; "SS" denotes that the maps were constructed from all-sky survey scan data.

Column (3).—Spatial extent code. A letter code has been assigned to indicate the degree of spatial extent evident in the *IRAS* surface brightness images of the galaxies and from which type of *IRAS* maps the galaxy total flux densities or upper limits were obtained. The code is given below.

E—The galaxy was observed as an extended source in one or more of the surface brightness wavelength maps; the total flux densities or upper limits were obtained from the surface brightness maps.

P—The galaxy was observed as an unresolved point source at all detected wavelengths; the total flux densities or upper limits were obtained from the point-source filtered maps.

N—The galaxy was not detected; the reported upper limits are 3 times the noise level of the surface brightness maps integrated over the *IRAS* beam.

Columns (4)–(7).—*IRAS* total flux density, f_ν, at 12, 25, 60, and 100 μm in janskys (10^{-26} W m^{-2} Hz^{-1}) measured from co-added maps, as described in § III*c*. The flux density of a faint extended source obtained from a point-source filtered map is followed by a "P." A colon following an entry denotes a larger flux density uncertainty because of poor background removal, the low sensitivity of a co-added survey data map, or for the reason listed in the notes to the table. (As in the PSC, flux densities have been calculated assuming an input energy distribution with f_ν proportional to ν^{-1}.)

Column (8).—Designation of the positionally associated *IRAS* point-source detection listed in the PSC. For galaxies associated with multiple PSC entries (cf. Table IIIA.2 in the *Cataloged Galaxies Observed in the IRAS Survey* [1985, hereafter Extragalactic Catalog]), the entry listed is the detection nearest the galaxy optical center. PSC flux densities are not reported for the SMC and the LMC; both galaxies generated many PSC sources.

Columns (9)–(12).—*IRAS* "point-source" flux densities as listed in the PSC (Version 1.0). A colon following an entry denotes a moderate quality flux density as described in the *IRAS* Supplement (§ V.H.5).

Special comments for several of the galaxies are presented in the notes to the table.

b) *Global Emission Properties*

Table 3 reports color-corrected total flux densities at 12, 25, 60, and 100 μm, along with the global emission of the galaxies at optical, near-infrared, and radio wavelengths compiled from the literature. The *IRAS* color corrections were calculated using a two-temperature thermal model fit to the measured flux densities or limits. The model is described below. The column entries of Table 3 are described below.

TABLE 2

IRAS FLUX DENSITIES[a]

Name (1)	Obs[b] (2)	Ext[c] (3)	Total Flux Density (Jy) 12 μm (4)	25 μm (5)	60 μm (6)	100 μm (7)	*IRAS* Name (8)	PSC Flux Density (Jy) 12 μm (9)	25 μm (10)	60 μm (11)	100 μm (12)
N45	SS	E	<0.12	<0.17	1.62	4.99	00115−2327	<0.25	<0.25	<0.45	2.75
N55	PO	E	1.34	6.25	77.00	174.09	00125−3928	0.56:	1.77	30.96	73.33:
N134	SS	E	1.77	2.67	17.23	61.18	00278−3331	1.39	1.97	19.02	53.33
N147	PO	N	<0.05	<0.06	<0.08	<0.36		...	...	...	...
N185	PO	P	0.04	<0.03	0.31	1.93	00362+4803	<0.29	<0.25	<0.44	2.11
N205	PO	E	0.15P	0.19P	0.60	3.78	00376+4124	<0.25	<0.24	<0.59	3.10
M31	PO	E	163.23	107.71	536.18	2928.40	00400+4059	1.15:	0.75:	7.53	14.37:
N247	SS	E	<0.12	<0.16	7.93	27.32	00446−2101	<0.94	<0.25	<0.78	6.07
N253	SS	E	55.84	155.65	998.73	1861.67	00450−2533	20.52	117.08	758.62	1044.83
SMC	PO(1)	E	67.03	270.18	6688.91	15021.93		...	...	...	...
N300	SS	E	0.53:	0.64:	23.08	74.45	00523−3756	<0.99	<0.78	<1.10	8.43
I1613	PO	E	<0.06	<0.14	1.42	3.69	01025+0153	<1.56	<0.29	1.01	2.64
M33	PO	E	32.69	40.26	419.65	1256.43	01310+3024	0.49	<0.37	9.93	<23.79
N628	SS	E	2.07	1.90	20.86	65.64	01340+1532	<0.25	<0.40	2.95	11.78
N660	SS	P	2.31	7.05	67.27	104.89	01403+1323	2.02	7.12	64.99	102.38
N891	PO	E	5.66	7.78	61.10	198.63	02193+4207	0.93	0.85:	34.08	146.28
N925	PO	E	0.26	0.66	7.65	26.68	02243+3321	<0.25	<0.25	2.82	11.90
N1023	SS	P	0.16	<0.09	<0.13	<0.30		...	...	...	...
Fornax Sys.	SS	N	<0.09	<0.11	<0.15	<0.43		...	...	...	...
N1097	PO	E	2.88	7.70	46.73	116.34	02441−3029	1.85	5.83	45.49	82.53
N1291	PO	E	0.18P	0.17P	1.76	10.13	03154−4117	<0.28	<0.24	1.68	5.56
N1313	PO	E	0.95	3.49	35.97	92.00	03176−6640	<0.25	0.57	10.23	30.15
N1365	PO	E	4.42	13.07	84.20	185.40	03317−3618	3.22	11.13	77.75	139.94
I342	PO	E	23.66	45.20	255.96	661.68	03419+6756	3.80	18.76	85.15	125.97
N1448	PO	P	0.89	1.08	9.92	34.07	03428−4448	0.64	0.69	7.92	26.22
N1560	PO	E	<0.05	<0.05	2.15	5.32	04271+7146	<0.25	<0.25	0.87	4.09
LMC	PO(1)	E	2781.90	7824.19	82917.00	184686.69		...	...	...	...
N2403	PO	E	3.34	6.29	51.55	148.49	07321+6543	<0.28	1.30	11.46	54.65
N2683	PO	E	0.93	0.52	8.33	34.02	08495+3336	<0.25	<0.25	4.79	24.02
N2841	PO	E	0.90	0.83	4.41	24.21	09185+5111	<0.25	<0.25	2.41	13.51
N2903	PO	E	5.00	7.64	52.38	147.36	09293+2143	0.86	2.33	27.93	102.64
N2997[d]	PO	E	3.13	5.06	32.28	85.14		...	...	...	...
M81	PO	E	5.86	5.42	44.73	174.02	09514+6918	0.67	0.75	6.88	25.21
M82	PO	E	66.61	285.03	1271.32	1351.09	09517+6954	53.21	273.98	1167.76	1145.11
N3109[d]	PO	E	<0.04	0.07P	3.41	7.97		...	...	...	...
N3115	SS	P	0.19	<0.11	<0.13	<0.30		...	...	...	...
Leo I	PO	N	<0.04	<0.10	<0.06	<0.23		...	...	...	...
N3198	SS	E	0.34	0.61	6.46	17.69	10168+4548	<0.25	0.46	3.66	14.33
I2574	PO	E	<0.05	0.08P	2.41	10.62:	10251+6843	<0.30	<0.25	1.09	2.55
N3521	SS	E	4.91	4.36	44.02	124.80	11032+0014	<0.98	0.92:	26.97	83.74
N3556	SS	E	2.25	4.09	32.19	80.77	11085+5556	0.61	1.80	23.26	60.13
N3621	PO	E	3.47	5.09	29.62	90.12	11158−3232	0.60:	0.71	13.66	50.74
N3623	SS	E	<0.12	<0.21	2.99	15.27	11163+1322	<0.25	<0.34	2.03	12.92
N3627	SS	E	4.17	7.72	56.31	144.96	11176+1315	0.72:	1.37:	33.69:	104.20
N3628	SS	E	3.08	5.30	48.51	122.17	11176+1351	2.61	4.67:	48.03	101.73

TABLE 2—*Continued*

Name (1)	Obs[b] (2)	Ext[c] (3)	Total Flux Density (Jy) 12 μm (4)	25 μm (5)	60 μm (6)	100 μm (7)	*IRAS* Name (8)	PSC Flux Density (Jy) 12 μm (9)	25 μm (10)	60 μm (11)	100 μm (12)
N3718	SS	P	0.15	0.11	0.76	2.52	11298+5320	<0.36	<0.62	<0.81	2.81
N4192	SS	E	0.65:	0.36:	7.19	23.18	12112+1510	<0.33	<0.45	5.02	18.38
N4216	SS	E	<0.12	<0.20	2.27	12.79	12133+1325	<0.34	<0.31	<0.93	7.42
N4236	PO	E	0.11P	0.57P	3.98	10.02	12140+6947	<0.25	0.29:	1.60	3.93
N4244	PO	E	<0.05	<0.07	4.20	16.06	12150+3804	<0.36	<0.25	<0.45	2.94
N4258[d]	PO	E	2.25	2.81	21.60	78.39		...	...	...	...
N4395	SS	E	<0.11	0.17P	4.21	12.90	12233+3348	<0.25	<0.25	2.07	5.68
N4438	SS	P	0.17	<0.15	4.28	12.05	12252+1317	<0.27	<0.27	4.00	10.44
N4472	SS	N	<0.13	<0.21	<0.19	<0.48		...	...	...	...
N4517	SS	E	0.61:	0.53:	6.92	20.20	12301+0023	<0.31	0.56	3.91	14.41
N4559	SS	E	0.49:	0.73:	9.69	27.05	12334+2814	<0.40	0.43	5.25	17.45
N4565	PO	E	1.53	1.70	9.83	47.23	12338+2615	<0.90	0.58:	5.94	24.69:
N4569	SS	E	0.75:	1.28:	9.19	27.33	12343+1326	<0.35	0.89	7.08	22.72
N4594	SS	E	0.74:	0.50:	4.26	22.86	12373-1120	<0.57	0.43:	3.12	11.72
N4631	PO	E	5.48	9.65	82.90	208.66	12396+3249	1.82	3.01	51.15	118.60
N4656	PO	E	0.10P	0.30P	5.90	11.46	12415+3226	<0.69	<0.34	2.17	6.08
N4725	SS	E	0.32:	0.20P	4.18	20.79	12480+2547	<0.59	<0.25	0.75	<7.00
N4736	PO	E	4.77	6.83	62.41	135.34	12485+4123	2.79	3.50	55.70	103.78
N4762	SS	P	0.14	<0.15	<0.15	<0.35		...	...	...	...
N4826	SS	P	1.71	2.00	33.86	77.38	12542+2157	1.83	2.57	36.89	74.47:
N4945	PO	E	23.65	43.28	588.11	1415.50	13025−4911	3.65	14.32	388.05	684.01
N5033	SS	E	1.38	1.77	17.20	51.05	13111+3651	0.78	1.06	13.08	43.55
N5055	PO	E	5.56	7.00	40.02	157.74	13135+4217	1.21:	1.15	27.64	99.84
N5102	SS	E	<0.10	<0.14	0.82	2.73	13191−3622	<0.25	<0.25	0.82	2.55
N5128	PO	E	23.03	30.74	217.57	501.20	13225−4245	11.20	15.07	171.12	335.73
N5170	SS	P	0.15	<0.16	1.08	4.84	13271−1742	<0.25	<0.31	1.02	3.59
M51	PO	E	11.02:	17.47:	108.68:	292.08:	13277+4727	1.37	2.40	31.68	121.42
M83	PO(2)	E	26.28	47.72	266.03	638.63	13341−2936	4.72	19.61	103.25	212.05
M101	PO	E	6.20	11.78	88.04	252.84	14013+5435	<0.52	0.35	3.83	29.90
U Mi	PO	N	<0.04	<0.05	<0.07	<0.24		...	...	...	...
N5907	PO	E	1.22	1.35	8.78	45.76	15146+5629	0.90	0.94	9.89	35.13
Draco Sys.	PO	N	<0.06	<0.08	<0.10	<0.30	17185+5756	<0.25	<0.25	0.65	1.11
N6744	PO	E	2.86	4.18	22.21	85.80	19047−6357	<0.25	<0.25	2.02	16.94
N6822	PO	E	0.25	2.46	47.63:	95.42:	19421−1455	<0.83	<0.33	1.91	<11.44
N6946	PO	E	12.13	21.18	136.69	344.37	20338+5958	2.17	6.56	52.07	126.37
I5201	SS	E	0.15P	<0.10	1.42	3.31	22179−4617	<0.25	<0.25	0.41:	3.11
N7331	SS	E	3.36	4.20	35.29	115.07	22347+3409	<0.46	<0.25	19.02:	80.89
N7640	SS	E	0.16P	<0.13	3.70	11.45	23197+4034	<0.25	<0.24	1.70	7.28
N7793	PO(2)	E	1.54	2.09	19.62	56.34	23552−3252	<0.30	<0.39	5.59	32.54
WLM	SS	E	<0.12	<0.20	0.32	1.04		...	...	...	...

[a]Flux densities have been calculated assuming an input energy distribution proportional to ν^{-1}. Version 1.0 PSC values are reported.

[b]Observation type: Maps were constructed from pointed observations (PO) or all-sky survey scans (SS). (1) LMC and SMC data are mean measurements from two sets of PO maps and one set of SS maps for each galaxy. (2) Maps constructed from single PO data.

[c]Extent code key: E—galaxy was observed as an extended source; the total flux densities were obtained from surface brightness maps. Entries followed by P were measured from point-source filtered maps. P—galaxy was observed as an "unresolved" source; the total flux densities were obtained from point-source filtered maps. N—galaxy was not detected.

[d]N2997, N3109, and N4258 were not covered in the all-sky survey but were the targets of pointed observations.

Remarks to Table 2

N45.—Nearby background galaxies detected at 3 σ level in the 60 and 100 μm maps.

N147.—Heavy cirrus in field.

N185.—Heavy cirrus in field; 100 μm source possibly confused due to cirrus.

SMC.—Integrated emission within 3° of 0051.00−7306.0; the 12 and 25 μm emission of the foreground source NGC 104 has been removed (cf. Schwering and Israel 1987).

I1613.—Prominent emission from cluster of H II regions northeast of the nucleus and low-level emission coincident with optical knots southeast of the nucleus.

REMARKS TO TABLE 2—*Continued*

N1097.—Low-level emission from disk at 12 and 25 μm.
N1291.—Emission from disk at 100 μm.
N1313.—Heavy cirrus in field.
N1365.—Low-level emission from disk at 12 and 25 μm.
N1448.—Possibly extended along cross-scan direction.
LMC.—Integrated emission within 4° of 0521.22−6807.2; the emission of foreground sources has not been removed (cf. Schwering 1987).
N2903.—Cirrus in field.
N3198.—Low-level emission from disk at 12 and 25 μm.
N3521.—Cirrus in field.
N3627.—Double source near nucleus at 12 and 25 μm.
N4438.—100 μm source possibly confused because of nearby source.
M51.—N5194 and N5195 were not totally resolved; the M51 total flux densities have been estimated as twice the measured emission of the hemisphere of the galaxy not containing the companion.
N6822.—Total flux density, above local "cirrus" background, within 14′ of galaxy center.
Draco System.—PSC detection is a background galaxy.

Column (1).—Galaxy name.

Column (2).—B_T^0, the total blue magnitude corrected for Galactic and internal extinction. The RC2 magnitudes have been recalculated using the correction formulae of RC2 and the Galactic extinction estimates of Burstein and Heiles (1984).

Columns (3)–(4).—$(B-V)_T^0$ and $(U-B)_T^0$, integrated color indices corrected for Galactic and internal extinction. The RC2 colors have been recalculated using the correction formulae of RC2 and the Galactic extinction estimates of Burstein and Heiles (1984).

Column (5).—Magnitude in the near-infrared H band (1.65 μm) as listed in Aaronson *et al.* (1982) and the sources cited therein. The magnitudes were corrected for Galactic extinction and refer to an aperture-to-diameter ratio log $(A/D) = -0.5$.

Columns (6)–(9).—*IRAS* color-corrected total flux densities at 12, 25, 60, and 100 μm.

Column (10).—Integrated flux density in H I 21 cm line emission as listed in Aaronson *et al.* (1982), Huchtmeier *et al.* (1983), and the sources cited therein.

Column (11).—Mean integrated radio continuum flux density at 1400 MHz as listed in RC2, Hummel (1980), and the sources cited therein.

Column (12).—Integrated flux density in CO from Sanders and Young (1986) and Verter (1985).

c) *Integrated Infrared Properties*

Since a single-temperature model cannot generally fit *IRAS* galaxy data (Extragalactic Catalog), a two-temperature model was used to estimate the total flux of the mid- and far-infrared emission of the galaxies. Both the warm and the cold component energy distributions of the model were Planck curves with an emissivity law proportional to λ^{-1}. The two distributions, convolved with the spectral response of the four *IRAS* bandpasses (*IRAS* Supplement, Table II.C.5), were iteratively fitted to the measured flux densities or limits reported in Table 2. While measurable flux densities at both 60 and 100 μm were requirements for using the model, if only upper limits at 12 and 25 μm were available these values were used. For an upper limit, the model fit was to one-half the 3 σ limit value with an uncertainty set equal to one-half the limit value. An uncertainty of 15% was assigned to measured flux densities. The mean correction was 14%, −15%, 4%, and 4% for the 12, 25, 60, and 100 μm flux densities, respectively.

The total fluxes of the warm and cold components of the model, and the total flux of the combined components, were obtained by integrating the two final fitted curves over all wavelengths. Warm and cold component dust temperatures were also derived from the fits.[5]

The model results are reported in Table 4. The fluxes were converted to luminosities using the distances listed in Table 1. The column entries are the following:

Column (1).—Galaxy name.

Column (2).—IR_T, the total flux (W m^{-2}) of the combined warm and cold component distributions of the two-temperature model.

Column (3).—$L(IR_T)$, IR_T converted to luminosity in solar units.

Column (4).—$IR_C/IR_T \equiv f_{C,T}$, the ratio of the total flux of the cold component distribution of the two-temperature model to the total flux of the combined distributions of the model.

Column (5).—$F_{\rm IR}$, the far-infrared flux (W m^{-2}), an estimate of the total flux between 42.5 and 122.5 μm, defined in the Extragalactic Catalog as

$$F_{\rm IR} = 1.26(2.58 f_\nu(60) + f_\nu(100)) \times 10^{-14},$$

where $f_\nu(60)$ and $f_\nu(100)$ are the flux densities at the two far-infrared wavelengths as reported in Table 2 (see also Helou *et al.* 1987).

Column (6).—$L(F_{\rm IR})$, $F_{\rm IR}$ converted to luminosity in solar units.

Column (7).—$F_{\rm IR}/IR_C \equiv f_{{\rm FIR},C}$, the ratio of the 42.5–122.5 μm flux to the total flux of the cold component distribution of the two-temperature model.

[5] While the two-temperature thermal model provides a better fit to the *IRAS* flux densities of galaxies, one should be cautious when applying physical interpretations to the total fluxes and dust temperatures derived from this simplified model. The true energy distribution of galaxies at mid- and far-infrared wavelengths is poorly understood (e.g., the relative contribution at the *IRAS* wavelengths of nonequilibrium emission from small dust grains). The derived quantities of the model are useful for statistical analyses intercomparing the infrared properties of the sample galaxies.

Note that the color-correction, total flux, and infrared temperature derivations may be affected by the sensitivity of the 12 and 25 μm wavelength bands. As discussed in § III*d*, the reported 12 and 25 μm flux densities (or limits) of faint extended sources may underestimate the total emission by excluding the contribution of low-level diffuse emission of the galaxy disk.

Column (8).— $IR_T/F_B^* \equiv f_{T,B}$, the ratio of the total flux of the combined distributions of the two-temperature model to the blue-light flux corrected for Galactic and internal reddening. Here, the blue-light flux is defined as $F_B^* = \nu f_\nu$ at 0.44 μm (de Jong *et al.* 1984; Soifer *et al.* 1984) and differs from the commonly used "in-band" blue-light flux.

Column (9).— $F_{IR}/F_B^* \equiv f_{FIR,B}$, the ratio of the 42.5–122.5 μm flux to the blue-light flux.

Column (10).— T_W, the dust temperature of the warm component. A colon following an entry means that the 12 or 25 μm flux density was an upper limit or both values were upper limits.

Column (11).— T_C, the dust temperature of the cold component.

The last three lines of the table list the median, the mean, and the standard deviation from the mean of the column

TABLE 3

GLOBAL EMISSION PROPERTIES

Name (1)	B_T^o (2)	$(B-V)_o$ (3)	$(U-B)_o$ (4)	1.65 μm (5)	Color–corrected (Jy) 12 μm (6)	25 μm (7)	60 μm (8)	100 μm (9)	HI (10)	21 cm (11)	CO (12)
N45	10.93	0.65	−0.07	9.65	...	...	1.71	5.21	236	...	...
N55	7.27	...	...	...	1.65	6.06	83.84	179.82	2450(3)	700(4)	...
N134	10.59	0.79	0.20	7.58	2.06	2.26	17.49	64.11	154	...	...
N147	9.69(1)	0.78	...	...	...	...	...	...	...	<50	...
N185	9.29	0.72	...	...	0.03	...	0.28	2.03	36(3)	<50	...
N205	8.71	0.81	...	...	0.17	0.16	0.52	3.97	...	<50	...
M31	3.68	0.76	0.36	0.91	164.33	82.42	489.85	3080.75	...	8000	...
N247	8.99	0.55	...	7.69	...	...	8.23	28.60	740	<50	...
N253	7.61	0.87	...	4.74	68.34	142.52	1095.99	1906.87	...	5500	23000
SMC	2.39	0.41	...	...	82.58	255.73	7337.85	15505.51	...	67600(4)	...
N300	8.50	...	...	...	0.60	0.53	24.20	77.81	2010(3)	...	...
I1613	9.94	0.59	...	...	...	...	1.53	3.83	500(3)	<50	...
M33	5.92	0.47	−0.16	4.38	37.03	33.29	442.56	1310.68	...	3100	...
N628	9.60	0.55	...	...	2.23	1.51	21.85	68.57	650(3)	200	...
N660	11.08	0.74	...	...	2.83	6.53	74.66	106.39	150(3)	390	...
N891	10.05	0.73	0.09	6.84	6.52	6.53	63.30	207.70	225	770	6800
N925	10.17	0.49	...	8.74	0.32	0.60	7.83	27.94	307	65	...
N1023	9.86	0.92	0.47	...	...	...	...	...	45(3)	<50	...
Fornax Sys.	9.02	...	...	...	...	...	...	...	...	...	...
N1097	10.05	0.96	...	...	3.52	7.02	49.94	120.68	137(3)	540(4)	...
N1291	9.37	0.92	0.43	...	0.20	0.14	1.60	10.66	72(3)	200(4)	...
N1313	9.24	...	...	...	1.17	3.30	38.59	95.49	440(3)	...	...
N1365	9.93	0.57	0.02	7.20	5.42	12.05	91.22	191.37	159	616(4)	...
I342	7.75	...	...	...	28.27	39.53	272.65	687.25	4908(3)	2500(4)	35000
N1448	10.77	...	...	8.38	1.01	0.89	10.20	35.67	134	...	...
N1560	11.07	0.45	...	9.31	...	...	2.35	5.51	191	<50(4)	...
LMC	0.31	0.47	...	...	3405.97	7157.10	90480.32	190632.61	...	616600(4)	...
N2403	8.52	0.42	...	6.45	3.99	5.49	54.43	154.75	1459	300	...
N2683	10.01	0.77	0.17	6.96	0.90	0.39	8.31	35.73	85	90	...
N2841	9.83	0.79	0.35	6.90	0.97	0.66	4.02	25.47	190	95	...
N2903	9.20	0.57	0.00	6.56	5.83	6.50	55.42	153.46	187	400	4900(5)
N2997	10.00	...	...	...	3.68	4.33	34.41	88.48	173(3)	708(4)	...
M81	7.39	0.85	...	4.38	6.33	4.32	44.82	182.65	266	380	...
M82	8.89	0.78	...	...	82.06	278.17	1375.27	1340.50	700(3)	8000	42000
N3109	9.69(1)	...	...	...	...	0.07	3.74	8.24	1280(3)	210	...
N3115	9.86	0.91	0.53	...	...	...	...	...	...	<50	...
Leo I	11.02	0.95	...	...	...	...	...	...	...	...	...
N3198	10.66	0.47	...	8.71	0.40	0.53	6.90	18.40	206	<100	...
I2574	10.68	0.39	...	10.07	...	0.07	2.36	11.16	499	<70	...
N3521	9.41	0.77	...	6.51	5.25	3.46	46.86	129.96	282	430	...
N3556	10.23	0.51	−0.08	...	2.67	3.55	34.63	83.78	144(3)	293	...
N3621	9.48(1)	...	...	7.40	4.03	4.31	30.88	94.08	668	420(4)	...
N3623	9.74	0.80	0.32	6.76	...	...	2.82	16.07	26	<50	...
N3627	9.40	0.63	0.17	6.70	4.97	6.72	60.30	150.51	61	500	8300
N3628	9.64	0.68	...	6.97	3.64	4.57	52.27	126.72	276	512	10000

TABLE 3—*Continued*

Name (1)	B_T^o (2)	$(B-V)_o$ (3)	$(U-B)_o$ (4)	1.65 μm (5)	Color–corrected (Jy) 12 μm (6)	25 μm (7)	60 μm (8)	100 μm (9)	HI (10)	21 cm (11)	CO (12)
N3718	11.02	0.68	...	...	0.15	0.09	0.79	2.64	...	<50	...
N4192	10.34	0.67	...	7.77	0.63	0.27	7.53	24.23	83	90	...
N4216	10.43	0.88	0.43	...	...	...	2.08	13.46	23(3)	<50	...
N4236	9.55	0.30	...	9.08	0.13	0.56	4.23	10.40	476	<50	...
N4244	9.85	0.29	...	8.75	...	...	4.27	16.85	418	<50	...
N4258	8.66	0.61	...	6.11	2.56	2.33	21.91	82.18	506	820	...
N4395	10.63	0.53	...	...	...	0.16	4.44	13.46	301(3)	<70	...
N4438	10.48	0.75	...	...	0.15	...	4.59	12.54	4(3)	125	...
N4272	9.30	0.94	...	...	...	...	...	...	<4(3)	250	...
N4517	10.45	0.58	...	...	0.65	0.42	7.35	21.05	103(3)	130	...
N4559	9.96	0.37	...	8.34	0.57	0.62	10.34	28.15	314	180	...
N4565	9.64	0.68	...	6.70	1.71	1.39	9.30	49.68	242	100	...
N4569	9.91	0.68	0.24	...	0.89	1.10	9.64	28.51	12(3)	90	...
N4594	8.86	0.88	...	...	0.75	0.38	3.94	24.05	...	300	...
N4631	9.20	0.41	...	...	6.49	8.35	89.26	216.44	639(3)	1300	...
N4656	10.16	0.29	...	...	0.12	0.28	6.54	11.75	393(3)	118	...
N4725	9.80	0.71	...	7.06	0.32	0.15	3.97	21.87	100	<100	...
N4736	8.78	0.74	0.15	...	5.51	5.76	68.36	139.52	62(3)	270	...
N4762	10.77	0.82	0.33	...	...	...	...	...	...	<50	...
N4826	9.00	0.76	0.14	6.10	1.91	1.64	37.11	79.93	56	90	...
N4945	8.15	...	...	...	28.09	37.53	639.41	1465.39	...	6600(4)	...
N5033	10.38	0.49	...	7.50	1.57	1.47	18.15	53.24	178	200	...
N5055	9.13	0.69	...	6.30	6.33	5.81	39.70	165.61	372	409	...
N5102	10.06	0.63	0.22	...	...	...	0.85	2.86	89(3)	...	...
N5128	7.42	0.86	...	...	26.37	25.69	236.32	518.10	...	1300000(4)	...
N5170	11.01(1)	...	...	8.38	0.14	...	1.05	5.09	87	...	...
M51	8.83	0.57	...	...	11.25	12.61	84.95	192.56	230(3)	1500	16000
M83	8.03	...	...	...	31.24	41.47	285.97	661.47	1600(3)	1650	...
M101	8.19	0.46	...	...	7.40	10.29	92.86	263.48	3900(3)	850	11000
U Mi	11.6 (2)	...	...	...	...	...	...	...	...	...	...
N5907	10.31	0.61	...	7.58	1.36	1.10	8.14	48.14	242	114	...
Draco Sys.	11.9 (2)	...	...	...	...	...	...	...	...	...	...
N6744	8.74	...	...	...	3.32	3.53	22.07	90.05	975(3)	...	...
N6822	8.46	...	...	...	0.29	2.59	58.59	196.71	2150(3)	<50	...
N6946	7.97	0.43	...	...	14.36	18.31	146.54	357.29	839(3)	1500	21000
I5201	11.06	...	...	...	0.12	...	1.56	3.42	...	...	...
N7331	9.67	0.69	0.12	6.44	3.82	3.48	36.59	120.33	212	486	...
N7640	10.41	0.32	...	8.97	0.14	...	3.91	11.95	360(3)	...	...
N7793	9.59	0.56	−0.12	7.89	1.77	1.75	20.80	58.70	271	...	...
WLM	10.94	0.29	−0.32	...	...	...	0.32	1.09	285(3)	...	...

NOTES.—Optical values have been corrected using the Galactic reddening estimates of Burstein and Heiles 1984. Units: 1.65 μm (mag); H I (Jy km s^{-1}); 21 cm (mJy); CO (mJy km s^{-1}).

SOURCES.—Optical: RC2; (1) RSA; (2) Kraan-Korteweg and Tammann 1979. 1.65 μm: Aaronson *et al.* 1982. H I: Aaronson *et al.* 1982; (3) Huchtmeier *et al.* 1983. 21 cm continuum: Hummel 1980; (4) RC2. CO: Sanders and Young 1986; (5) Verter 1985.

entries. The warm component dust temperature statistics exclude the values determined using a limit.

d) *Far-Infrared Diameters*

The far-infrared isophotal diameter of the largest infrared extended galaxies least affected by the *IRAS* beam was obtained from the 60 μm surface brightness map. The diameter was measured along the galaxy optical major axis to the 25 mJy $arcmin^{-2}$ isophotal brightness level. Table 5 reports the results. The column entries are:

Column (1).—Galaxy name.

Column (2).—The RC2 morphological classification T index and bar parameter letter.

Column (3).— D_{IR}, the 60 μm isophotal diameter.

Column (4).— D_{IR}/D_B, the ratio of the 60 μm isophotal diameter to the blue-light isophotal major diameter statistically corrected for Galactic extinction. The corrected blue diameter was calculated using the interpolation formula

adopted from RC2:

$$\log D_B = \log D_{25} + A_B(0.12 - 0.007T),$$

where A_B is the Galactic reddening from Burstein and Heiles (1984) and T is the RC2 morphological classification T index.

Column (5).—$(A_e/D)_{\rm IR}$, the ratio of the "effective" aperture diameter to the isophotal diameter of the 60 μm emission. As in RC2, the 60 μm emission effective aperture is defined here as the circular aperture, centered on the galaxy image, from which one-half of the galaxy total 60 μm emission was measured.

Column (6).—$(A_e/D)_B$, the ratio of the effective aperture diameter of the isophotal major diameter of the blue-light emission. Both diameters were obtained from RC2.

Uncertain infrared diameter measurements, possibly affected by the beam or by confusion due to local "cirrus" emission, are followed by a colon. The last two lines report the mean and standard deviation of the column entries.

TABLE 4

INTEGRATED INFRARED PROPERTIES

Name (1)	IR_T (W m^{-2}) (2)	$L(IR_T)$ ($L_\odot$) (3)	$f_{C,T}$ (4)	$F_{\rm IR}$ (W m^{-2}) (5)	$L(F_{\rm IR})$ ($L_\odot$) (6)	$f_{{\rm FIR},C}$ (7)	$f_{T,B}$ (8)	$f_{{\rm FIR},B}$ (9)	T_W (K) (10)	T_C (K) (11)
N45	2.04E−13	7.25E+08	0.897	1.16E−13	4.10E+08	0.631	0.201	0.114	216.1:	30.4
N55	7.62E−12	2.38E+09	0.875	4.70E−12	1.47E+09	0.704	0.257	0.159	148.7	34.1
N134	2.87E−12	9.13E+10	0.779	1.33E−12	4.23E+10	0.595	2.064	0.956	210.3	28.5
N185	9.56E−14	1.59E+06	0.818	3.44E−14	5.73E+05	0.440	0.021	0.007	406.2:	23.7
N205	2.08E−13	3.46E+06	0.755	6.71E−14	1.12E+06	0.428	0.026	0.009	224.0	23.2
M31	1.68E−10	2.79E+09	0.685	5.43E−11	9.05E+08	0.473	0.207	0.067	295.6	24.6
N247	1.02E−12	3.18E+08	0.980	6.02E−13	1.88E+08	0.602	0.168	0.099	224.4:	29.2
N253	1.03E−10	5.58E+10	0.735	5.59E−11	3.04E+10	0.741	4.742	2.583	172.8	36.8
SMC	6.22E−10	1.18E+08	0.934	4.07E−10	7.73E+07	0.700	0.235	0.153	156.5	34.4
N 300	2.90E−12	5.23E+08	0.939	1.69E−12	3.04E+08	0.619	0.304	0.177	230.4	29.9
I1613	1.51E−13	3.41E+06	0.913	9.27E−14	2.09E+06	0.671	0.060	0.037	183.0:	32.4
M33	5.71E−11	1.45E+09	0.808	2.95E−11	7.46E+08	0.639	0.556	0.287	227.2	30.6
N628	3.06E−12	2.84E+10	0.785	1.51E−12	1.39E+10	0.626	0.885	0.435	255.6	30.1
N660	5.82E−12	7.02E+10	0.802	3.51E−12	4.23E+10	0.751	6.569	3.959	170.9	40.1
N891	9.23E−12	7.00E+10	0.787	4.49E−12	3.41E+10	0.618	4.031	1.962	217.7	29.6
N925	1.10E−12	8.60E+09	0.890	5.85E−13	4.59E+09	0.600	0.535	0.285	176.7	28.8
N1097	5.73E−12	1.18E+11	0.758	2.98E−12	6.15E+10	0.687	2.502	1.304	174.1	32.5
N1291	4.59E−13	3.13E+09	0.875	1.85E−13	1.26E+09	0.460	0.107	0.043	251.8	24.3
N1313	4.00E−12	3.40E+09	0.858	2.33E−12	1.98E+09	0.678	0.829	0.483	158.5	32.4
N1365	9.37E−12	2.86E+11	0.759	5.07E−12	1.55E+11	0.714	3.665	1.985	169.1	34.2
I342	3.40E−11	2.33E+10	0.723	1.67E−11	1.14E+10	0.678	1.785	0.875	194.0	32.1
N1448	1.54E−12	2.08E+10	0.807	7.52E−13	1.01E+10	0.603	1.309	0.638	228.1	29.0
N1560	2.10E−13	1.43E+08	0.962	1.37E−13	9.37E+07	0.679	0.234	0.153	264.4:	33.2
LMC	8.48E−09	8.61E+08	0.839	5.02E−09	5.10E+08	0.706	0.471	0.279	172.2	34.4
N2403	6.78E−12	2.70E+09	0.806	3.55E−12	1.41E+09	0.649	0.724	0.379	194.9	30.9
N2683	1.57E−12	3.13E+09	0.800	6.99E−13	1.39E+09	0.556	0.662	0.295	321.9	27.4
N2841	1.24E−12	7.89E+09	0.768	4.48E−13	2.86E+09	0.471	0.442	0.160	254.3	24.5
N2903	7.23E−12	2.01E+10	0.751	3.56E−12	9.91E+09	0.655	1.444	0.711	209.6	31.2
N2997	4.31E−12	3.44E+10	0.733	2.12E−12	1.69E+10	0.671	1.800	0.886	205.5	32.0
M81	8.27E−12	3.29E+09	0.774	3.65E−12	1.45E+09	0.569	0.312	0.138	254.2	27.7
M82	1.17E−10	4.67E+10	0.649	5.84E−11	2.32E+10	0.767	17.602	8.760	156.3	47.6
N3109	3.16E−13	6.57E+07	0.968	2.11E−13	4.39E+07	0.691	0.099	0.066	152.3:	34.0
N3198	7.86E−13	4.84E+09	0.834	4.33E−13	2.67E+09	0.661	0.602	0.332	198.5	31.7
I2574	4.10E−13	1.57E+08	0.967	2.12E−13	8.12E+07	0.535	0.320	0.166	164.6:	26.6
N3521	6.17E−12	3.03E+10	0.747	3.00E−12	1.48E+10	0.651	1.495	0.728	259.5	31.3
N3556	3.90E−12	3.04E+10	0.777	2.06E−12	1.61E+10	0.682	2.011	1.065	197.6	32.7
N3621	4.53E−12	1.07E+10	0.728	2.10E−12	4.96E+09	0.636	1.171	0.542	212.5	30.2
N3623	6.09E−13	3.47E+09	0.962	2.90E−13	1.65E+09	0.494	0.200	0.095	199.6:	25.3
N3627	7.03E−12	3.09E+10	0.768	3.66E−12	1.61E+10	0.677	1.689	0.878	196.2	32.3
N3628	5.74E−12	3.71E+10	0.798	3.12E−12	2.01E+10	0.680	1.721	0.933	201.5	32.7
N3718	1.40E−13	2.05E+09	0.658	5.65E−14	8.26E+08	0.613	0.149	0.060	281.7	29.4
N4192	1.07E−12	1.60E+10	0.793	5.26E−13	7.87E+09	0.619	0.612	0.300	325.1	29.9
N4216	5.26E−13	7.87E+09	0.957	2.35E−13	3.51E+09	0.467	0.326	0.146	202.9:	24.5
N4236	4.59E−13	1.41E+08	0.810	2.56E−13	7.88E+07	0.688	0.126	0.070	143.7	32.2
N4244	5.99E−13	4.64E+08	0.986	3.39E−13	2.63E+08	0.574	0.218	0.123	219.5:	28.1

TABLE 4—*Continued*

Name (1)	IR_T (W m^{-2}) (2)	$L(IR_T)$ ($L_\odot$) (3)	$f_{C,T}$ (4)	F_{IR} (W m^{-2}) (5)	$L(F_{IR})$ ($L_\odot$) (6)	$f_{FIR,C}$ (7)	$f_{T,B}$ (8)	$f_{FIR,B}$ (9)	T_W (K) (10)	T_C (K) (11)
N4258	3.63E−12	1.23E+10	0.791	1.69E−12	5.71E+09	0.589	0.441	0.205	225.5	28.4
N4395	5.02E−13	5.80E+08	0.943	2.99E−13	3.46E+08	0.632	0.374	0.223	167.1:	30.4
N4438	5.15E−13	7.71E+09	0.868	2.91E−13	4.35E+09	0.651	0.334	0.189	382.0:	31.6
N4517	9.38E−13	7.44E+09	0.794	4.79E−13	3.80E+09	0.644	0.592	0.303	262.2	31.0
N4559	1.18E−12	8.73E+09	0.852	6.56E−13	4.87E+09	0.655	0.473	0.264	212.1	31.5
N4565	2.30E−12	3.94E+10	0.782	9.15E−13	1.57E+10	0.509	0.688	0.274	235.7	25.6
N4569	1.28E−12	1.92E+10	0.780	6.43E−13	9.62E+09	0.642	0.494	0.247	201.5	30.5
N4594	1.13E−12	1.07E+10	0.789	4.27E−13	4.06E+09	0.479	0.165	0.062	292.3	24.8
N4631	9.91E−12	4.55E+10	0.789	5.32E−12	2.44E+10	0.681	1.980	1.063	199.9	32.7
N4656	5.14E−13	2.50E+09	0.904	3.36E−13	1.64E+09	0.723	0.249	0.163	171.9	36.6
N4725	8.98E−13	1.53E+10	0.883	3.98E−13	6.77E+09	0.502	0.312	0.138	303.9	25.6
N4736	6.93E−12	1.03E+10	0.760	3.73E−12	5.56E+09	0.709	0.941	0.507	216.0	34.8
N4826	3.54E−12	5.43E+09	0.841	2.08E−12	3.18E+09	0.696	0.589	0.345	234.7	34.2
N4945	6.28E−11	9.40E+10	0.855	3.70E−11	5.53E+10	0.688	4.772	2.806	198.1	33.4
N5033	2.34E−12	2.36E+10	0.800	1.20E−12	1.21E+10	0.641	1.388	0.712	223.7	30.7
N5055	7.69E−12	2.91E+10	0.756	3.29E−12	1.24E+10	0.566	1.441	0.616	224.7	27.5
N5102	1.17E−13	1.76E+08	0.851	6.11E−14	9.14E+07	0.611	0.052	0.027	216.4:	29.4
N5128	2.70E−11	4.05E+10	0.708	1.34E−11	2.00E+10	0.699	1.048	0.519	220.9	33.9
N5170	2.33E−13	4.81E+09	0.778	9.61E−14	1.98E+09	0.531	0.246	0.102	329.7:	26.5
M51	1.05E−11	3.85E+10	0.669	4.91E−12	1.80E+10	0.697	1.493	0.697	209.4	33.4
M83	3.42E−11	1.05E+11	0.703	1.67E−11	5.13E+10	0.694	2.327	1.135	197.5	33.1
M101	1.18E−11	2.12E+10	0.791	6.05E−12	1.09E+10	0.651	0.926	0.476	194.3	30.9
N5907	2.17E−12	1.65E+10	0.816	8.62E−13	6.54E+09	0.486	1.206	0.479	236.1	25.0
N6744	4.17E−12	2.29E+10	0.757	1.80E−12	9.91E+09	0.571	0.545	0.236	212.6	27.6
N6822	7.23E−12	1.04E+08	0.950	4.21E−12	6.08E+07	0.613	0.730	0.425	122.1	29.3
N6946	1.75E−11	2.47E+10	0.736	8.78E−12	1.24E+10	0.682	1.125	0.565	200.2	32.5
I5201	2.08E−13	1.38E+09	0.612	8.79E−14	5.82E+08	0.691	0.230	0.097	463.0:	34.0
N7331	5.34E−12	8.28E+10	0.788	2.60E−12	4.03E+10	0.617	1.644	0.800	225.6	29.6
N7640	4.73E−13	2.73E+09	0.889	2.65E−13	1.48E+09	0.629	0.288	0.161	308.1:	30.4
N7793	2.61E−12	3.57E+09	0.796	1.35E−12	1.85E+09	0.649	0.746	0.386	219.1	31.1
WLM	6.03E−14	4.82E+06	0.628	2.35E−14	1.88E+06	0.621	0.060	0.023	202.9:	29.1
Median		8.60E+09	0.796		4.35E+09	0.642	0.592	0.295	212.1	30.7
Mean			0.811			0.625			215.0	30.6
RMS			0.086			0.079			42.7	3.9

NOTES.—$f_{C,T} \equiv IR_C/IR_T$, the ratio of the total flux of the cold component distribution to the total infrared flux. $f_{FIR,C} \equiv F_{IR}/IR_C$, the ratio of the 42.5 to 122.5 μm flux to the total flux of the cold component distribution. $f_{T,B} \equiv IR_T/F_B^*$, the ratio of the total infrared flux to the blue light flux (see § IV.C). $f_{FIR,B} \equiv F_{IR}/F_B^*$.

V. ATLAS OF INFRARED PROFILES AND MAPS

a) *Profile Plots*

Radial infrared brightness profiles *along the IRAS scanning direction* are displayed in Figure 1 for all detected galaxies, excluding the SMC and LMC. (The profile plots of surface brightness images with peak intensities less than 6 σ are not displayed.) The profiles are centered on the optical center of the galaxies and are scaled by the peak intensity found along the cut. The position angle of the in-scan cuts is noted above each set of plots. The wavelength profile of IRC +10011, a representative *IRAS* point source, is also displayed.

b) *IRAS Surface Brightness Maps*

The atlas plates (Figs. 2–33 [Pls. 136–168]) display optical light photographs and *IRAS* surface brightness contour maps of the catalog galaxies for which interesting spatial structure was observed. Table 6 lists the galaxies displayed. Except for M31, the orientation of the optical photographs and infrared maps is (equatorial) north to the top and east to the left. The orientation of the M31 images is marked on the optical photograph.

Color-coded *IRAS* images are displayed in Figure 34 (Plate 169) for M31 (Fig. 34*a*), the SMC (Fig. 34*b*), and the LMC (Fig. 34*c*). These images were produced by combining the 12 (coded blue), 60 (coded green), and 100 μm (coded red) maps after smoothing the 12 and 60 μm maps to the resolution of the 100 μm map.

i) *Optical Photographs*

The optical photographs are reproductions of Palomar Sky Survey or ESO blue prints. The mosaics of the SMC and

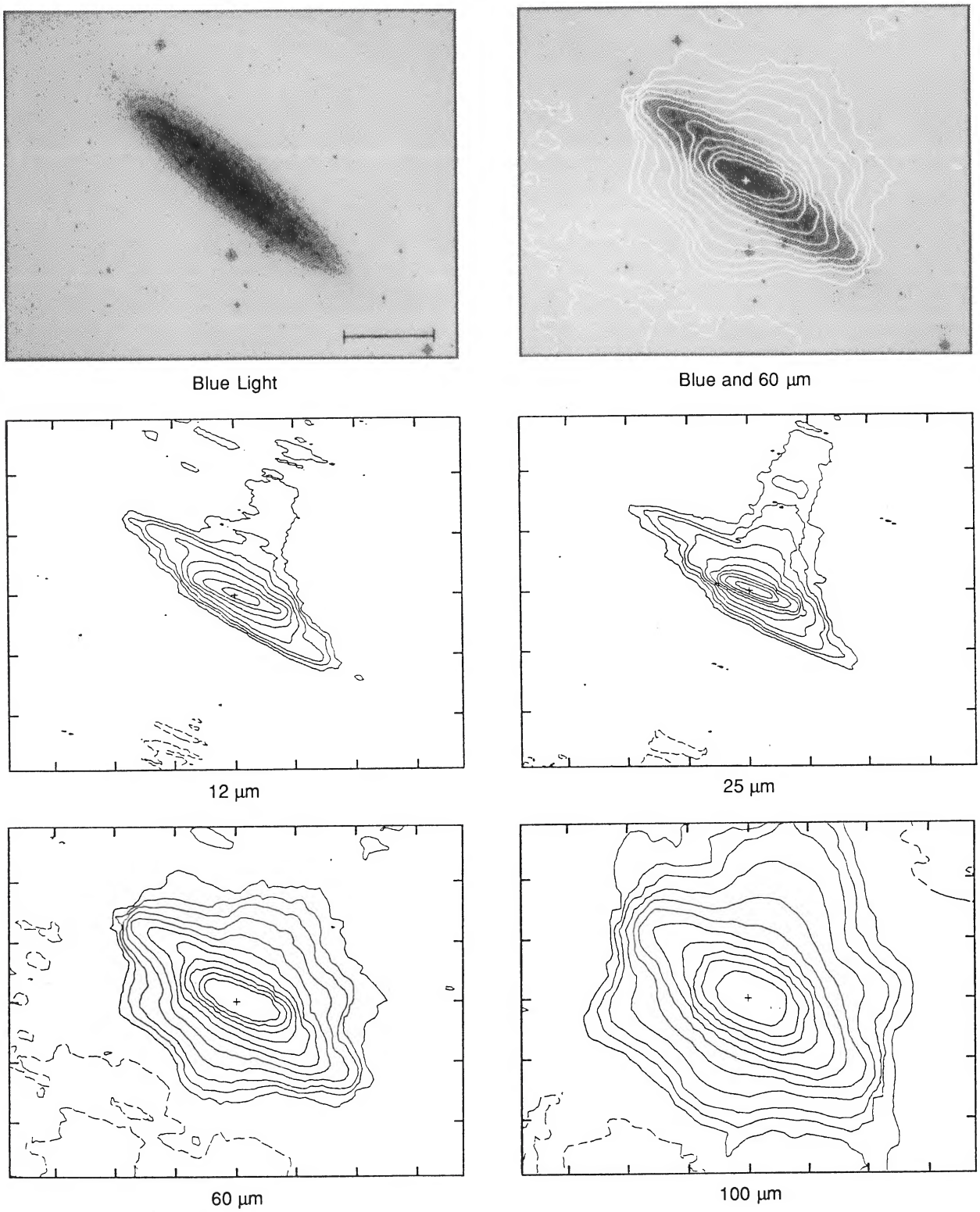

FIG. 5.—NGC 253. The tick marks on the infrared maps are spaced by 5′.4. (Optical photographs reproduced by permission of the European Southern Observatory.)

RICE *et al.* (*see* **68**, 102)

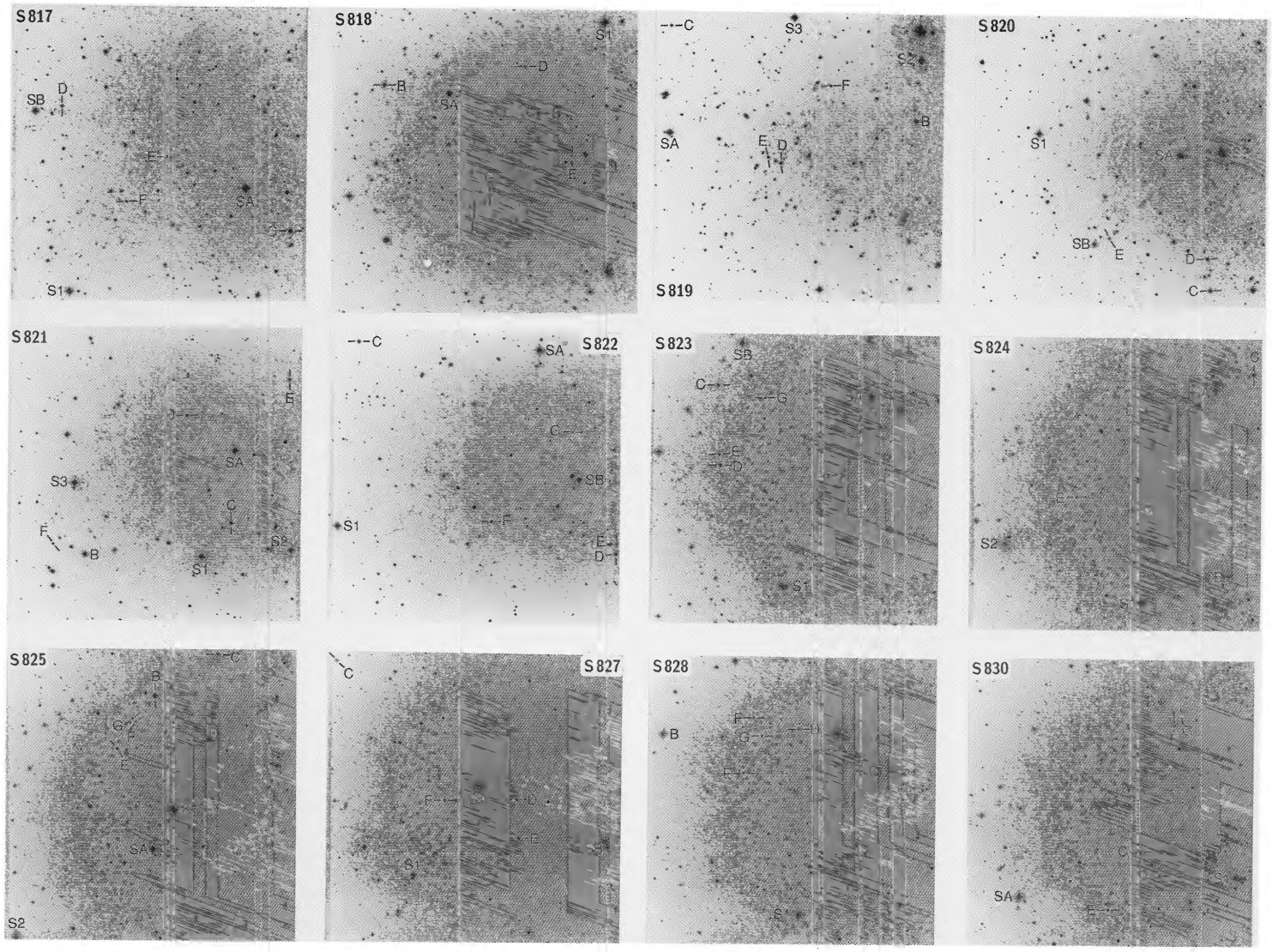

FIG. 121.—Finding charts for fields S817–S830. Northeast is to the upper left, and the fields are 0°.5 in size. *Note the breaks in continuous field sequencing*: charts S826 and S829, which are oversized, are given in Fig. 132.

LASKER, STURCH, *et al.* (*see* **68**, 10)

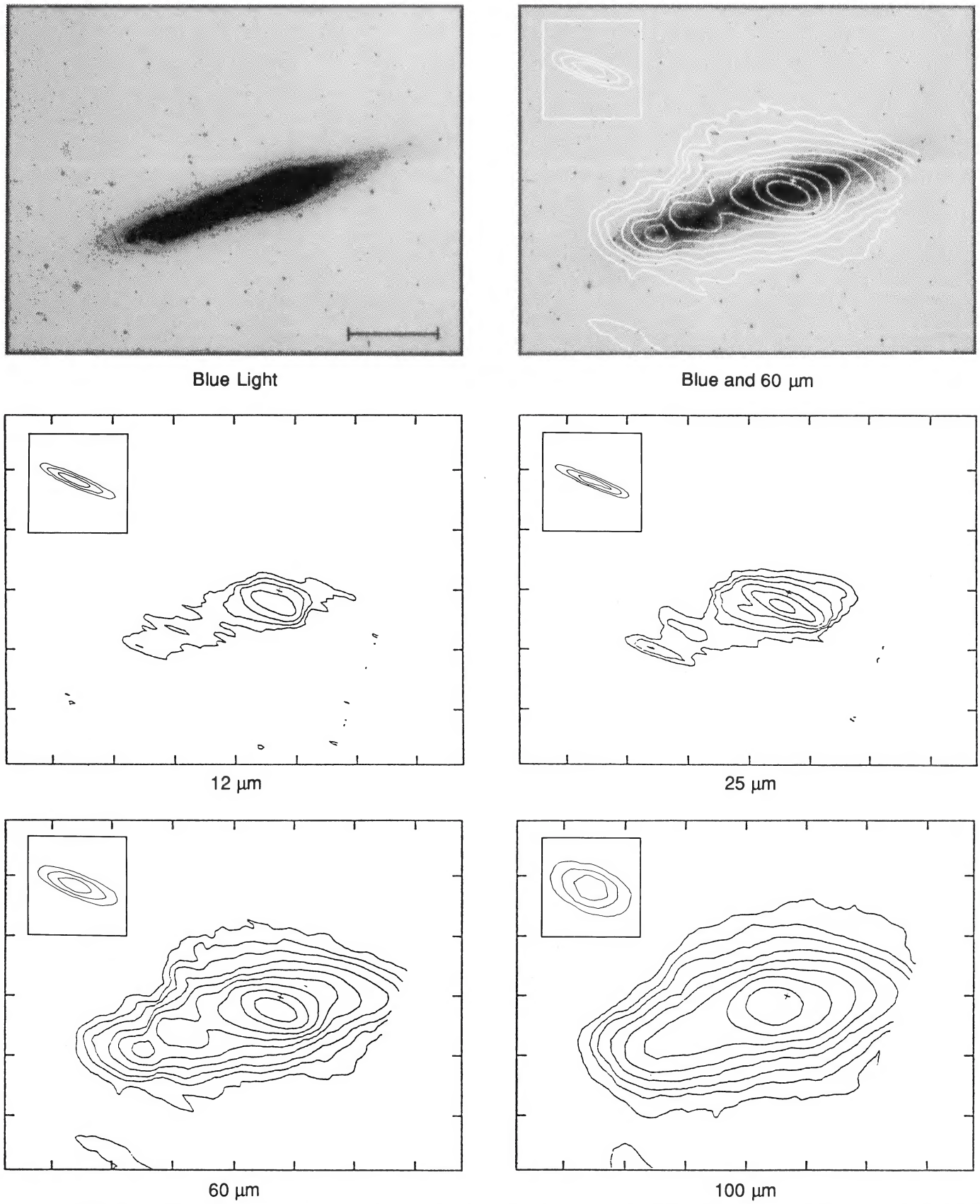

FIG. 2.—NGC 55. The tick marks on the infrared maps are spaced by 5′.4. The boxed image in the upper left-hand corner of the contour maps is the *IRAS* beam represented by the $\frac{1}{4}$, $\frac{1}{2}$, and $\frac{3}{4}$ power brightness level contours of the star IRC +10011, a representative *IRAS* point source. (Optical photographs reproduced by permission of the European Southern Observatory.)

RICE *et al.* (*see* **68**, 102)

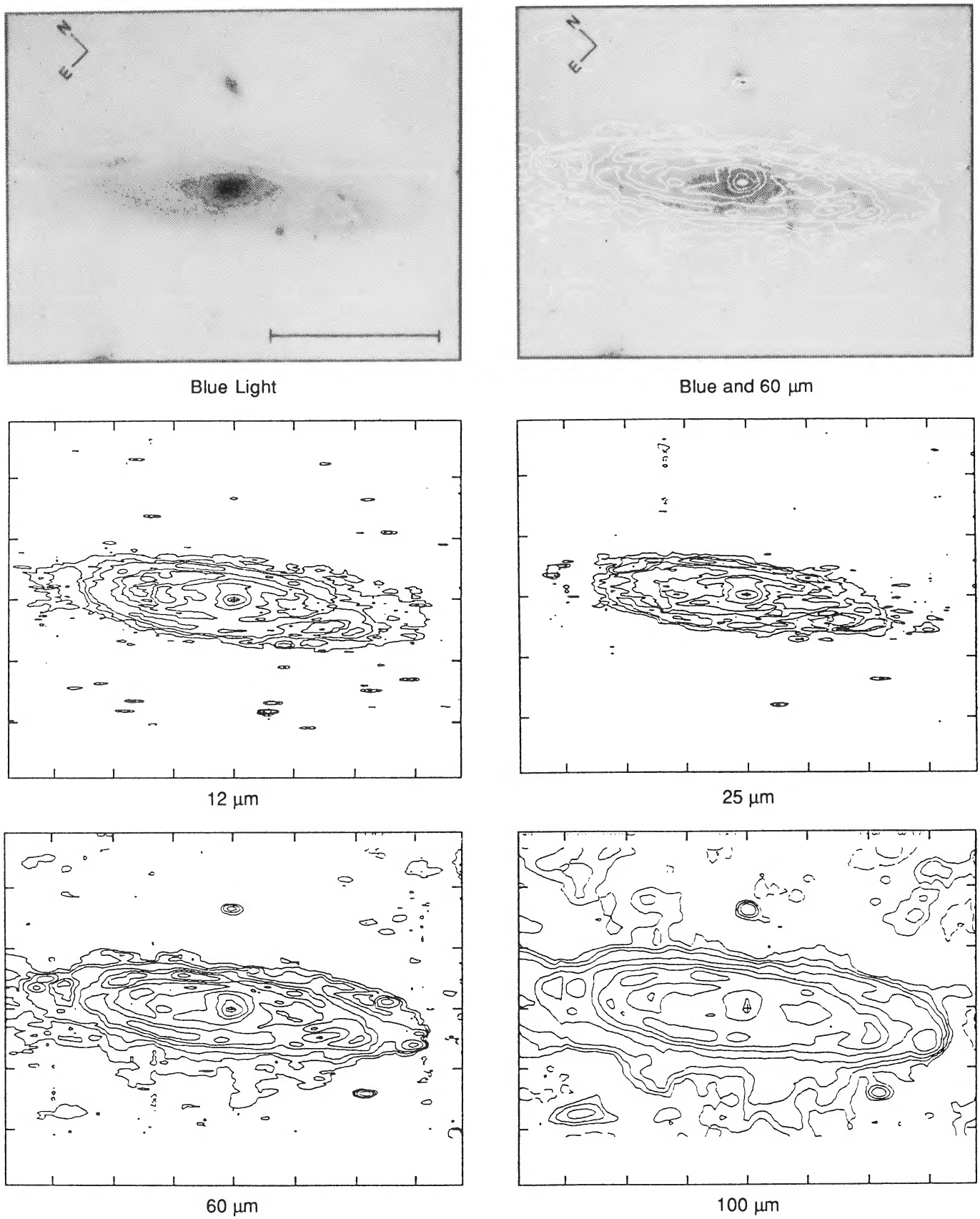

FIG. 3.—NGC 224. The scale marked on the photographs is 1°. The tick marks on the infrared maps are spaced by 21′.7. (Optical photographs reproduced by permission of the California Institute of Technology. © 1960 National Geographic Society–Palomar Sky Survey.)

RICE *et al.* (*see* **68**, 102)

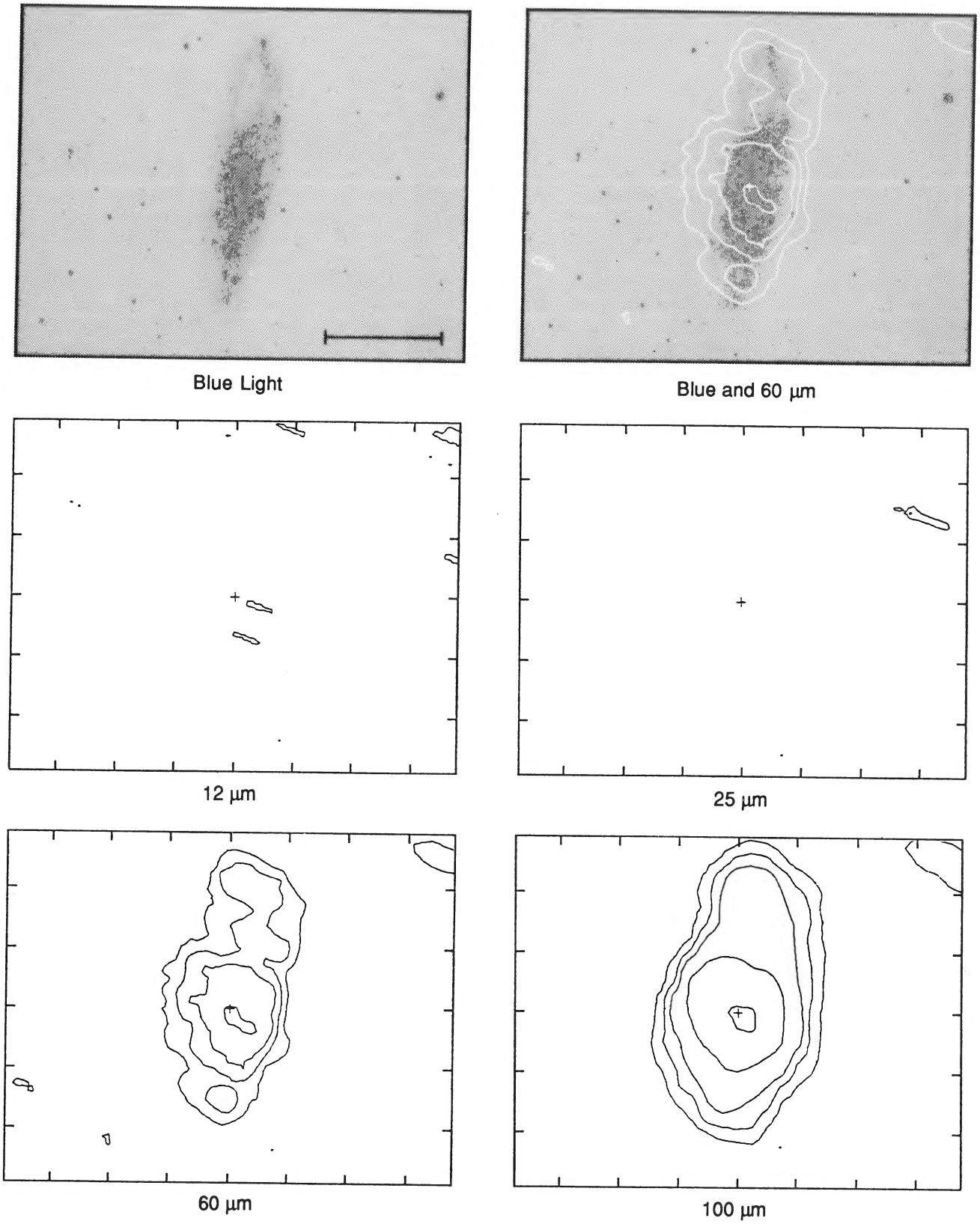

FIG. 4.—NGC 247. (Optical photographs reproduced by permission of the European Southern Observatory.)

RICE *et al.* (*see* **68**, 102)

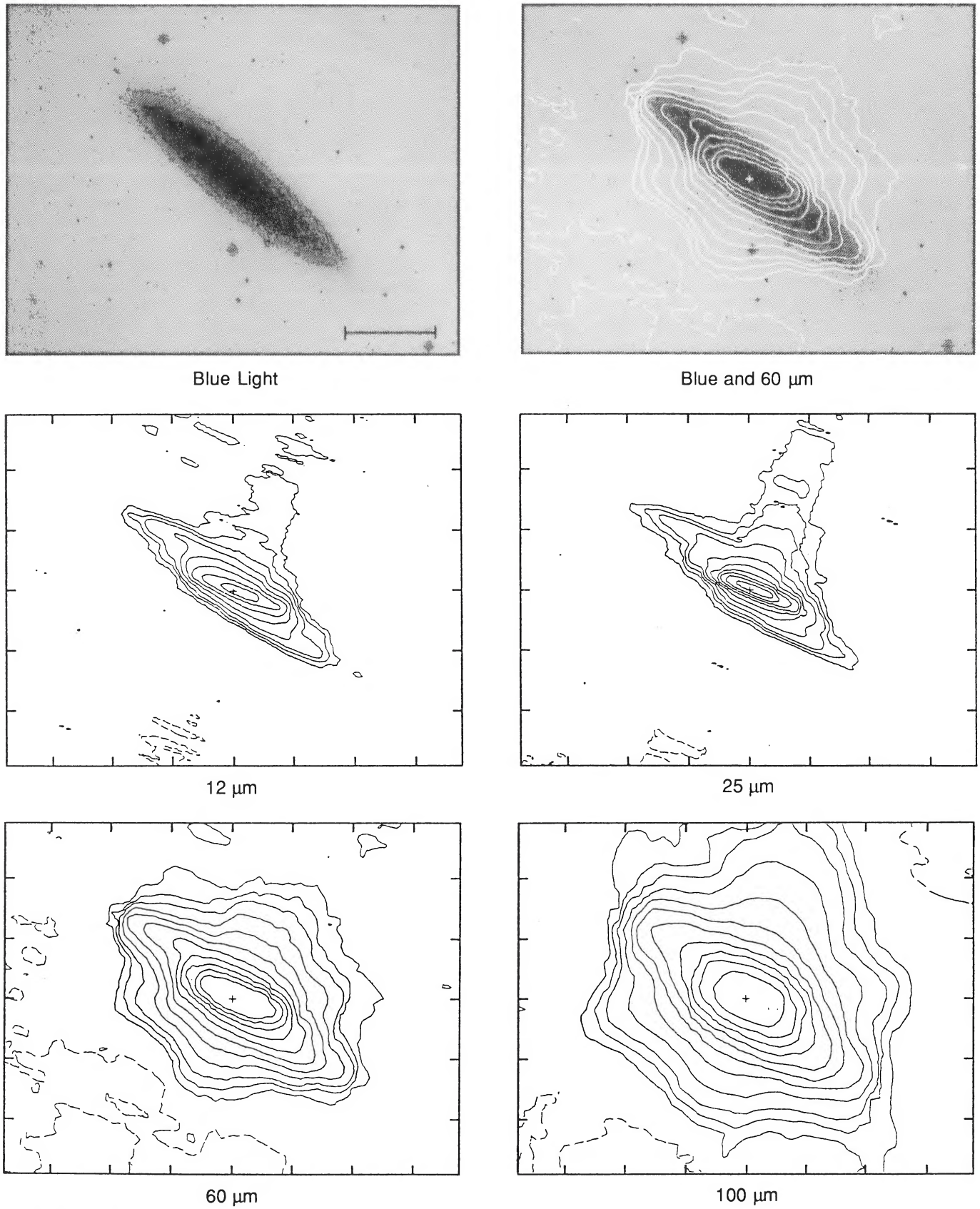

FIG. 5.—NGC 253. The tick marks on the infrared maps are spaced by 5′.4. (Optical photographs reproduced by permission of the European Southern Observatory.)

RICE *et al.* (*see* **68**, 102)

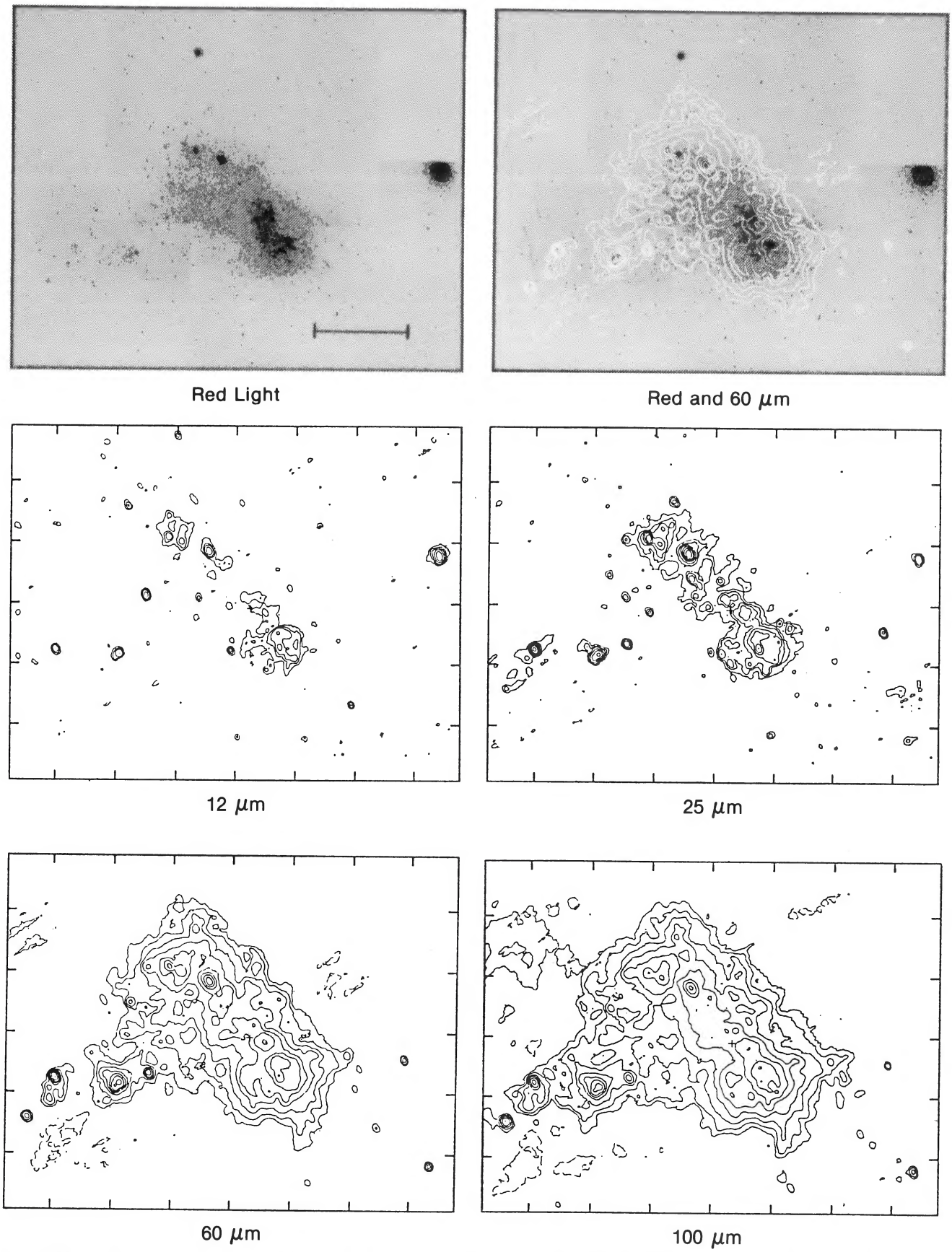

FIG. 6.—SMC. The scale marked on the photograph is 1°. The tick marks on the infrared map are spaced by 42′. The 12, 25, and 60 μm maps have been smoothed to the resolution of the 100 μm map. The contour levels of the 60 and 100 μm maps are at (*dashed*) 9 σ below the map mean background level and at (*solid*) 10 σ and with brighter contours scaled logarithmically by 2 from 10 σ. (Optical photographs reproduced by permission of the Mount Wilson and Las Campanas Observatories, Carnegie Institution of Washington.)

RICE *et al.* (*see* **68**, 102)

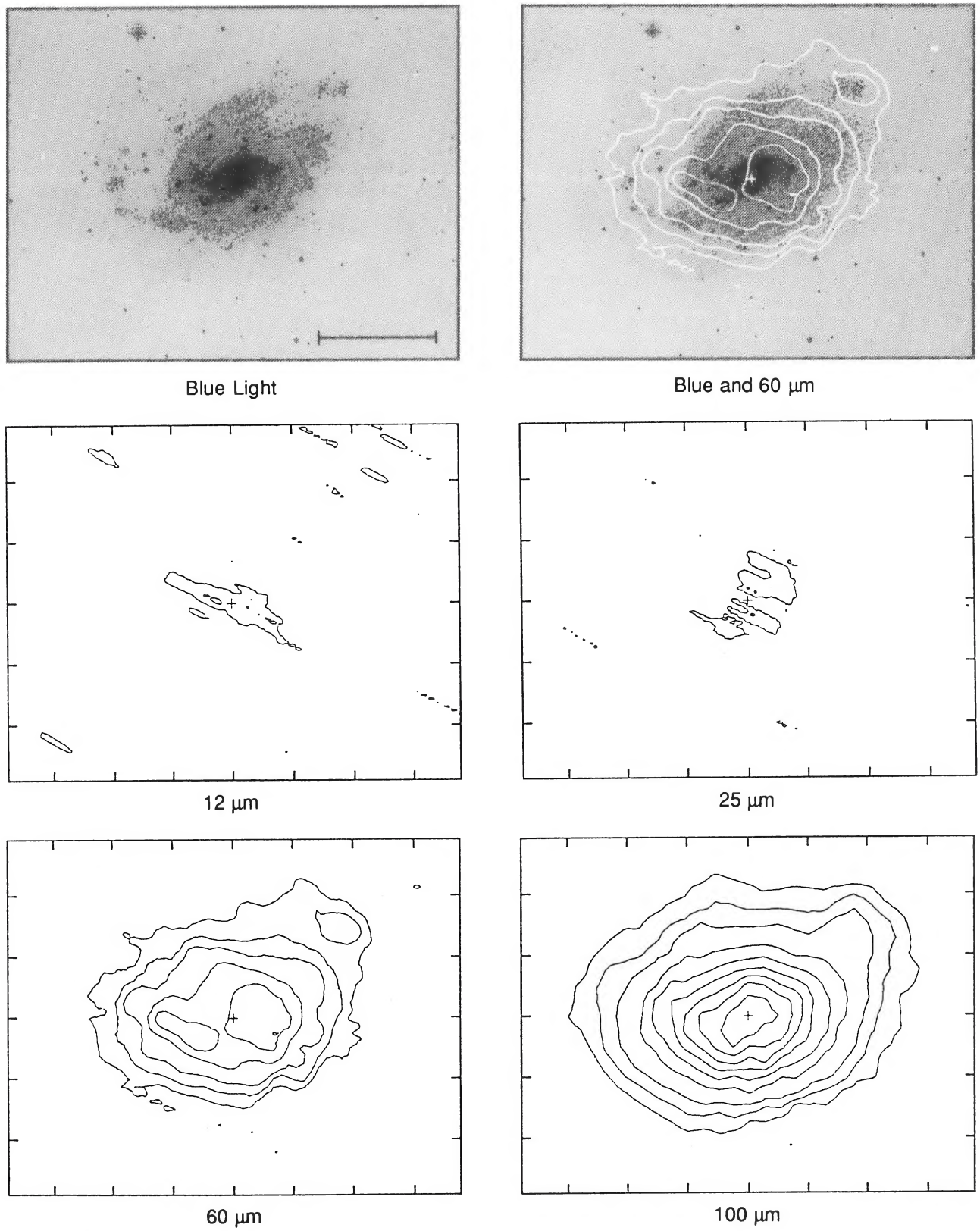

FIG. 7.—NGC 300. The map contour levels are at (*dashed*) 3, 6, and 9 σ below the map mean background level and at (*solid*) 3, 6, and 10 σ with brighter levels at increments of 10 σ. (Optical photographs reproduced by permission of the European Southern Observatory.)

RICE *et al.* (*see* **68**, 102)

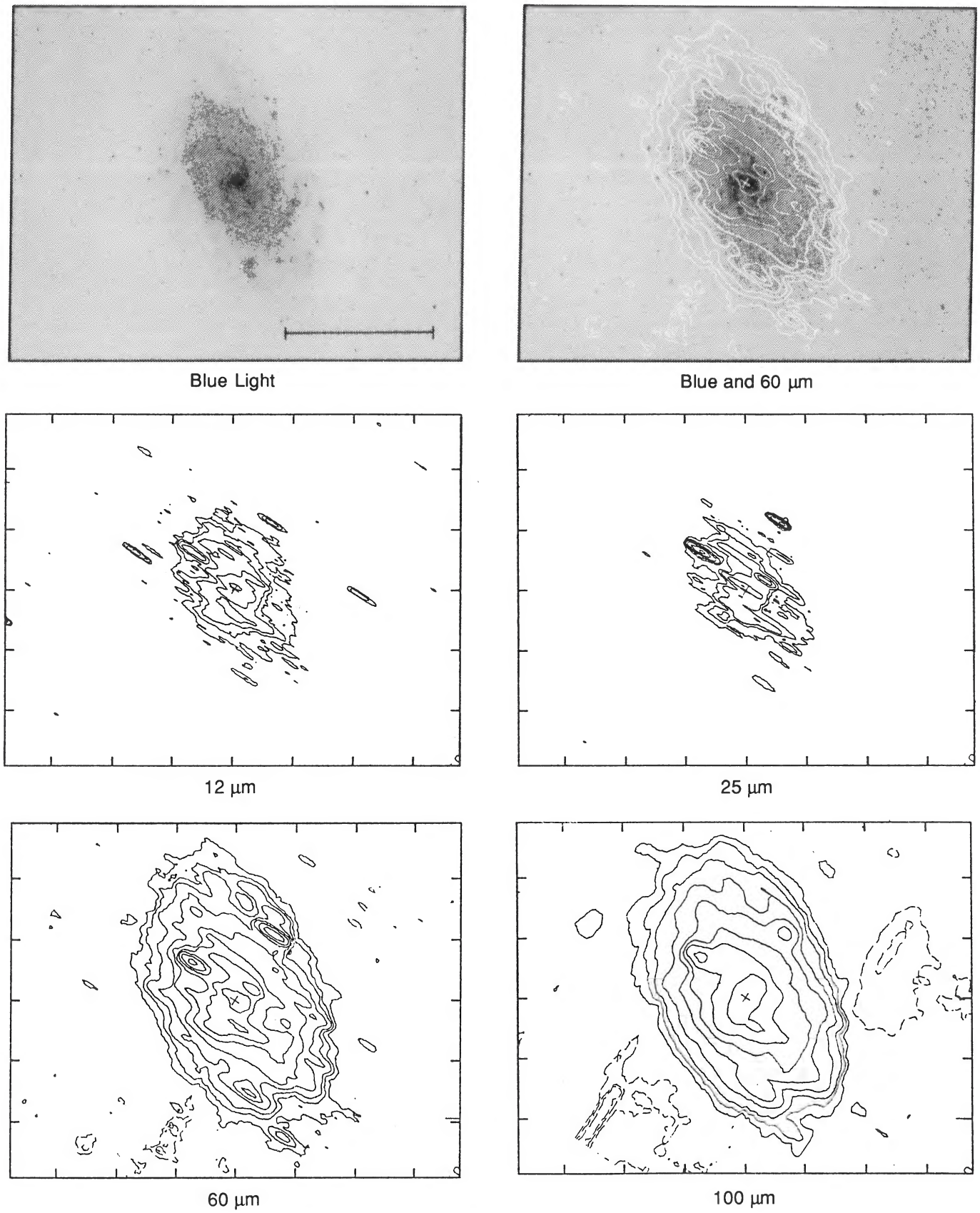

FIG. 8.—NGC 598. The scale marked on the photographs is 30′. The tick marks on the infrared maps are spaced by 12′.4. (Optical photographs reproduced by permission of the California Institute of Technology. © 1960 National Geographic Society–Palomar Sky Survey.)

RICE *et al.* (*see* **68**, 102)

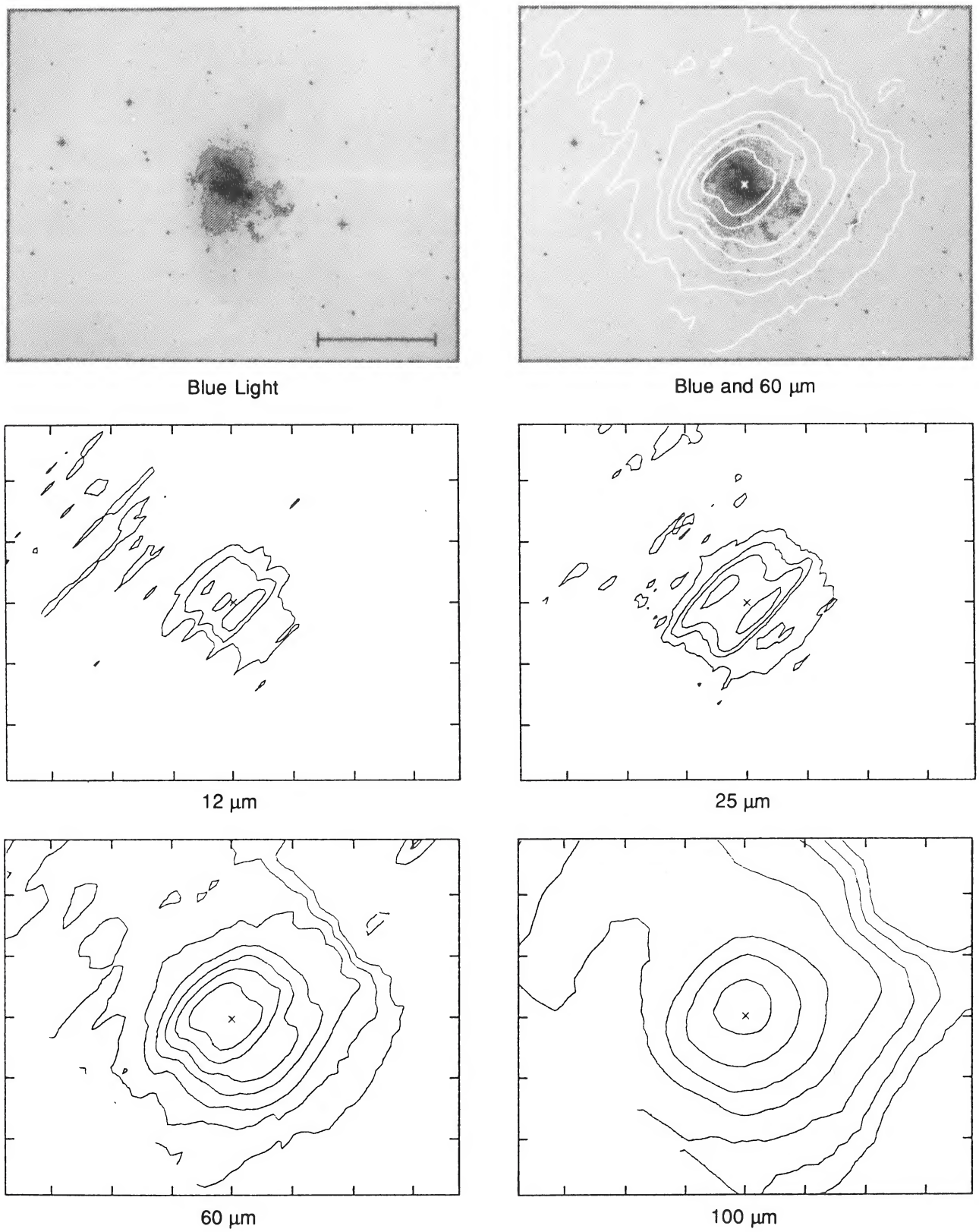

FIG. 9.—NGC 1313. (Optical photographs reproduced by permission of the European Southern Observatory.)

RICE *et al.* (*see* **68**, 102)

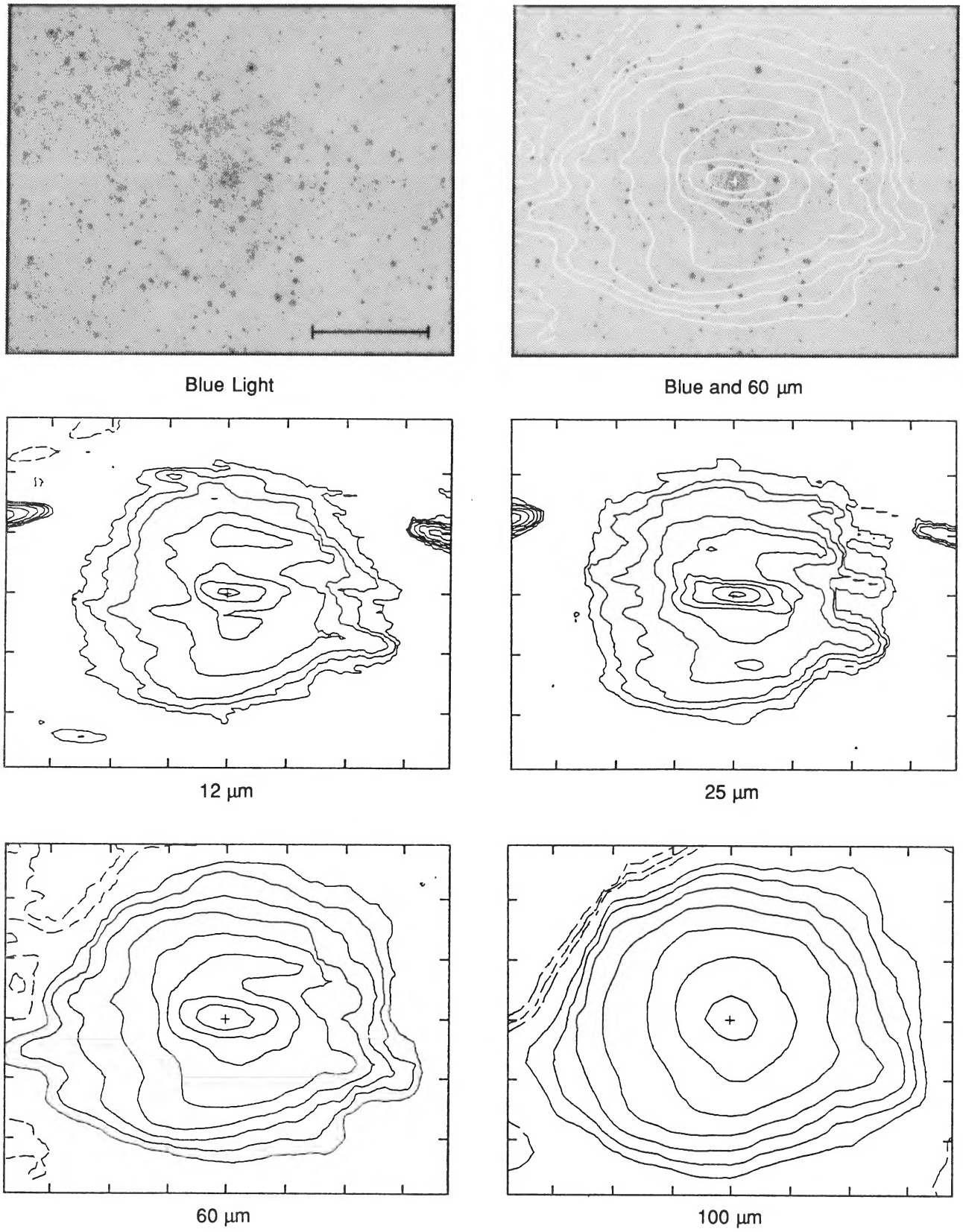

FIG. 10.—IC 342. The solid contour levels of the 60 and 100 μm maps are at (*dashed*) 3, 6, and 9 σ below the map mean background level and at (*solid*) 10 σ and with brighter contours scaled logarithmically by 2 from 10 σ. (Optical photographs reproduced by permission of the California Institute of Technology. © 1960 National Geographic Society–Palomar Sky Survey.)

RICE *et al.* (*see* **68**, 102)

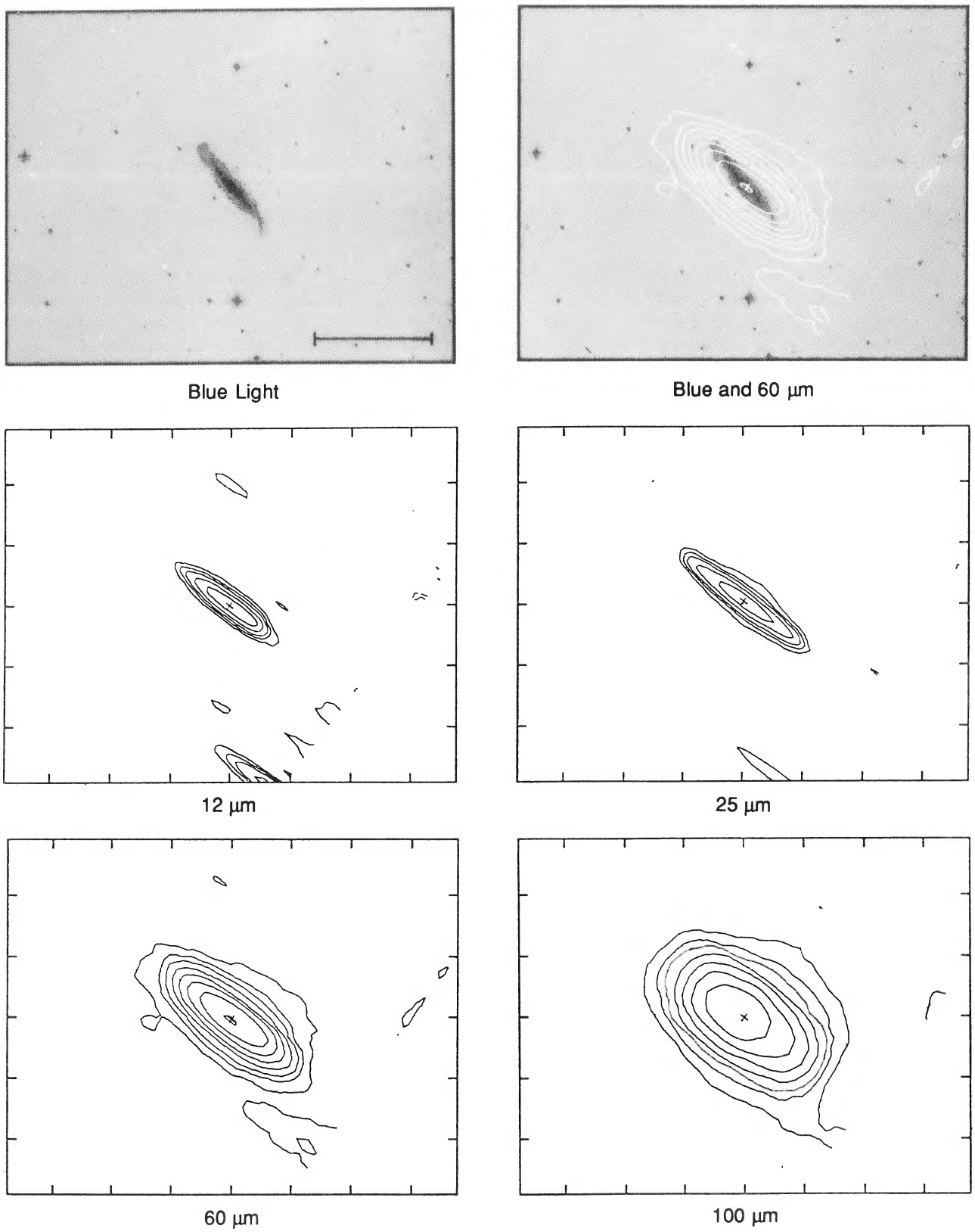

FIG. 11.—NGC 1448. (Optical photographs reproduced by permission of the European Southern Observatory.)

RICE *et al.* (*see* **68**, 102)

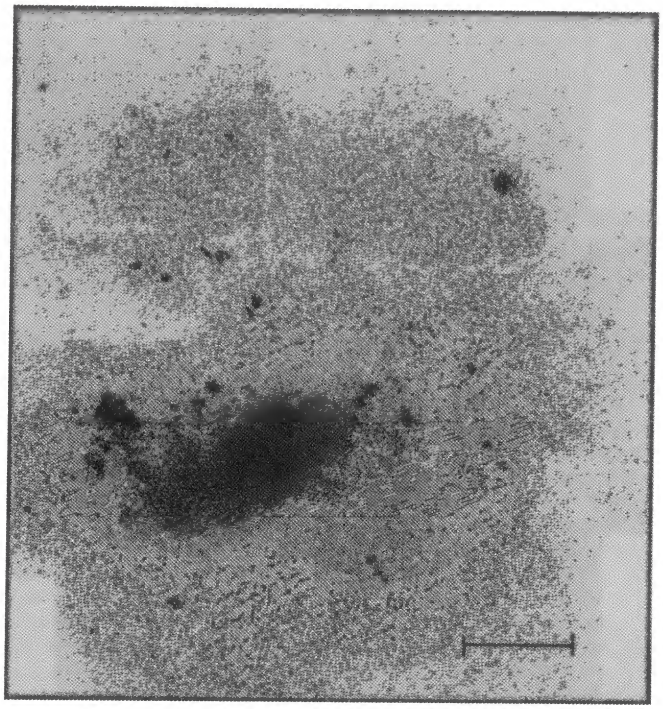

Red Light

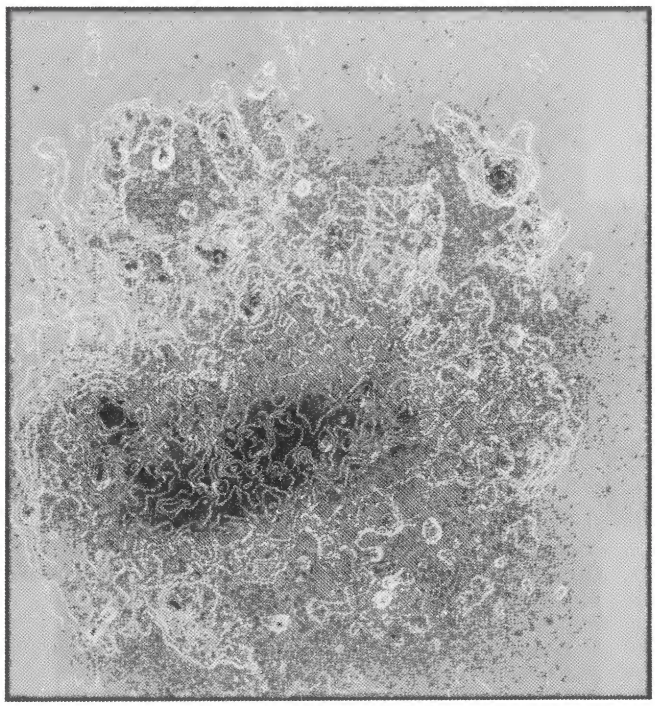

Red and 60 μm

FIG. 12.—LMC. The scale marked on the photograph is 1°. The tick marks on the infrared map are spaced by 61′. The 12, 25, and 60 μm maps have been smoothed to the resolution of the 100 μm map. The contour levels of the 60 and 100 μm maps are at (*dashed*) 9 σ below the map mean background level and at (*solid*) 10 σ and with brighter contours scaled logarithmically by 2 from 10 σ. (Optical photographs reproduced by permission of the Mount Wilson and Las Campanas Observatories, Carnegie Institution of Washington.)

RICE *et al.* (*see* **68**, 102)

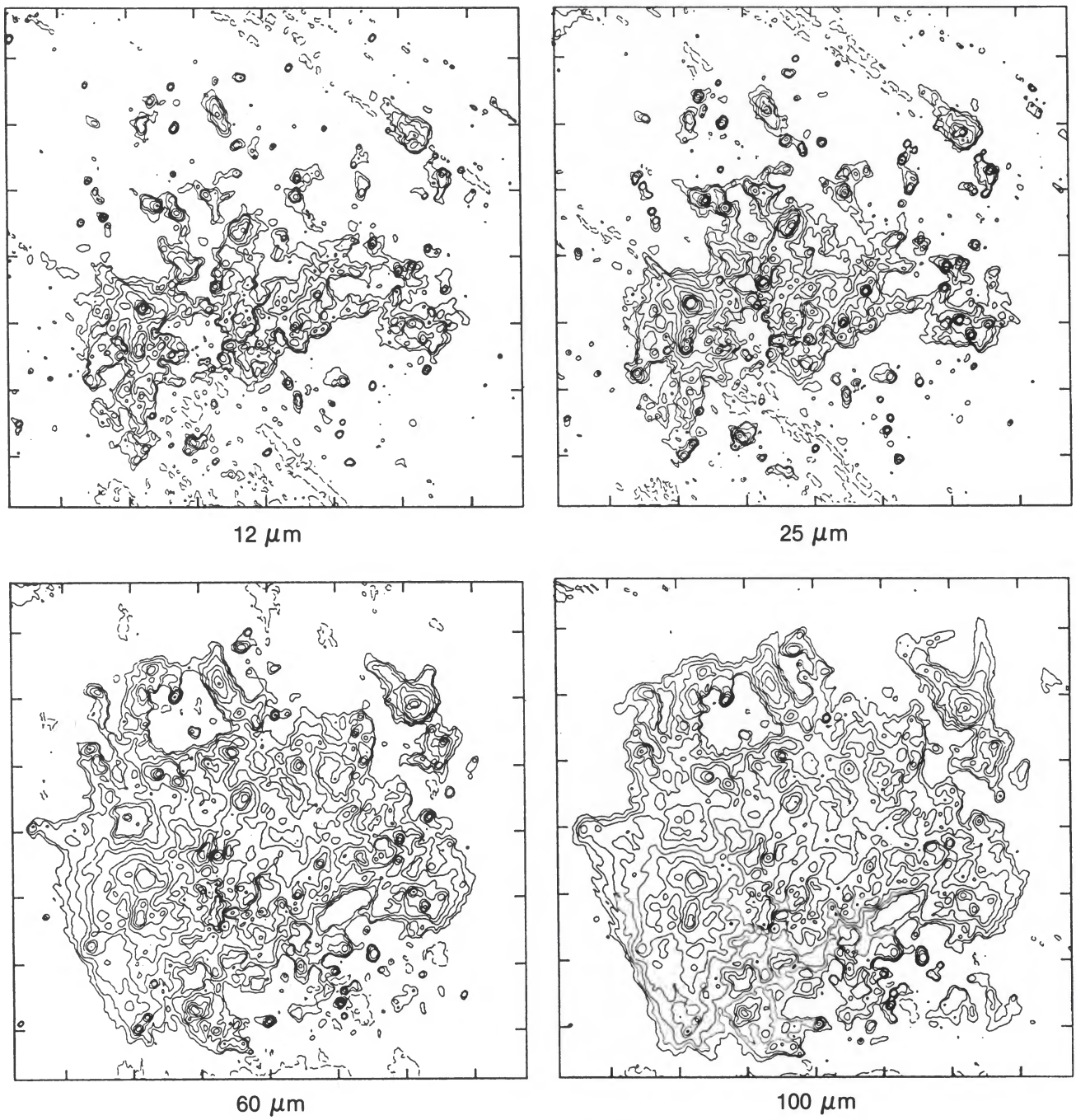

FIG. 12—*Continued*

RICE *et al.* (*see* **68**, 102)

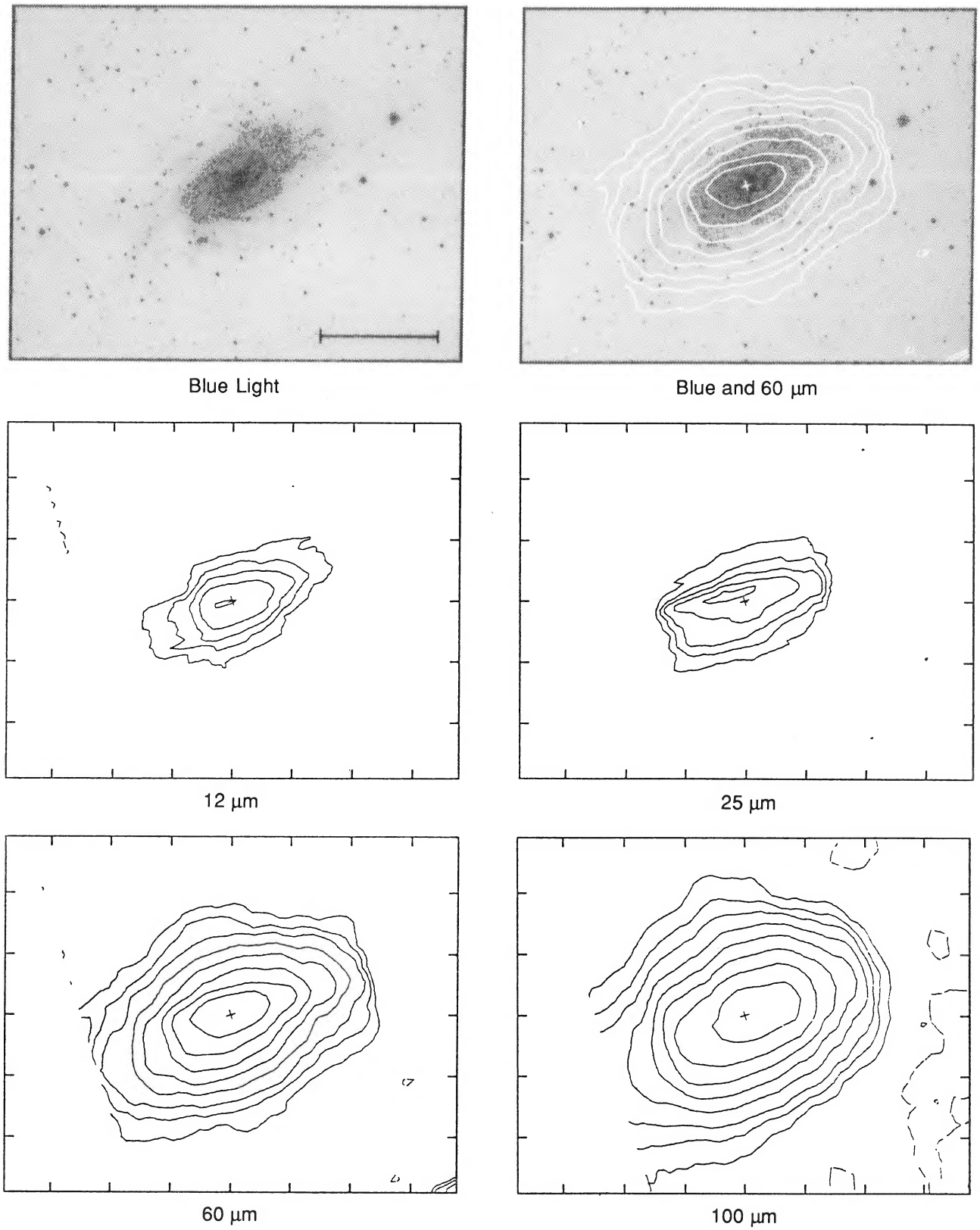

FIG. 13.—NGC 2403. (Optical photographs reproduced by permission of the California Institute of Technology. © 1960 National Geographic Society–Palomar Sky Survey.)

RICE *et al.* (*see* **68**, 102)

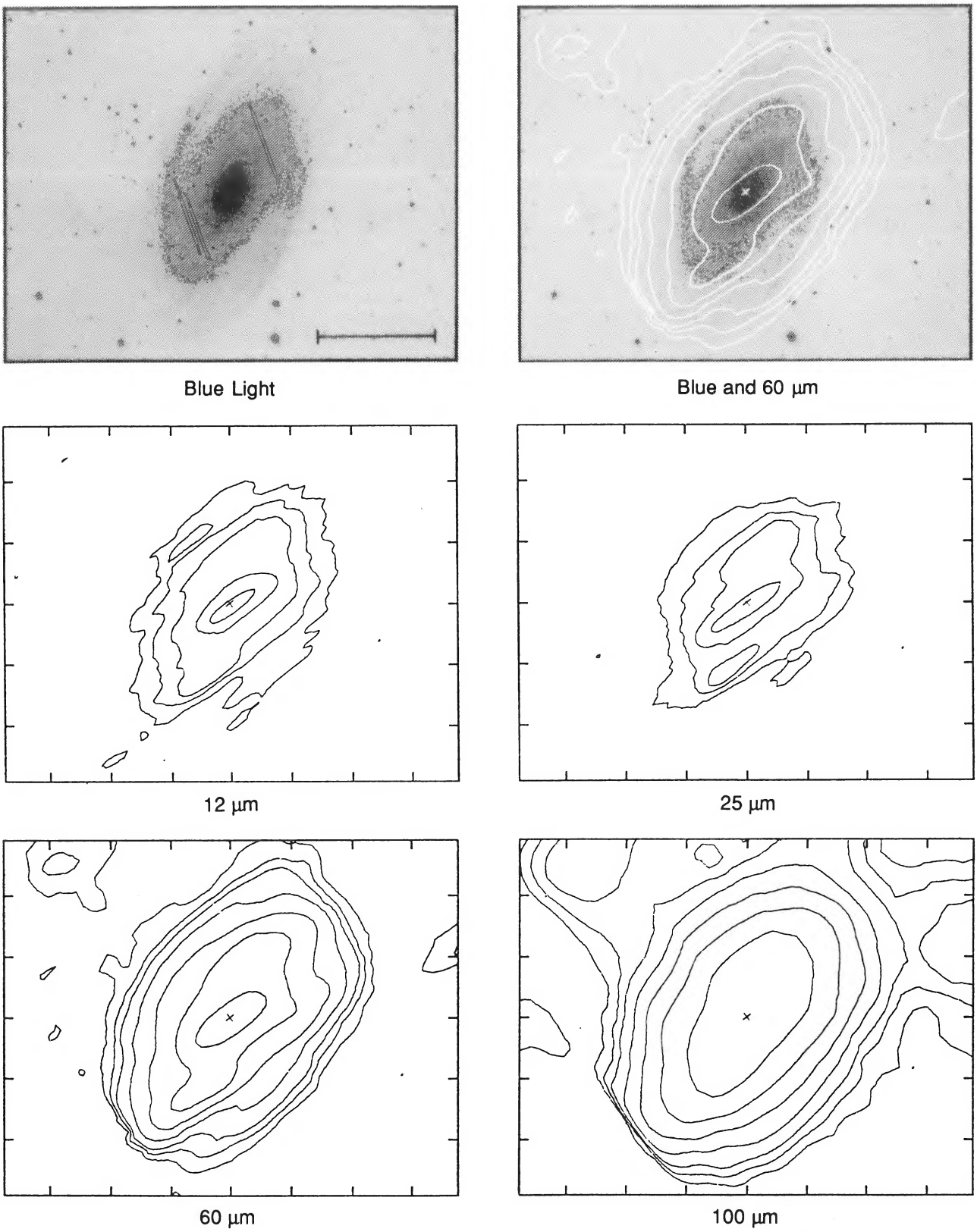

FIG. 14.—NGC 3031. (Optical photographs reproduced by permission of the California Institute of Technology. © 1960 National Geographic Society–Palomar Sky Survey.)

RICE *et al.* (*see* **68**, 102)

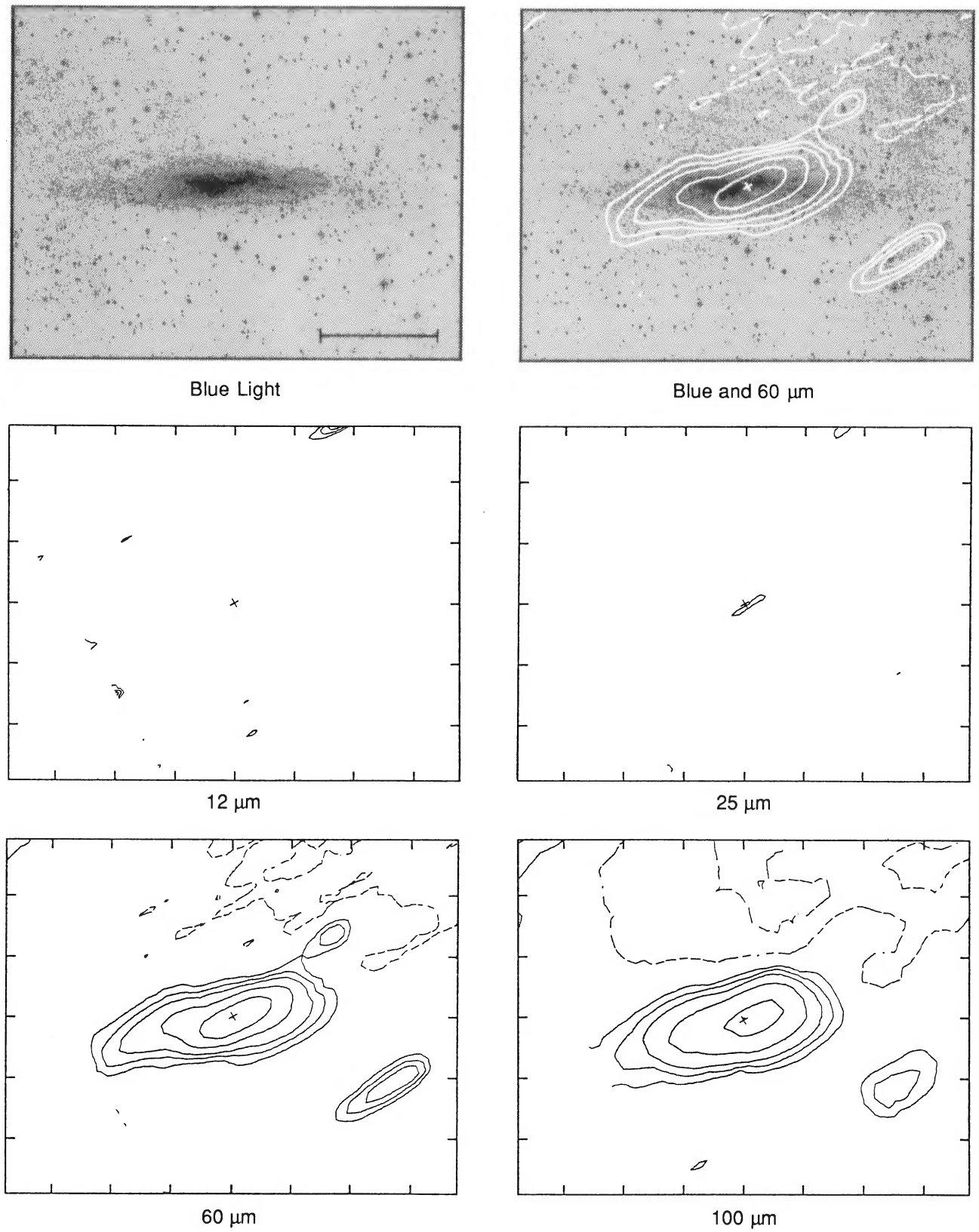

FIG. 15.—NGC 3109. (Optical photographs reproduced by permission of the European Southern Observatory.)

RICE *et al.* (*see* **68**, 102)

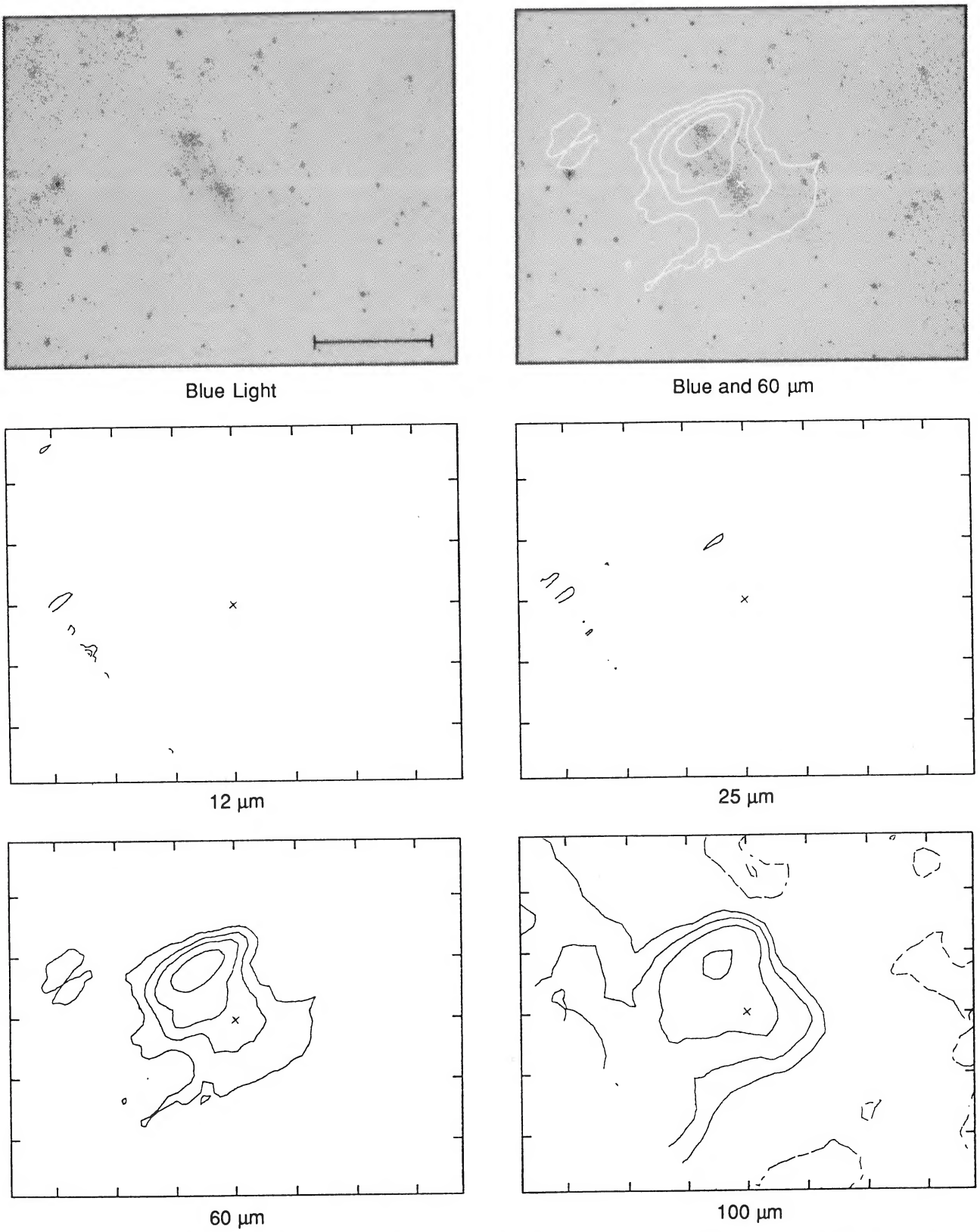

FIG. 16.—IC 2574. (Optical photographs reproduced by permission of the California Institute of Technology. © 1960 National Geographic Society–Palomar Sky Survey.)

RICE *et al.* (*see* **68**, 102)

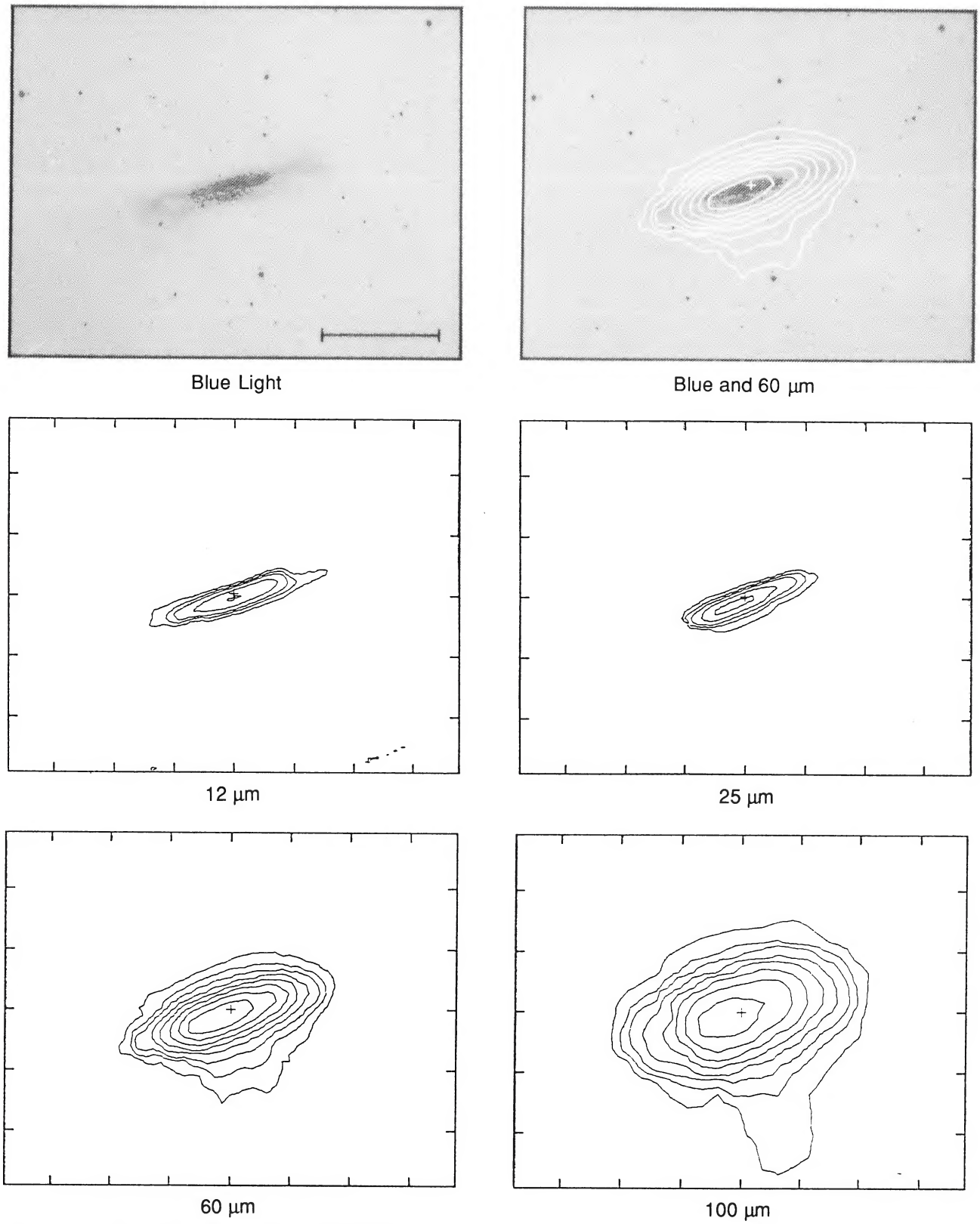

FIG. 17.—NGC 3628. (Optical photographs reproduced by permission of the California Institute of Technology. © 1960 National Geographic Society–Palomar Sky Survey.)

RICE *et al.* (*see* **68**, 102)

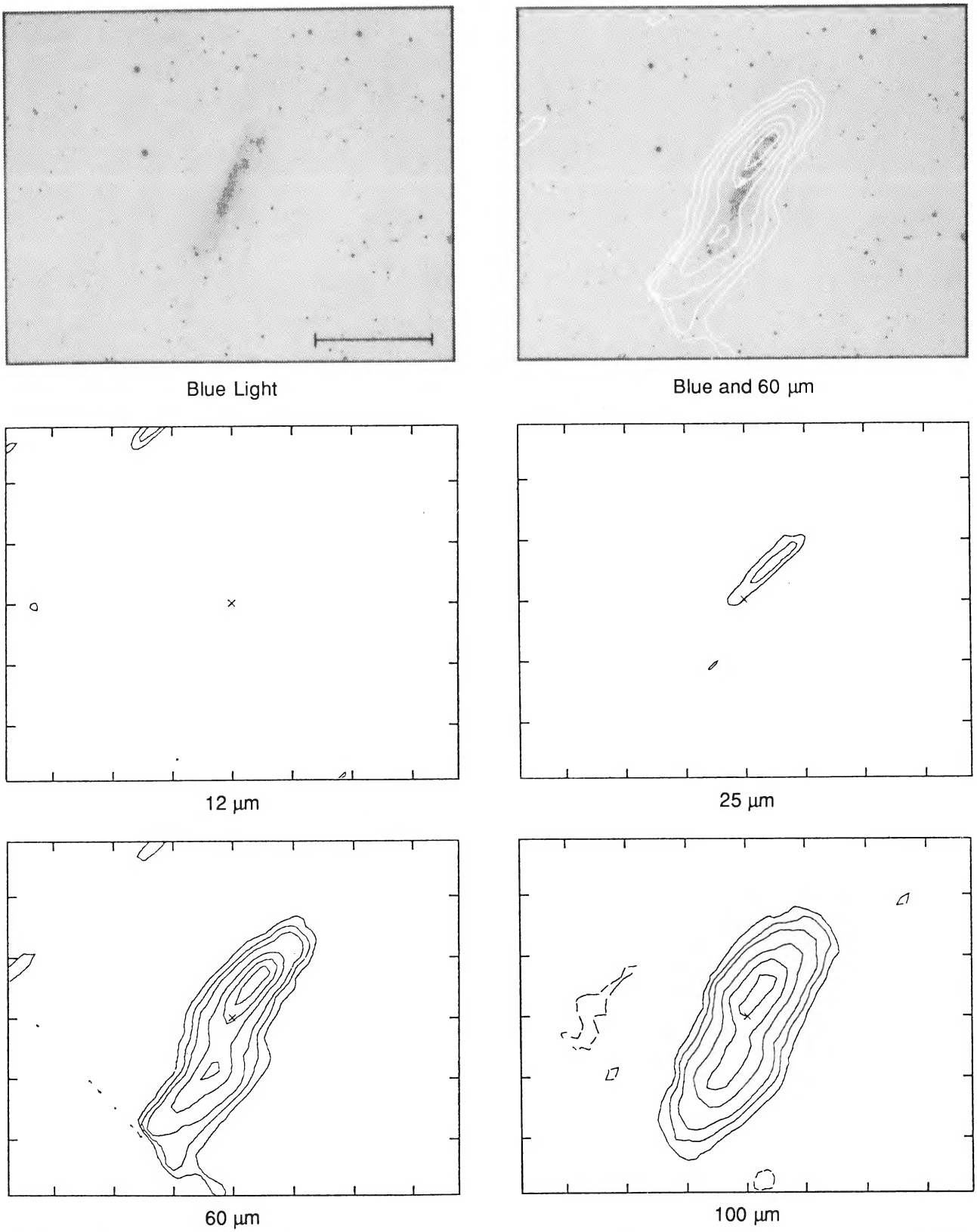

FIG. 18.—NGC 4236. The map contour levels are at (*dashed*) 3, 6, and 9 σ below the map mean background level and at (*solid*) 3, 6, and 10 σ with brighter levels at increments of 10 σ. (Optical photographs reproduced by permission of the California Institute of Technology. © 1960 National Geographic Society–Palomar Sky Survey.)

RICE *et al.* (*see* **68**, 102)

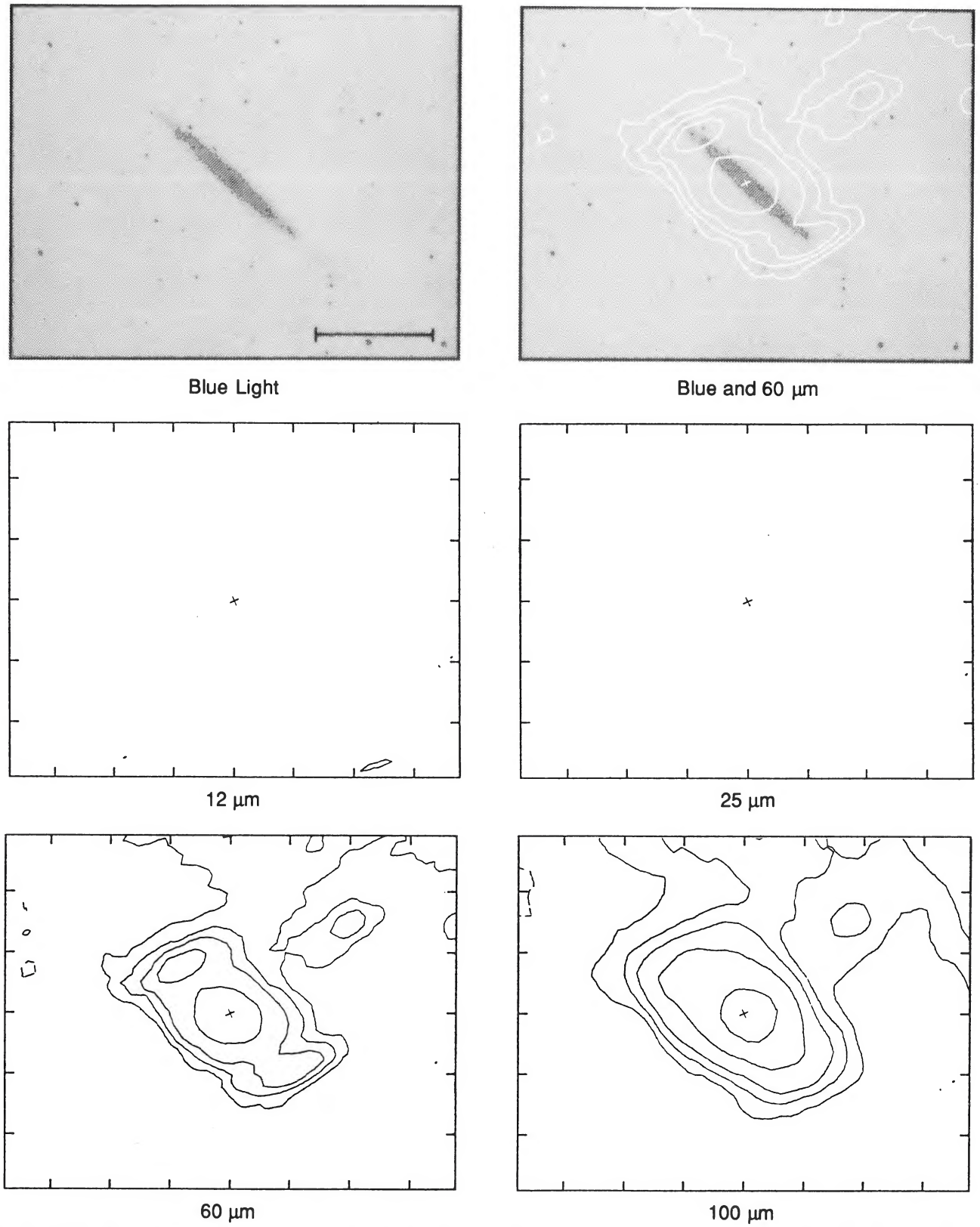

FIG. 19.—NGC 4244. (Optical photographs reproduced by permission of the California Institute of Technology. © 1960 National Geographic Society–Palomar Sky Survey.)

RICE *et al.* (*see* **68**, 102)

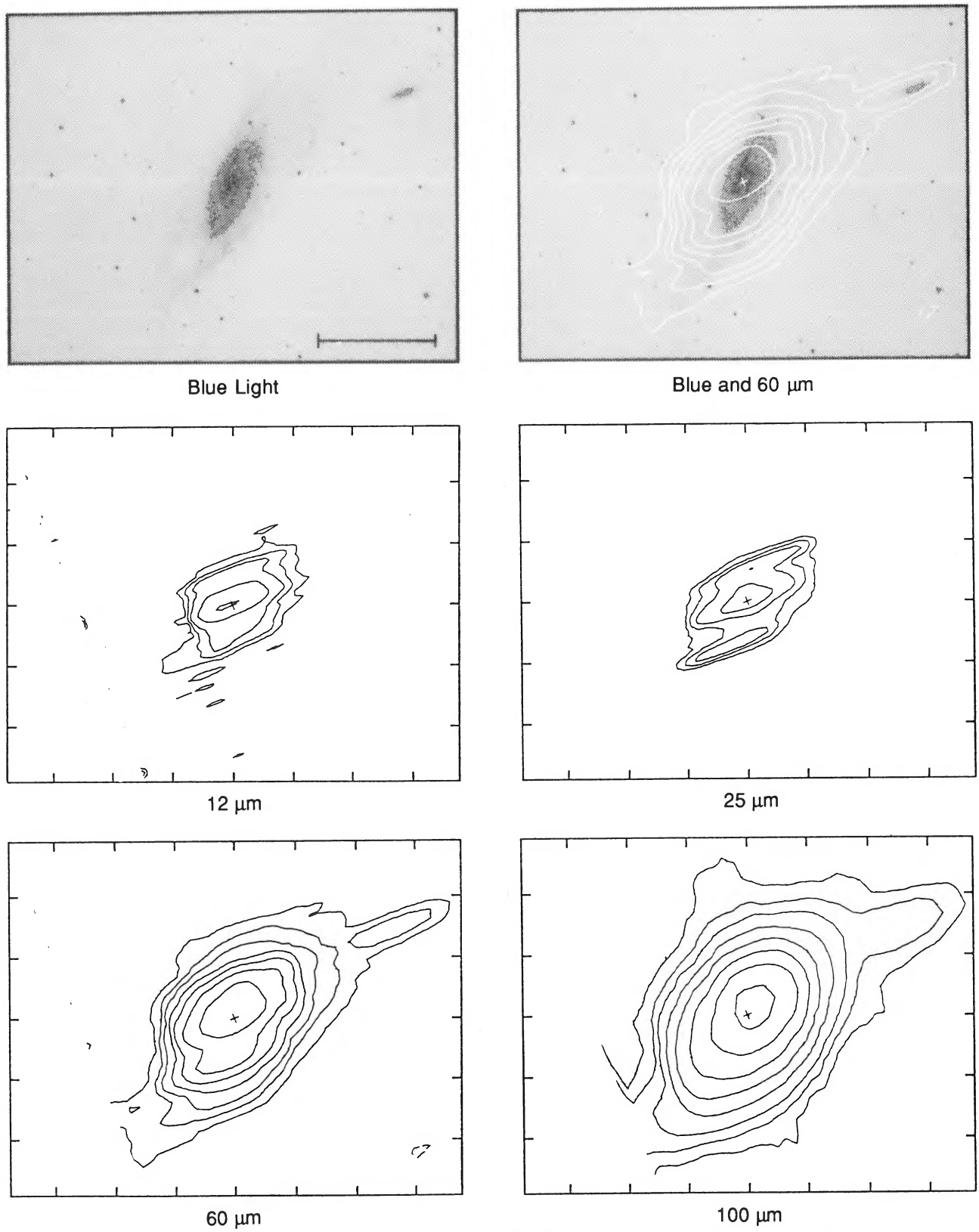

FIG. 20.—NGC 4258. (Optical photographs reproduced by permission of the California Institute of Technology. © 1960 National Geographic Society–Palomar Sky Survey.)

RICE *et al.* (*see* **68**, 102)

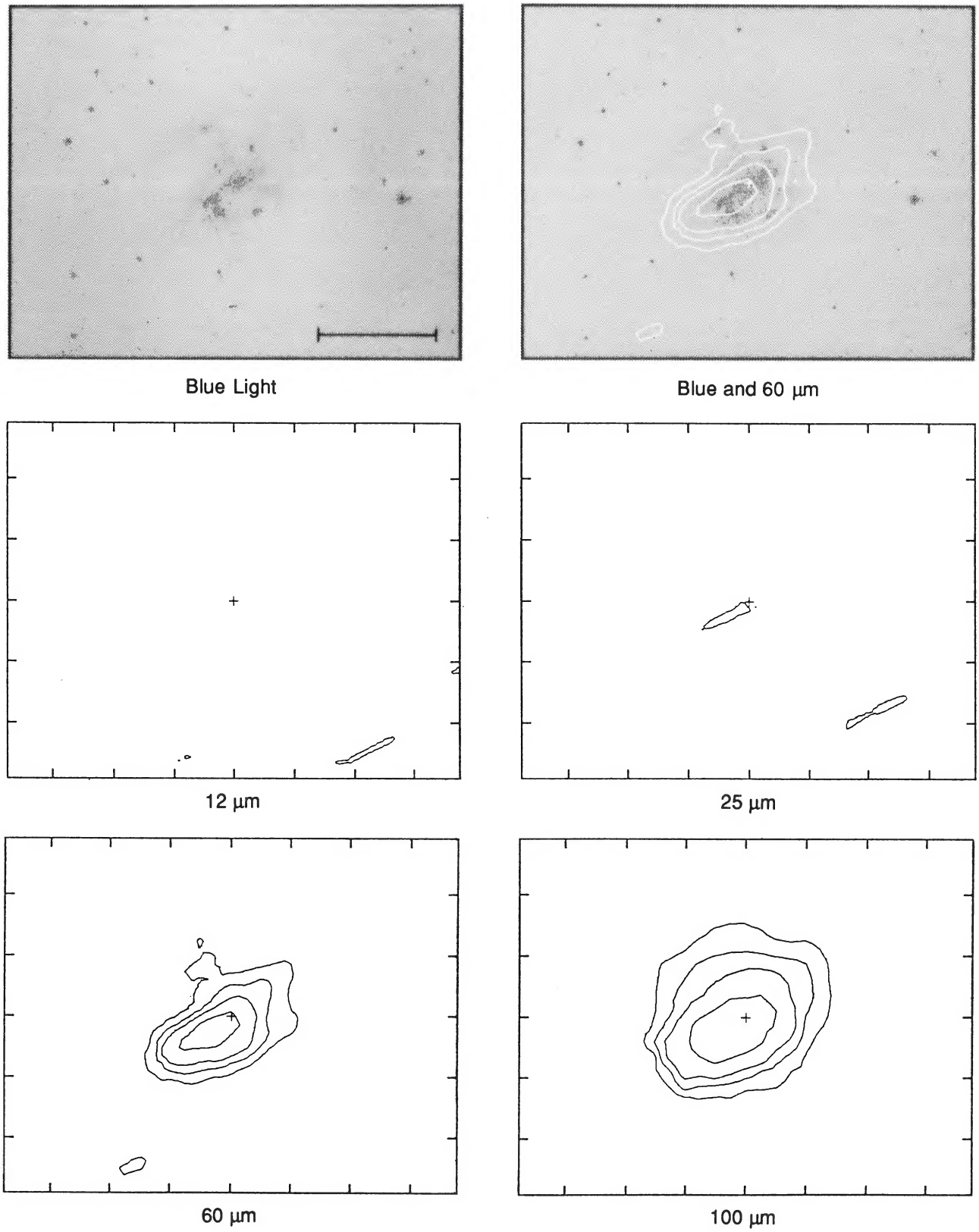

FIG. 21.—NGC 4395. (Optical photographs reproduced by permission of the California Institute of Technology. © 1960 National Geographic Society–Palomar Sky Survey.)

RICE *et al.* (*see* **68**, 102)

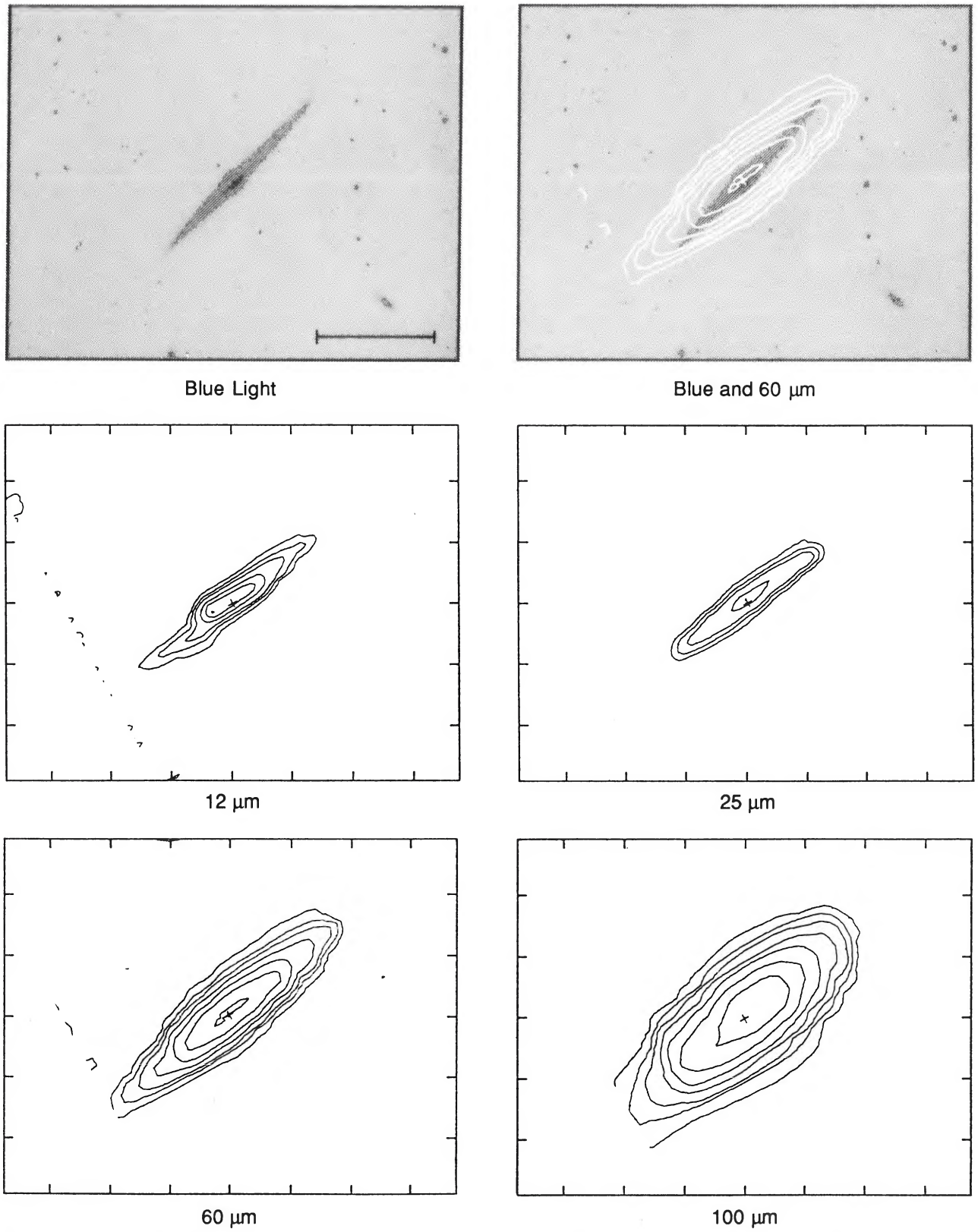

FIG. 22.—NGC 4565. For the 12 and 25 μm maps, the contour levels are at (*dashed*) 3, 6, and 9 σ below the map mean background level and at (*solid*) 3, 6, and 10 σ with brighter levels at increments of 10 σ. (Optical photographs reproduced by permission of the California Institute of Technology. © 1960 National Geographic Society–Palomar Sky Survey.)

RICE *et al.* (*see* **68**, 102)

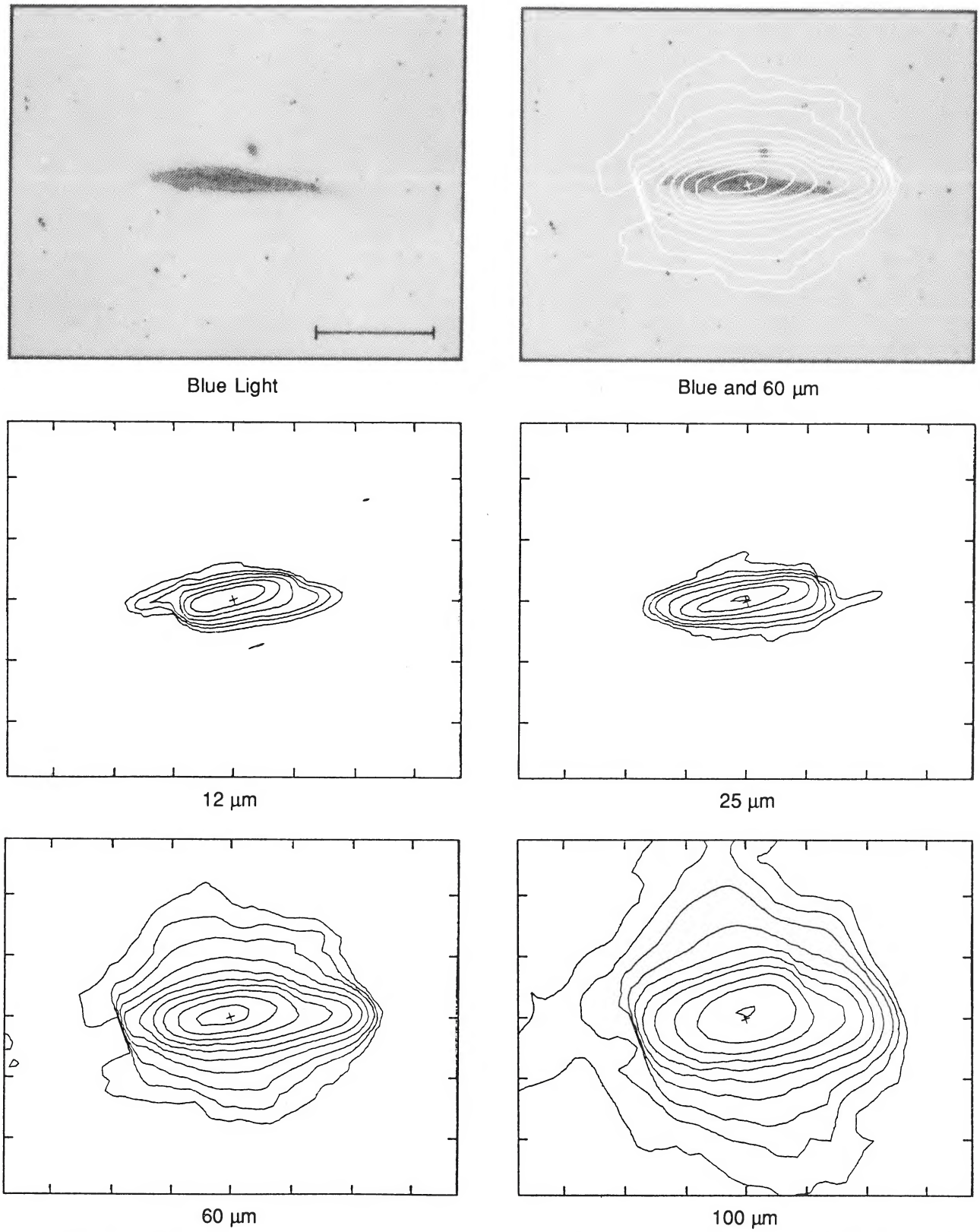

FIG. 23.—NGC 4631. (Optical photographs reproduced by permission of the California Institute of Technology. © 1960 National Geographic Society–Palomar Sky Survey.)

RICE *et al.* (*see* **68**, 102)

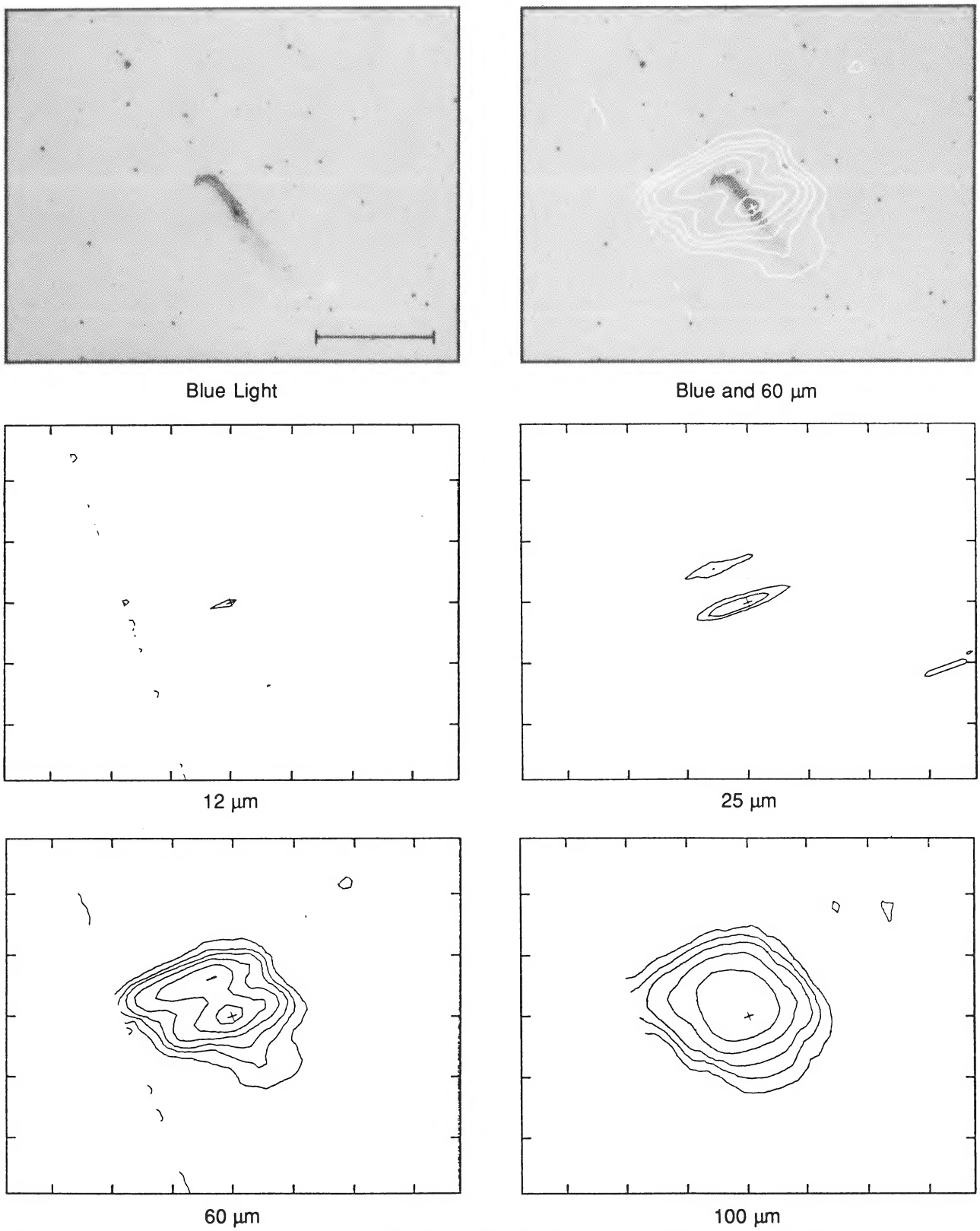

FIG. 24.—NGC 4656. (Optical photographs reproduced by permission of the California Institute of Technology. © 1960 National Geographic Society–Palomar Sky Survey.)

RICE *et al.* (*see* **68**, 102)

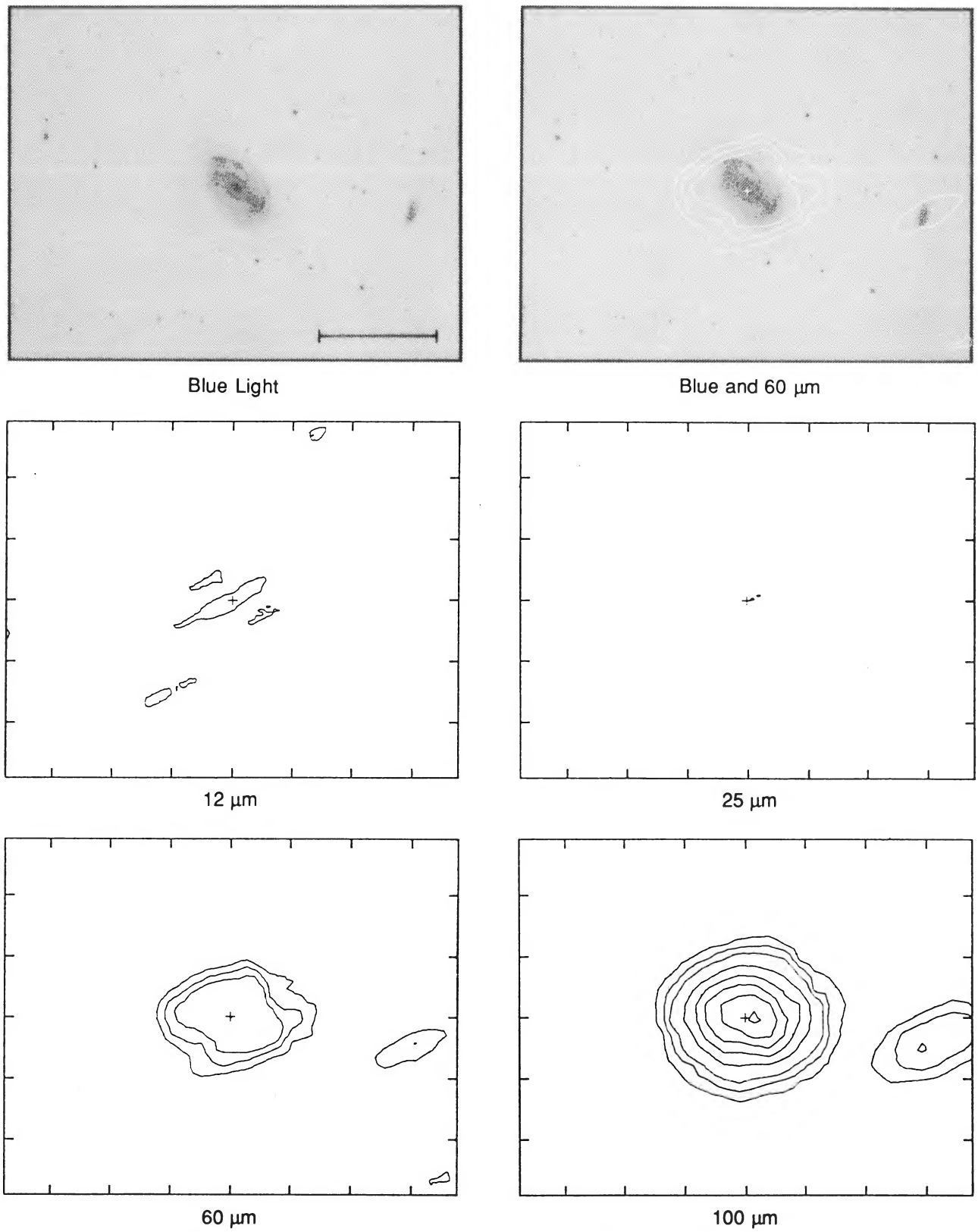

FIG. 25.—NGC 4725. The map contour levels are at (*dashed*) 3, 6, and 9 σ below the map mean background level and at (*solid*) 3, 6, and 10 σ with brighter levels at increments of 10 σ. (Optical photographs reproduced by permission of the California Institute of Technology. © 1960 National Geographic Society–Palomar Sky Survey.)

RICE *et al.* (*see* **68**, 102)

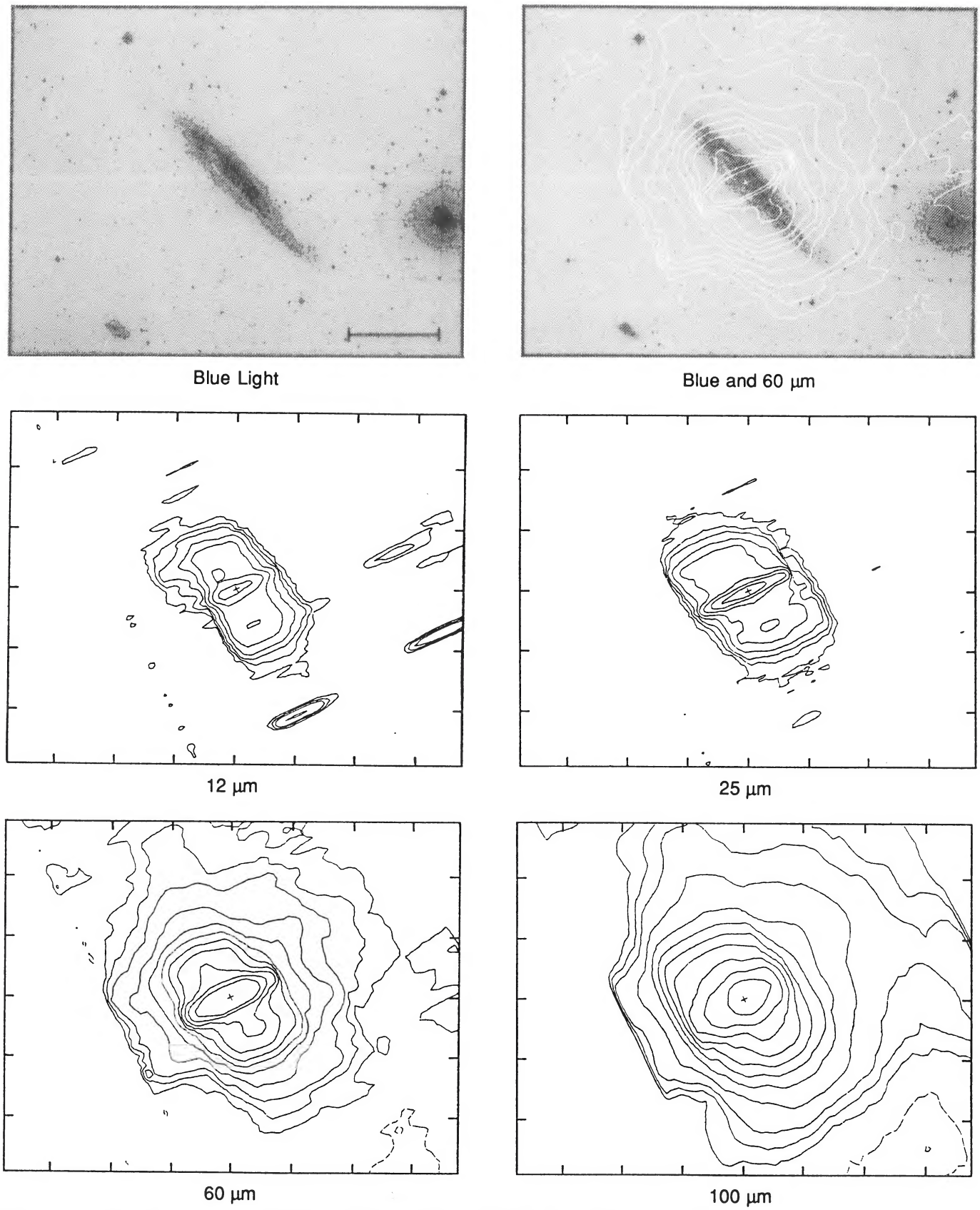

FIG. 26.—NGC 4945. The tick marks on the infrared maps are spaced by 5′.4. (Optical photographs reproduced by permission of the European Southern Observatory.)

RICE *et al.* (*see* **68**, 102)

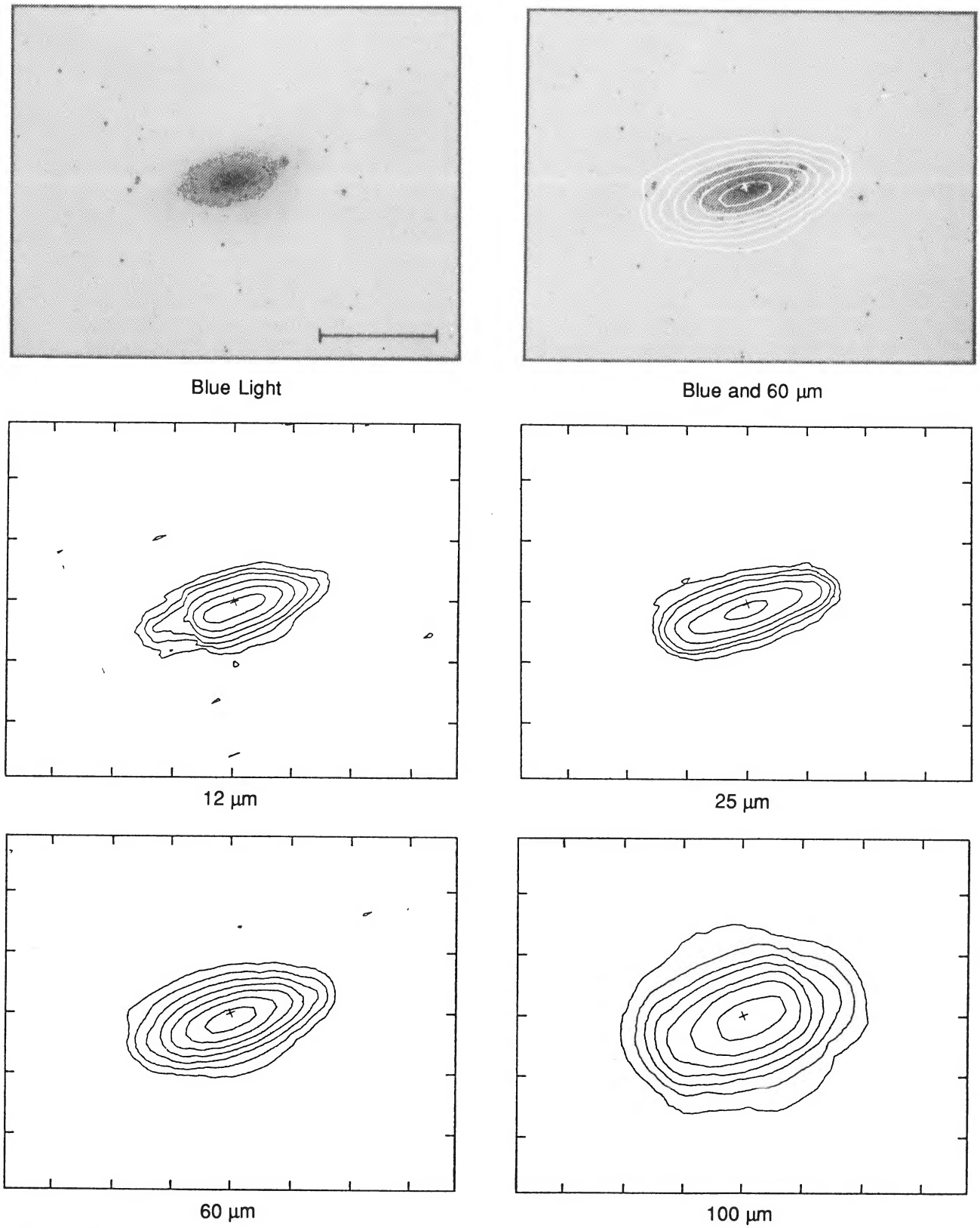

FIG. 27.—NGC 5055. The map contour levels are at (*dashed*) 3, 6, and 9 σ below the map mean background level and at (*solid*) 10 σ with brighter levels at increments of 10 σ. (Optical photographs reproduced by permission of the California Institute of Technology. © 1960 National Geographic Society–Palomar Sky Survey.)

RICE *et al.* (*see* **68**, 102)

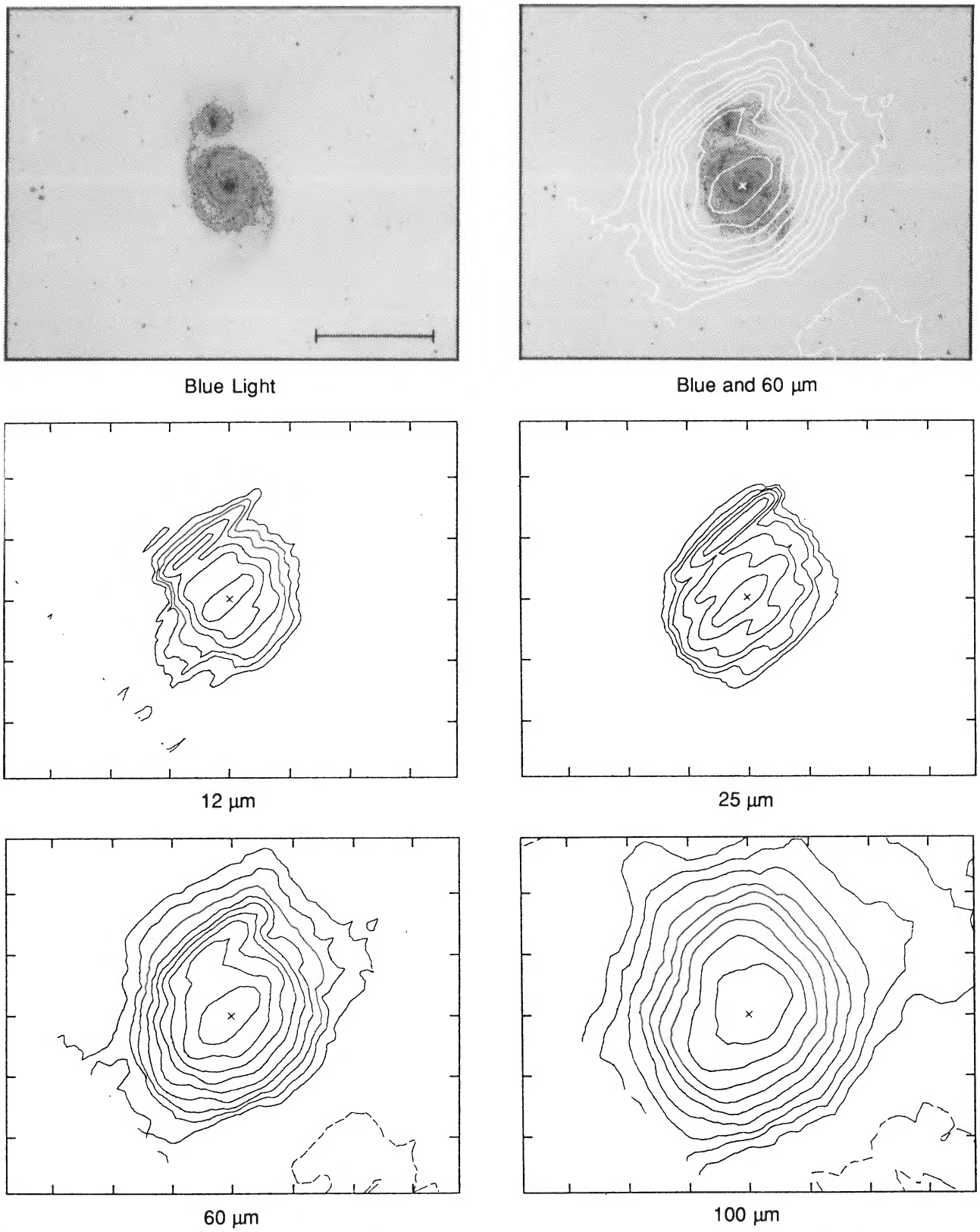

FIG. 28.—NGC 5194. (Optical photographs reproduced by permission of the California Institute of Technology. © 1960 National Geographic Society–Palomar Sky Survey.)

RICE *et al.* (*see* **68**, 102)

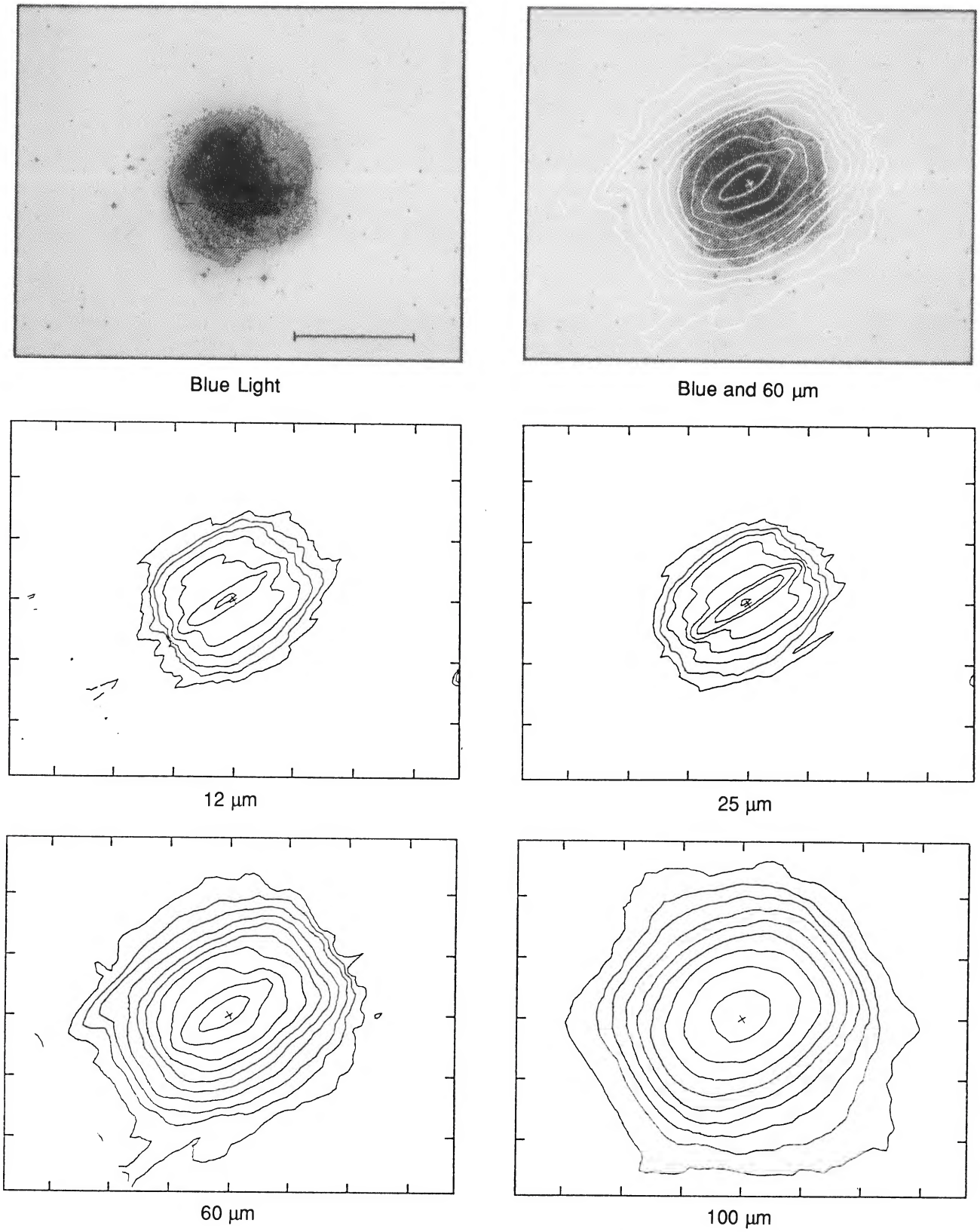

FIG. 29.—NGC 5236. (Optical photographs reproduced by permission of the European Southern Observatory.)

RICE *et al.* (*see* **68**, 102)

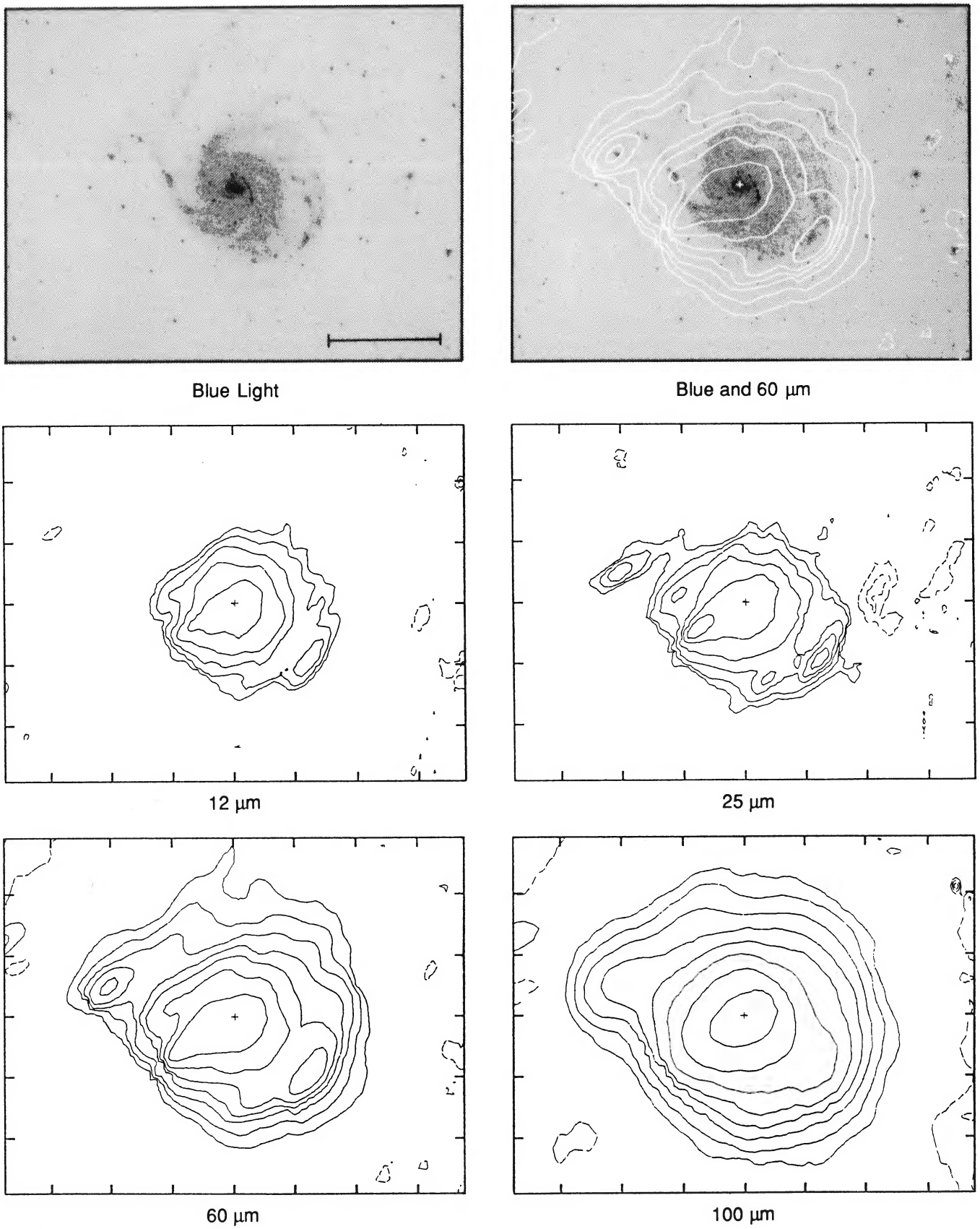

FIG. 30.—NGC 5457. The map contours are at (*dashed*) 3, 6, and 9 σ below the map mean background level and at (*solid*) 6 and 10 σ for the 12 and 25 μm map, and 10 σ for the 60 and 100 μm maps with brighter contours scaled logarithmically by 2 from 10 σ. The tick marks on the infrared maps are spaced by 5′.4. (Optical photographs reproduced by permission of the California Institute of Technology. © 1960 National Geographic Society–Palomar Sky Survey.)

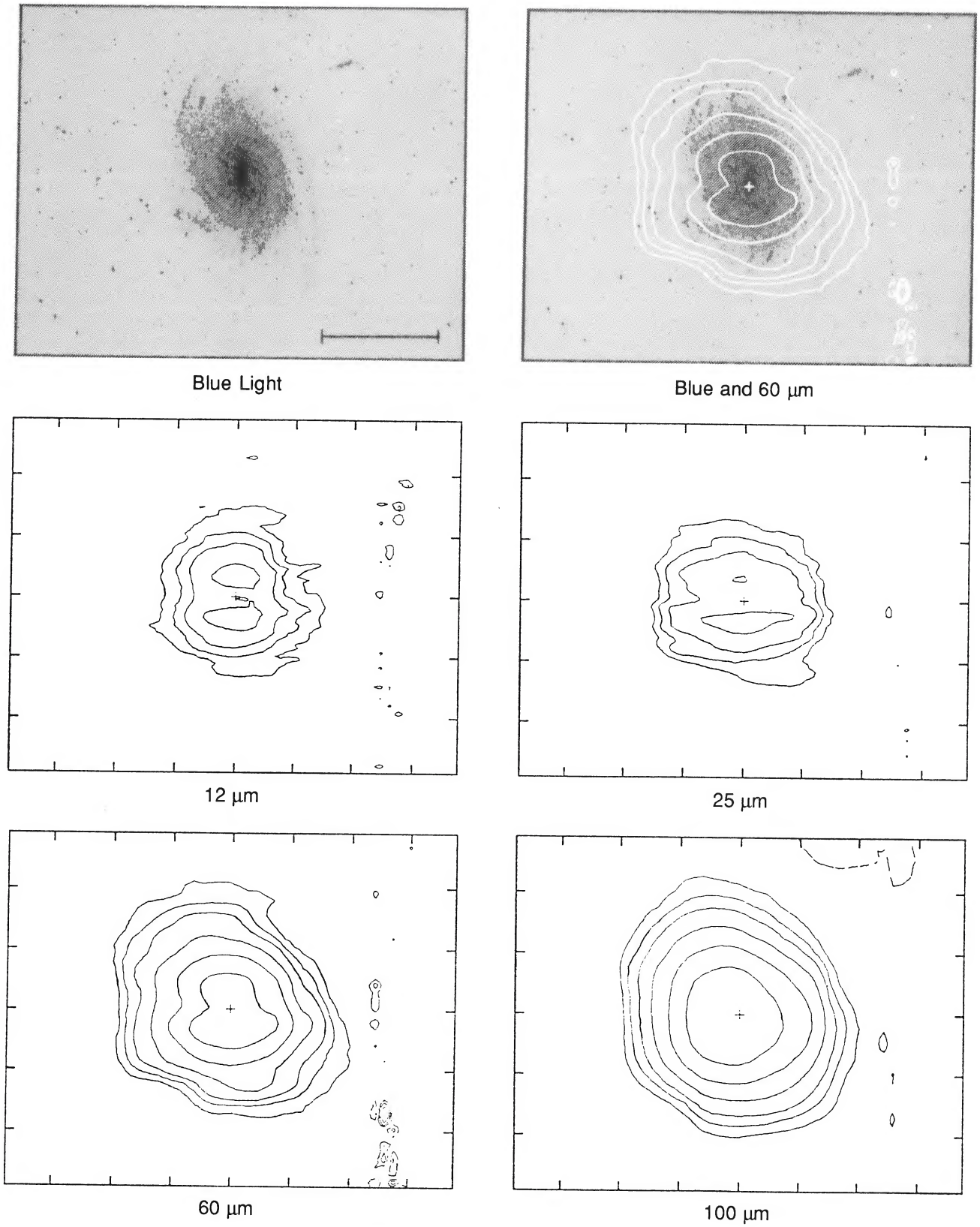

FIG. 31.—NGC 6744. (Optical photographs reproduced by permission of the European Southern Observatory.)

RICE *et al.* (*see* **68**, 102)

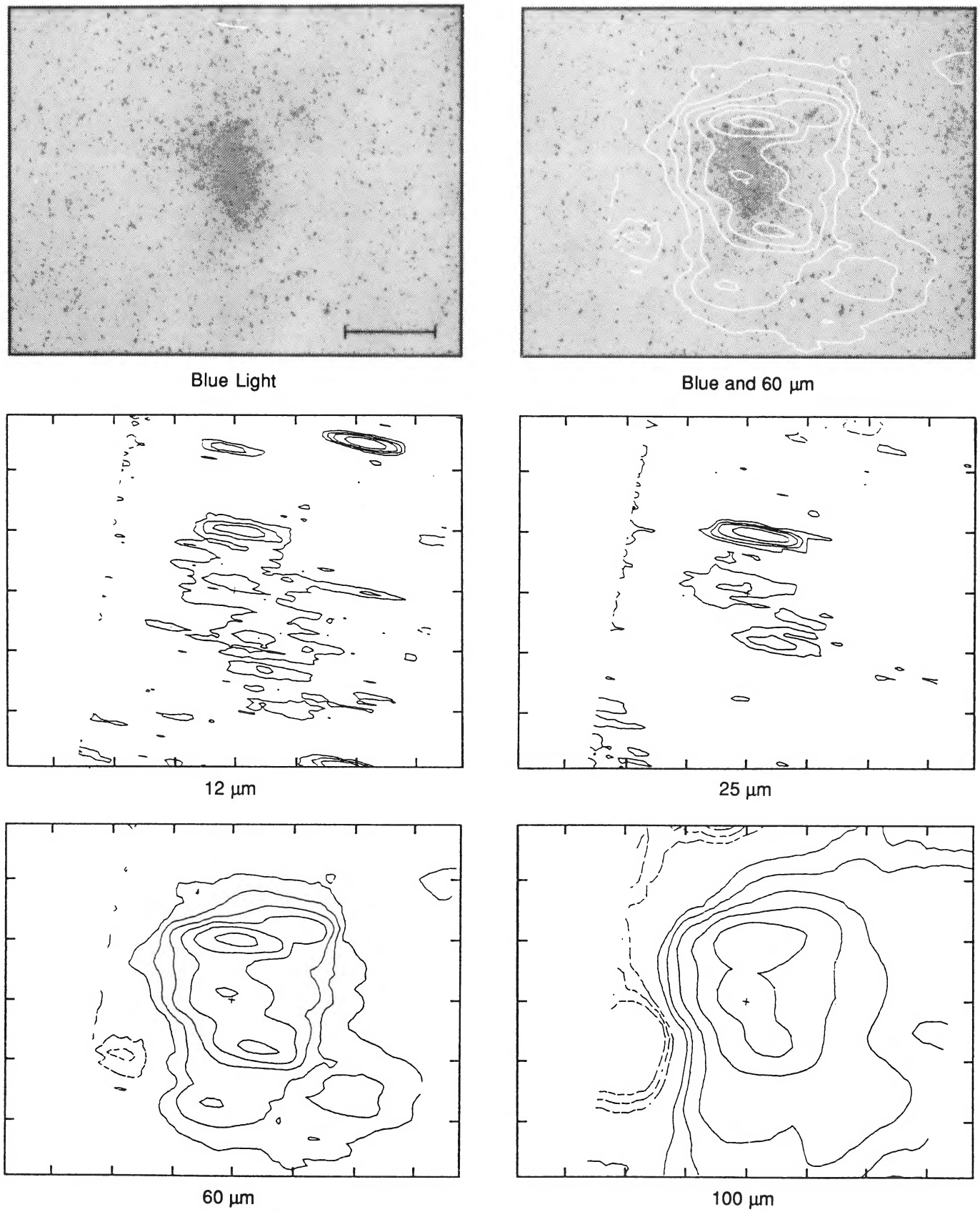

FIG. 32.—NGC 6822. For the 60 and 100 μm maps the contours are at (*dashed*) 3, 6, and 9 σ below the map mean background level and at (*solid*) 10 σ with brighter contours scaled logarithmically by 2 from 10 σ. The tick marks on the infrared maps are spaced by 5′.4. (Optical photographs reproduced by permission of the California Institute of Technology. © 1960 National Geographic Society–Palomar Sky Survey.)

RICE *et al.* (*see* **68**, 102)

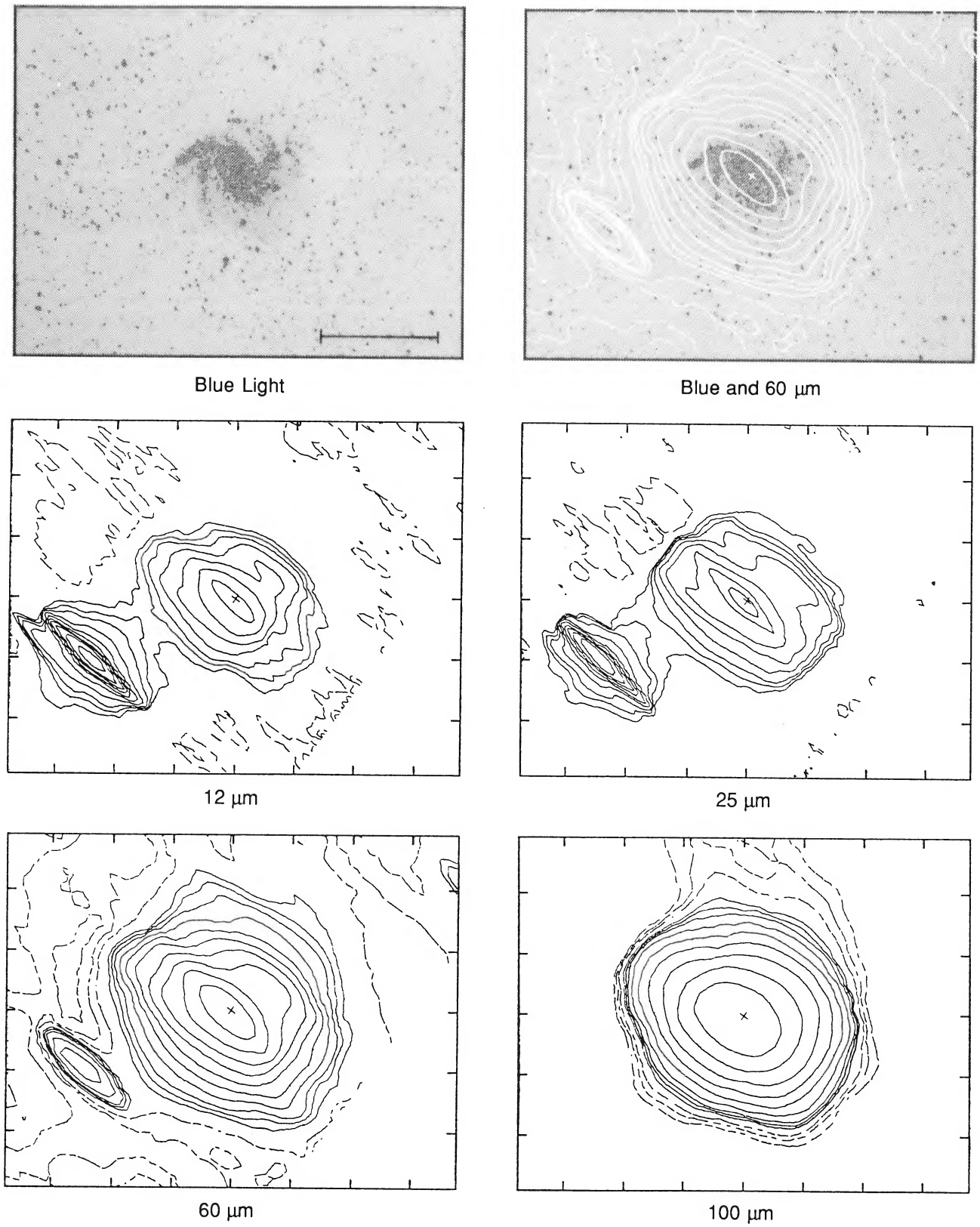

FIG. 33.—NGC 6946. (Optical photographs reproduced by permission of the California Institute of Technology. © 1960 National Geographic Society–Palomar Sky Survey.)

RICE *et al.* (*see* **68**, 102)

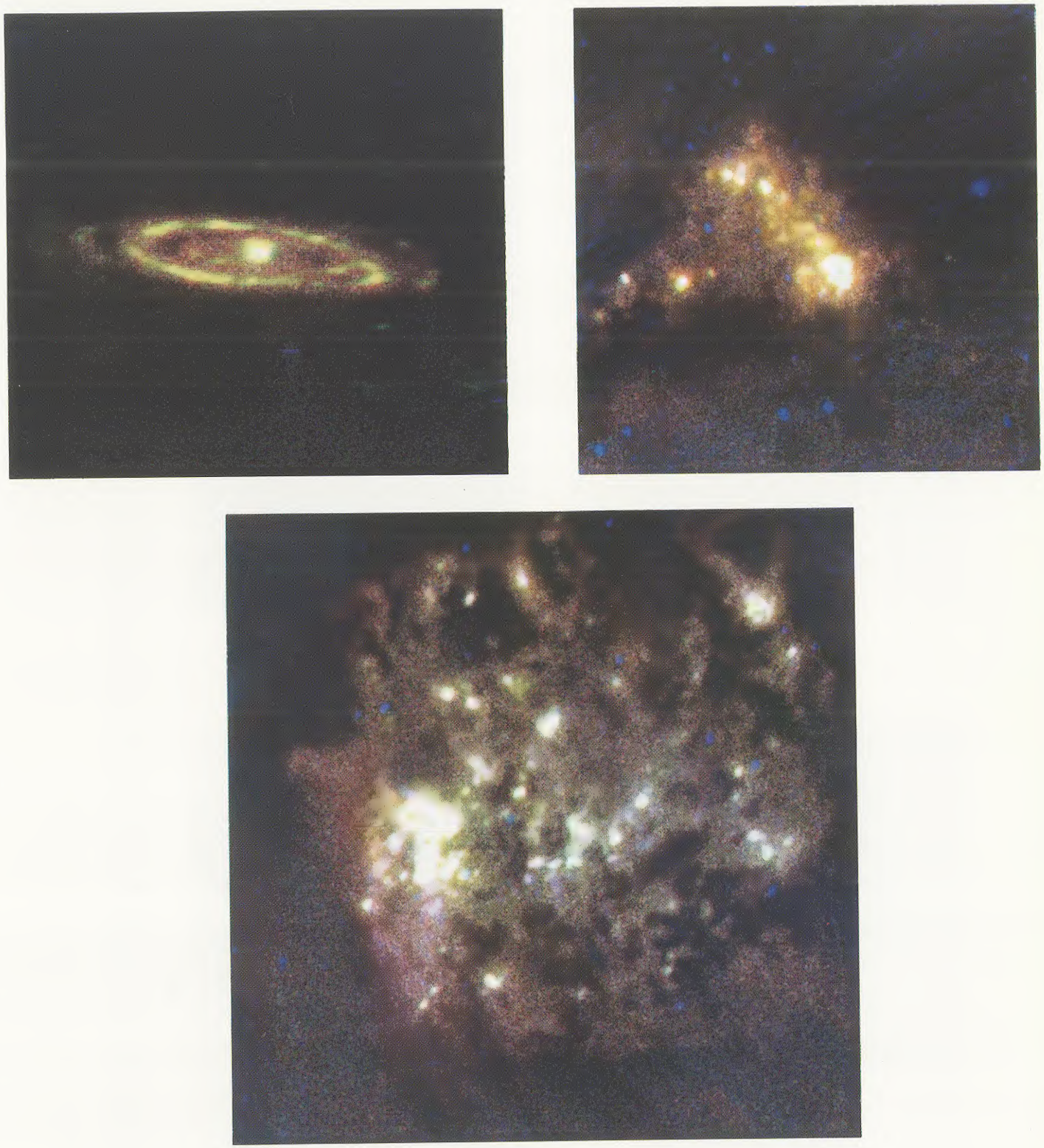

FIG. 34.—Color-coded infrared images of (*a*) M31, (*b*) the SMC, and (*c*) the LMC, produced by combining the 12 (*coded blue*), 60 (*coded green*), and 100 μm (*coded red*) *IRAS* surface brightness images of the galaxies. All maps have been smoothed to the resolution of the 100 μm map.

FIG. 34*a*

FIG. 34*b*

FIG. 34*c*

TABLE 5

FAR-INFRARED[a] AND OPTICAL[b] DIAMETERS

Name (1)	T (2)	D_{IR} (3)	D_{IR}/D_B (4)	$(A_e/D)_{IR}$ (5)	$(A_e/D)_B$ (6)
N55	9B	26.8	0.83	0.10	...
M31	3A	157.1	0.83	0.17	0.28
N247	7X	18.3	0.91	0.18	0.50
N253	5X	26.5:	1.06	0.08:	0.28
N300	7A	18.0	0.89	0.21	...
M33	5A	51.3	0.81	0.17	0.43
I342	6X	20.9	0.92	0.19	0.79
M81	2A	20.3	0.76	0.20	0.28
N3109	9B	12.4	0.84	...	...
N3628	3	14.3	0.96	< 0.14	...
N4244	6A	13.0:	0.80	0.24:	0.28
N4258	4X	14.1	0.77	...	0.31
N4565	3A	16.2	0.99	0.14:	0.22
N4631	7B	16.8:	1.11	0.13:	0.30
N4945	6B	21.1:	0.92	0.10:	...
N5055	4A	14.7	1.20	...	0.29
M51[c]	4A	11.8:	1.07	...	0.36
M83	5X	15.6:	1.36	0.16	...
M101	6X	23.1	0.86	0.18	0.42
N6744	4X	14.0	0.87	0.22	...
N6822	10B	21.1:	1.87	0.26	...
N6946	6X	13.3:	0.90	0.19	0.46
Mean	...	...	0.98	0.17	0.37
RMS	...	...	0.25	0.05	0.15

[a]Diameters measured from the 60 μm map along the optical major axis to a brightness level of 25 mJy arcmin^{-2}.

[b]Optical diameters statistically corrected for Galactic extinction, as described in RC2.

[c]The reported diameter is twice the isophotal radius measured from the center of M51 to the southwest along the *IRAS* in-scan direction.

TABLE 6

GALAXIES DISPLAYED IN THE ATLAS

		MAP NOISE LEVEL (mJy arcmin^{-2})			
FIGURE	NAME	12 μm	25 μm	60 μm	100 μm
2	N55	3.98	5.26	3.77	7.82
3	M31	5.74	7.32	4.52	8.44
4	N247	11.71	15.88	8.73	11.28
5	N253	11.59	14.59	8.70	11.21
6	SMC	4.74	4.84	3.91	6.06
7	N300	11.20	13.57	9.38	13.09
8	M33	6.61	10.95	4.68	9.82
9	N1313	5.15	6.07	4.94	9.86
10	I342	4.91	5.85	4.27	11.30
11	N1448	3.52	3.97	2.99	5.73
12	LMC	5.81	5.97	7.21	16.39
13	N2403	5.19	7.45	3.93	7.56
14	M81	4.56	5.86	3.84	7.30
15	N3109	4.03	5.42	3.07	5.72
16	I2574	4.96	6.05	4.41	7.51
17	N3628	12.40	20.55	8.83	11.91
18	N4236	4.36	5.35	3.62	5.93
19	N4244	4.71	6.82	3.61	5.95
20	N4258	4.51	5.97	3.51	6.40
21	N4395	11.27	13.96	8.35	10.98
22	N4565	5.01	6.88	3.93	7.06
23	N4631	4.65	6.52	3.53	5.70
24	N4656	4.72	6.46	3.57	5.28
25	N4725	11.36	15.05	8.15	9.82
26	N4945	5.73	6.78	5.62	12.30
27	N5055	4.51	5.51	3.59	6.71
28	M51	5.07	6.30	3.93	6.61
29	M83	8.63	14.84	7.58	18.96
30	M101	1.26	1.49	1.16	1.86
31	N6744	3.99	4.57	4.36	11.56
32	N6822	3.24	6.94	2.58	4.13
33	N6946	3.61	3.95	3.13	8.06

LMC were constructed from red prints provided by the Mount Wilson and Las Campanas Observatories. A second copy of the optical photograph with the 60 μm map superposed is also displayed. The optical photographs and infrared maps are at the same scale; the angular scale marked on the photograph is 8′ for all galaxies except the Magellanic Clouds, M31 and M33. The scale of these images is noted in the figure captions.

ii) *Infrared Contour Maps and the IRAS Beam*

The contour levels of the infrared images are scaled by the map 1 σ mean noise level. The noise level of each wavelength map in units of mJy arcmin^{-2} is listed in Table 6. Unless otherwise noted in the figure caption, the dashed contours are at 3, 6, and 9 σ below the map background level, and the solid contours are at 3, 6, and 10 σ, with brighter levels scaled logarithmically by 2 from 10 σ (i.e., 20, 40, 80 σ, etc.). The faintest contours of the maps should be viewed with caution given the emission from foreground Galactic "cirrus" and the possibility of inadequate background emission removal.

The optical center of the galaxy, as given in Table 1, is marked on each infrared map. For all but the largest galaxies, the tick marks on the maps are spaced by 4′. For the galaxies with maps at a different scale (NGC 55, M31, NGC 253, SMC, M33, LMC, NGC 4945, M101, and NGC 6822), the tick mark spacing is noted in the figure caption.

Note that even in those maps showing structural features, the "resolved" features may reflect both the noncircular, undeconvolved *IRAS* beam shape and the various scanning directions of the individual pointed observation or survey scan maps co-added to produce the maps shown. The beam shape, represented by the $\frac{1}{4}$, $\frac{1}{2}$, and $\frac{3}{4}$ power brightness level contours of an *IRAS* point source, is displayed on the maps of NGC 55 (Fig. 2). The beam has been oriented along the scanning direction of the observations of the galaxy.

VI. ANALYSIS AND DISCUSSION

A preliminary analysis of the catalog and a discussion of the atlas maps are presented below. The detailed discussion of these data, including the radial distribution of the infrared surface brightness and colors, arm/disk and nuclear/disk contrasts, comparisons with optical, H I and CO images and profiles, and an intercomparison among the atlas galaxies of all these parameters, is deferred to Paper II.

a) *Detection Rates*

The distribution by optical morphological type of the catalog galaxies and of their *IRAS* detection rates are tabulated in Table 7. The six galaxies not detected are all ellipticals, and the two ellipticals detected, NGC 185 and NGC 205, are well known to have low levels of star formation (Hodge 1963, 1973; Gallagher and Mould 1981). Seventy-five percent (59 of 79) of the detected galaxies were observed at all four *IRAS* wavelengths, and all but three galaxies—the S0 galaxies NGC 1023, NGC 3115, and NGC 4762, which were seen only at 12 μm—were detected at both 60 and 100 μm.

b) *Far-Infrared and Optical Sizes*

The mean ratio of the 60 μm to blue-light isophotal diameters, reported in Table 5, is 0.98 ± 0.25. The most discrepant ratio is for NGC 6822. NGC 6822, a member of the Local Group, is a low surface brightness dwarf irregular system at low Galactic latitude ($b = -18\overset{\circ}{.}4$). These two factors, and possibly confusion due to "cirrus," may account for the discrepant optical and infrared sizes of this galaxy.

For the 11 galaxies for which both infrared and optical effective aperture diameter measurements are available, the mean radial distribution of the infrared emission, $\langle (A_e/D)_{\rm IR} \rangle = 0.17 \pm 0.05$, is more centrally concentrated than that of the blue-light emission $\langle (A_e/D)_B \rangle = 0.37 \pm 0.15$. While a discussion of this result is deferred to Paper II, one factor likely to contribute to the larger ratio of the blue-light distribution is the extinction of the blue light toward the central regions of the galaxies.

While galaxies with infrared extents that significantly exceed their optical sizes may exist, the overall agreement between the optical and far-infrared sizes of the galaxies best resolved by *IRAS* presented in this catalog suggests that the RC2 "large optical galaxy" sample, along with the secondary sample presented in the Appendix, comprise a complete set of galaxies likely to have 60 μm extents greater than 8′ (and for which, because of source extent, the data reduction techniques of this study are needed to obtain "total" *IRAS* flux densities).

c) *General Far-Infrared Morphology*

Although the *IRAS* spatial resolution decreases with increasing wavelength, the infrared images and profiles presented in the atlas are typically most interesting at 60 μm. Galaxies emit substantially more flux at the longer *IRAS* wavelengths, and, in some cases the large galaxies studied here do not emit strongly enough in the outer regions to be detected as extended sources at 12 and 25 μm.

We have attempted to "classify" the 60 μm images and brightness profiles of the galaxies displayed in the atlas according to a simple scheme that parallels the Hubble bulge-to-disk classification scheme for optical morphology. The basic criterion used here was the shape of the 60 μm in-scan radial profile, in particular, the degree of central concentration of the 60 μm emission in relation to the disk emission. (Note that in this far-infrared "bulge-to-disk" reclassification scheme, the 60 μm bulge emission does not correspond to the galaxy stellar nuclear bulge.) This classification scheme is limited by the varying linear scale sizes resolvable in the galaxies and the orientation of the *IRAS* scanning direction with respect to the galaxy position and inclination angles. Therefore, we have separated the 25 highest resolution images into four bins only, and refer to them as "groups" rather than as well-defined classes. A fifth group contains highly inclined galaxies which were scanned in a direction close to the minor axis, and for which there is insufficient resolution to place them in one of the other four groups.

This grouping scheme is based only on the 60 μm images and profiles and not on the data at the other wavelengths.

Group 1: IC 342, NGC 4656, NGC 4945, NGC 5236 (M83), NGC 6946.—These five galaxies show the largest contrast of the 60 μm "bulge-to-disk" emission among the atlas galaxies

TABLE 7

MORPHOLOGICAL DISTRIBUTION AND DETECTION RATES

	Type							
Sample	E	S0	S0/a–Sab	Sb–Sbc	Sc—Scd	Sd–Im	I0	Total
Optical	8	5	12	17	22	20	1	85
12 μm detection	2	4	11	16	21	12	1	67
25 μm detection	1	1	10	16	18	15	1	62
60 μm detection	2	2	12	17	22	20	1	76
100 μm detection	2	2	12	17	22	20	1	76
4 band detection	1	1	10	16	18	12	1	59
No detection	6	0	0	0	0	0	0	6

FIG. 1.—Profile cuts along the *IRAS* scanning direction of the 12, 25, 60, and 100 μm surface brightness images of the "large optical galaxies." Wavelength profile plots of all galaxies detected brighter than 6 σ are presented (the SMC and the LMC are excluded). The cuts are centered on the galaxy optical center and are scaled by the maximum intensity found along the cut. For each galaxy the position angle of the in-scan cuts is indicated. The lighter curve marked with small circles is the in-scan profile of IRC +10011, a representative *IRAS* point source. An offset has been applied to redefine the profile zero level of the images for which Galactic "cirrus" resulted in poor background removal.

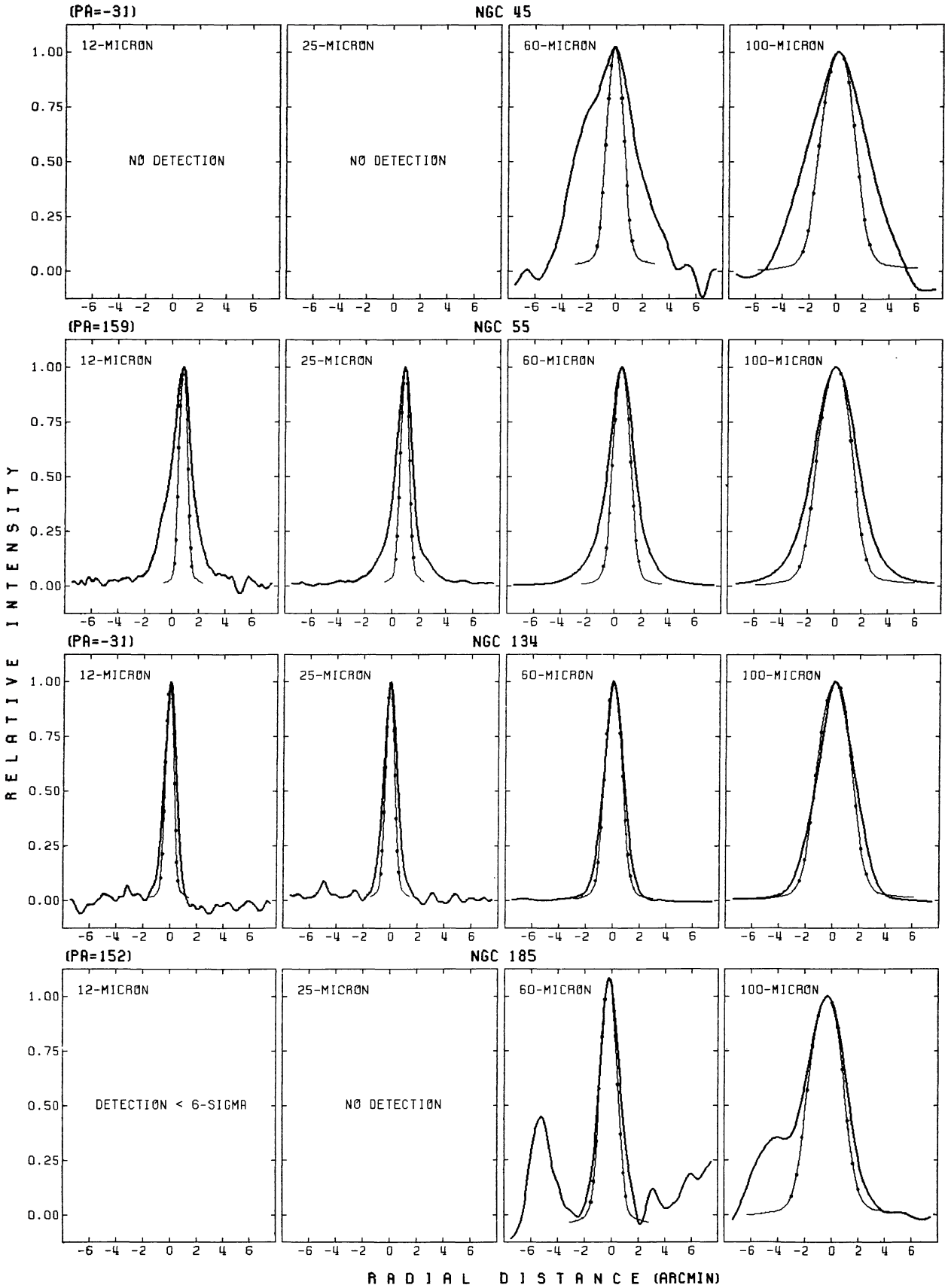

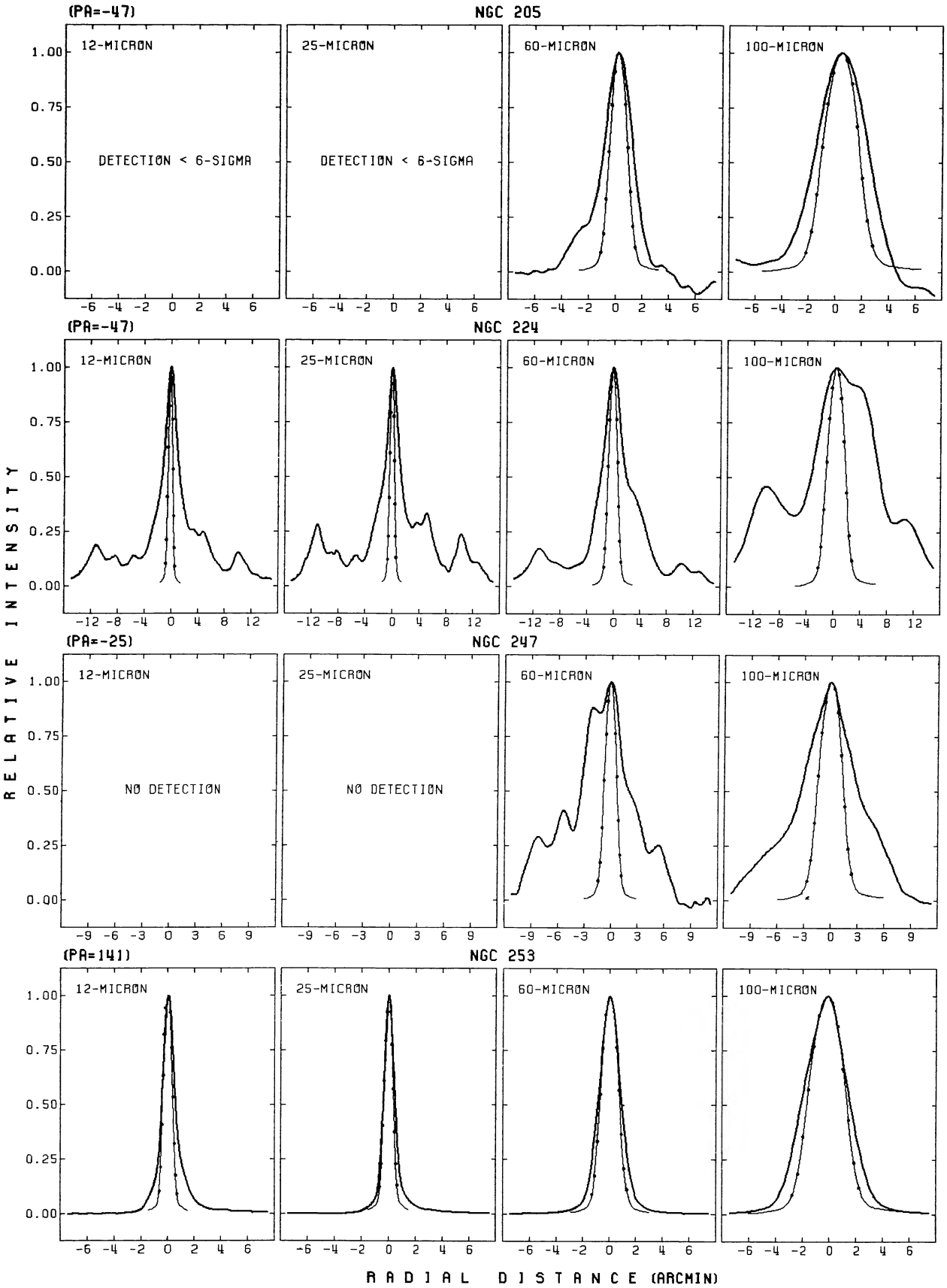

FIG. 1—*Continued*

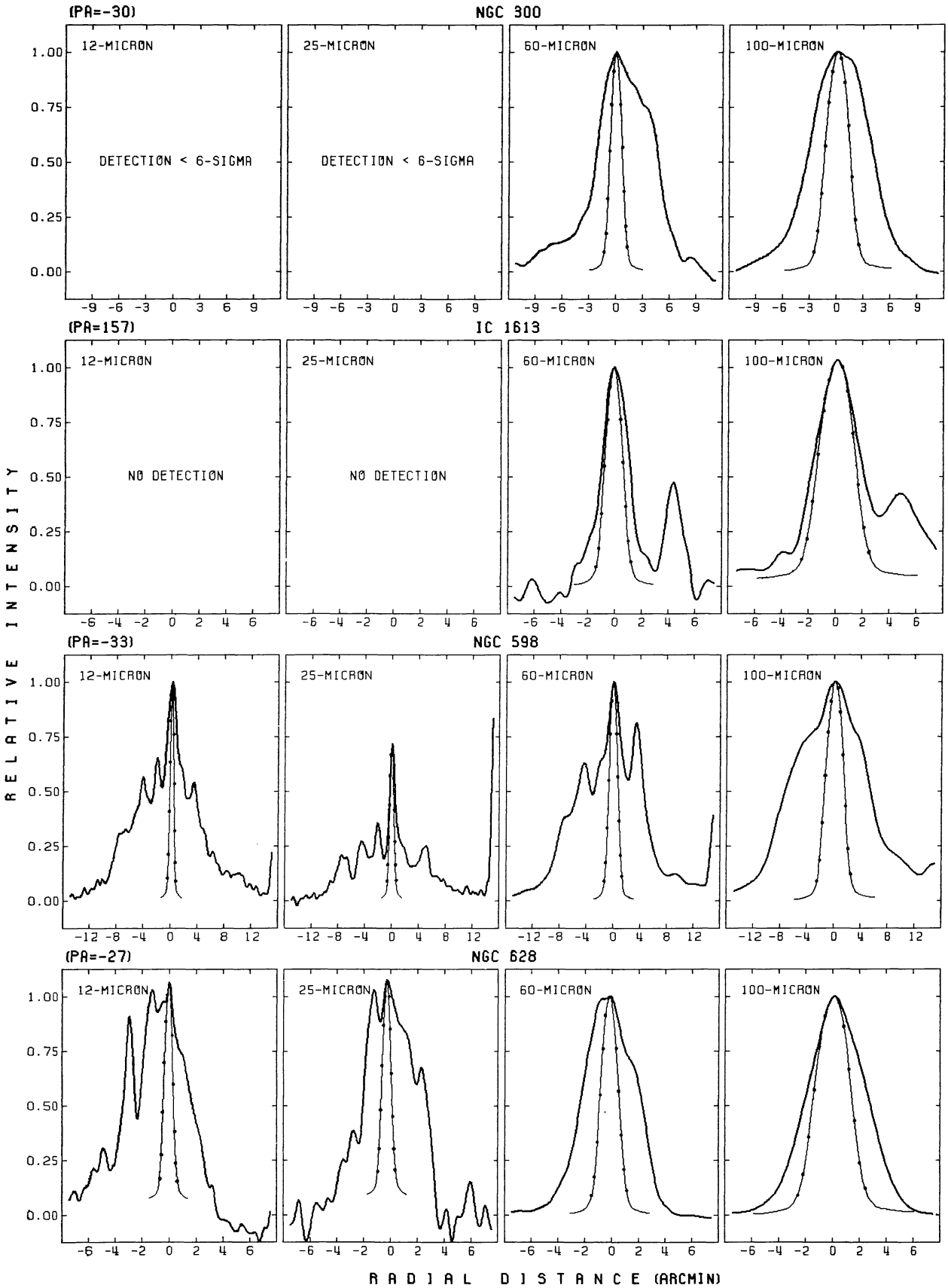

FIG. 1—*Continued*

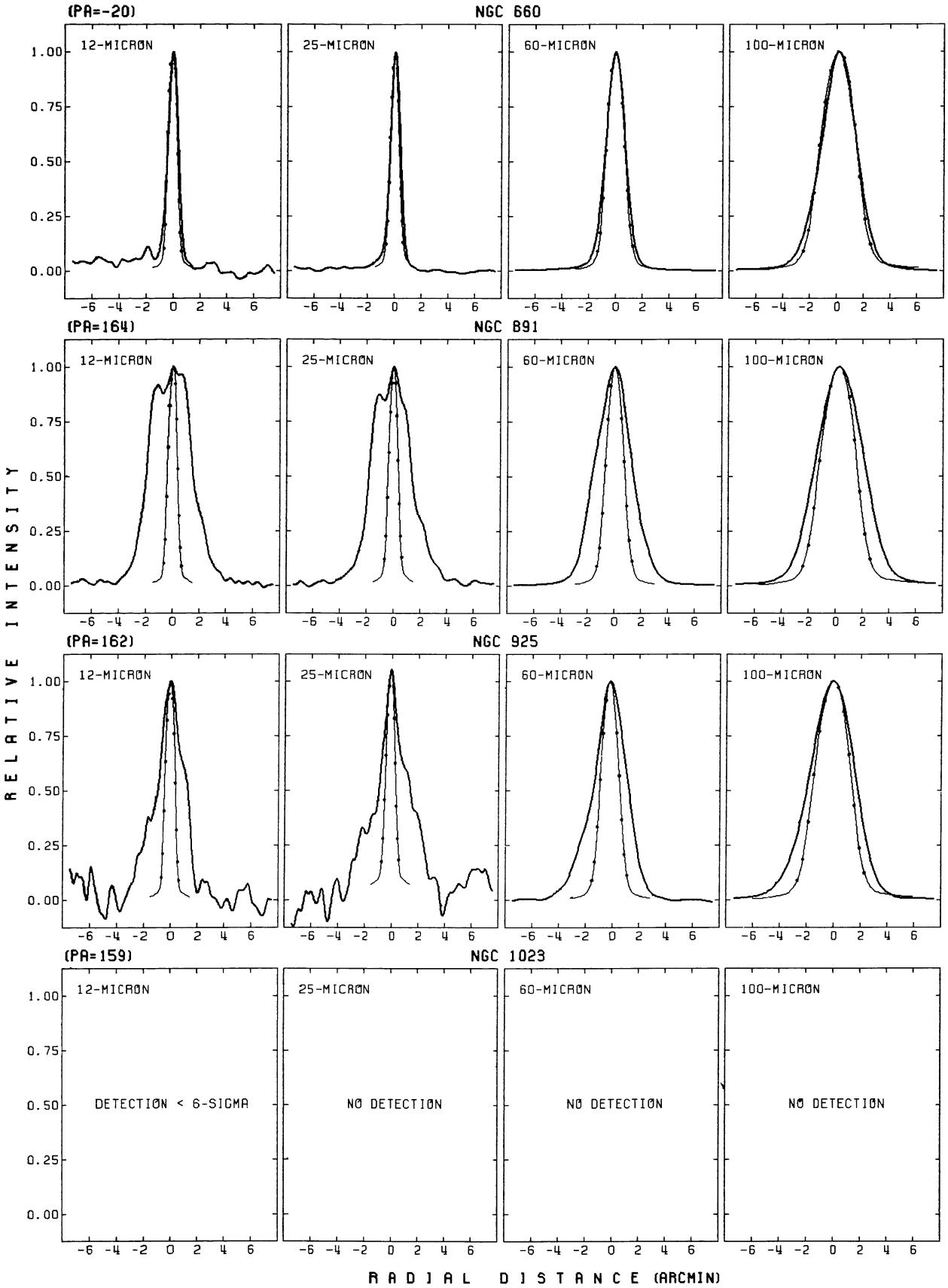

FIG. 1—*Continued*

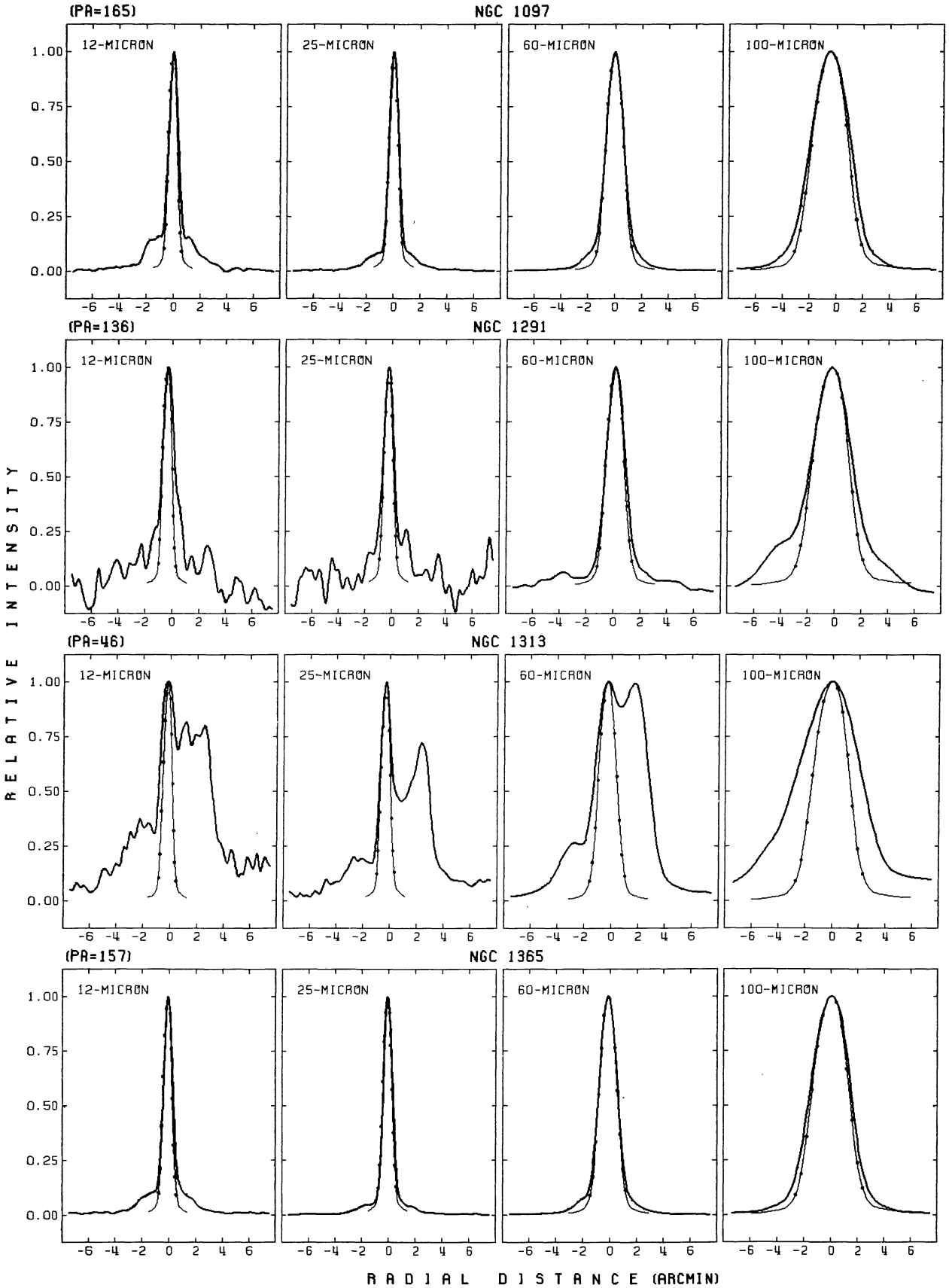

FIG. 1—*Continued*

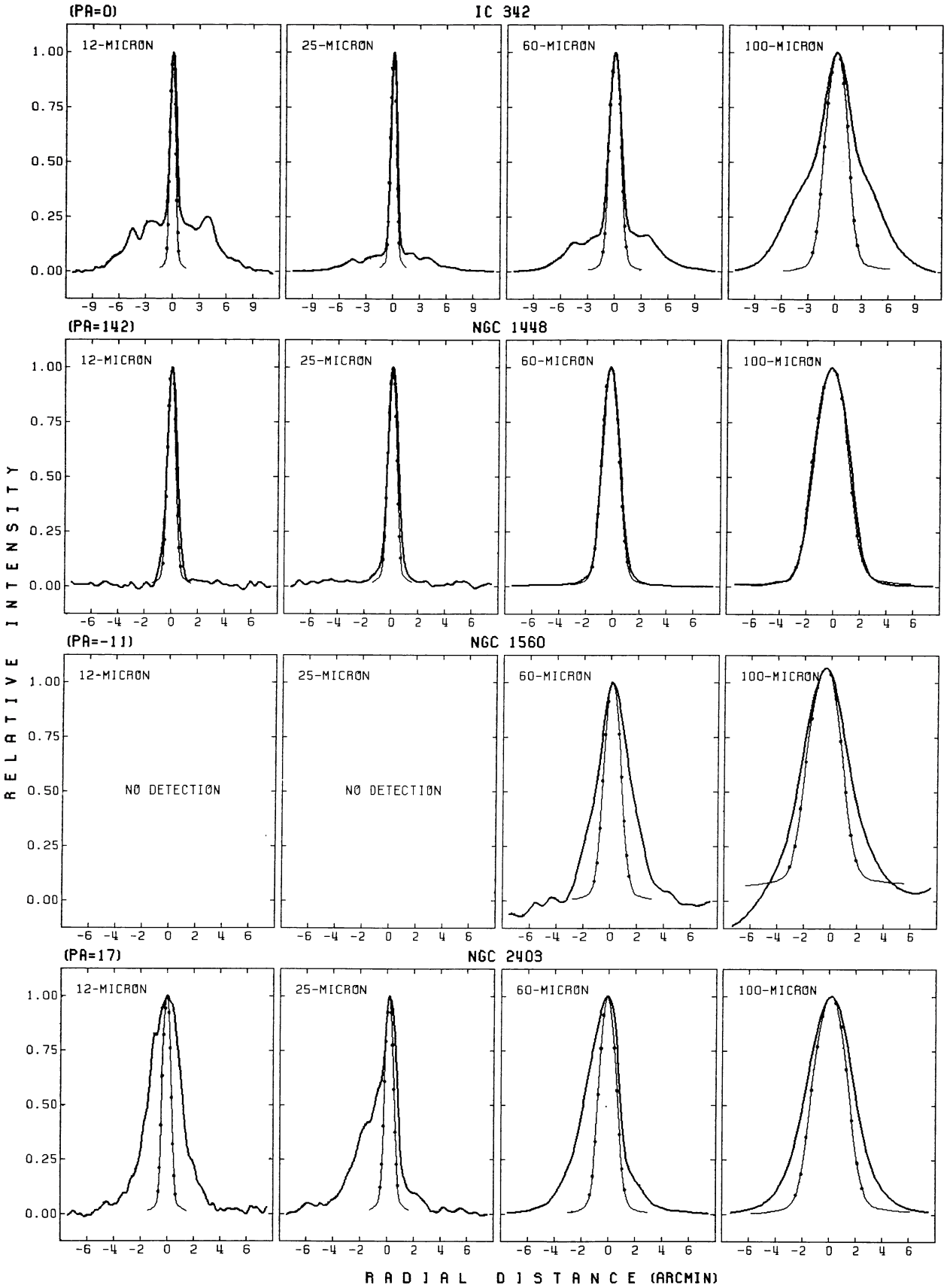

FIG. 1—*Continued*

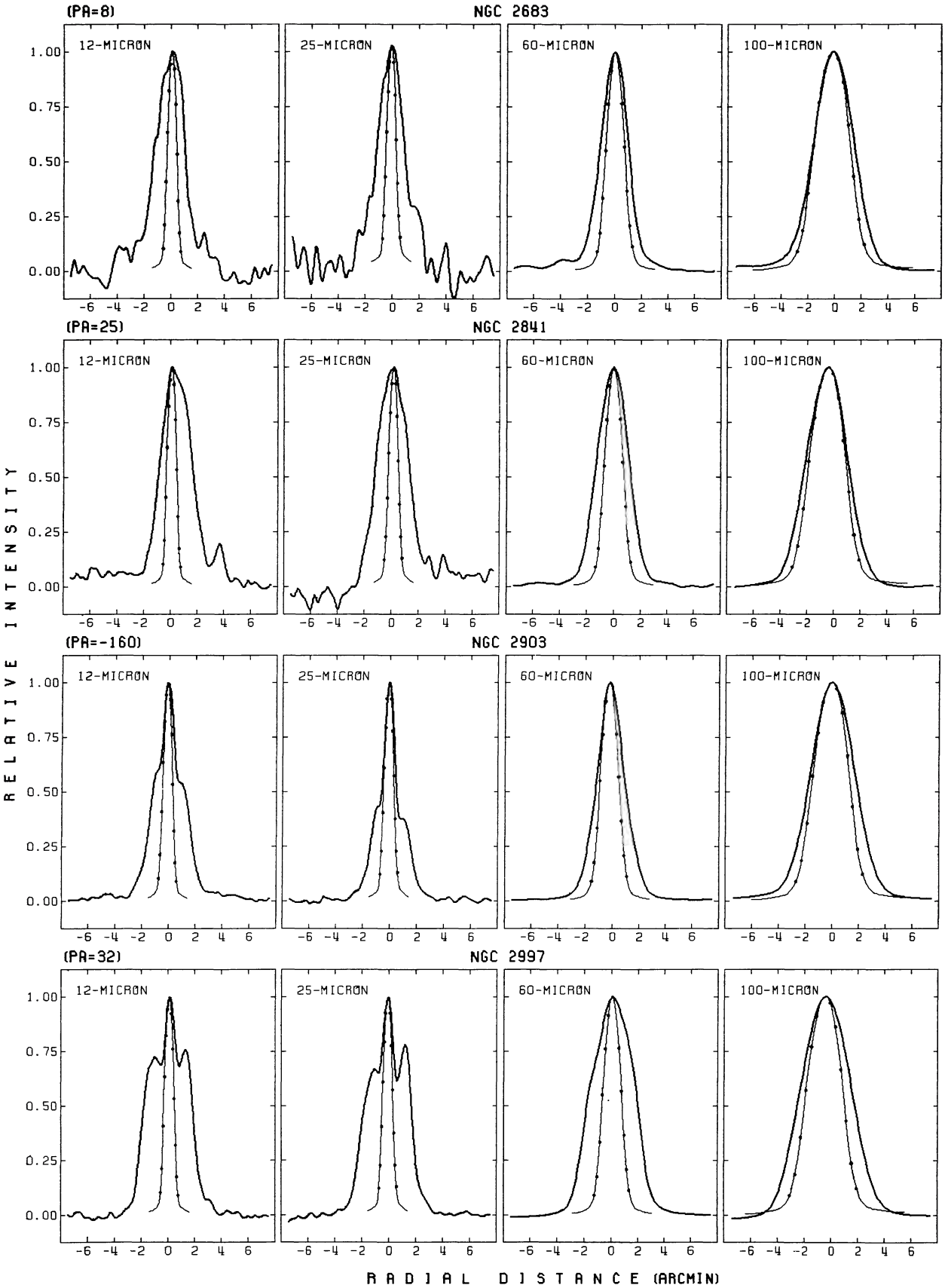

FIG. 1—*Continued*

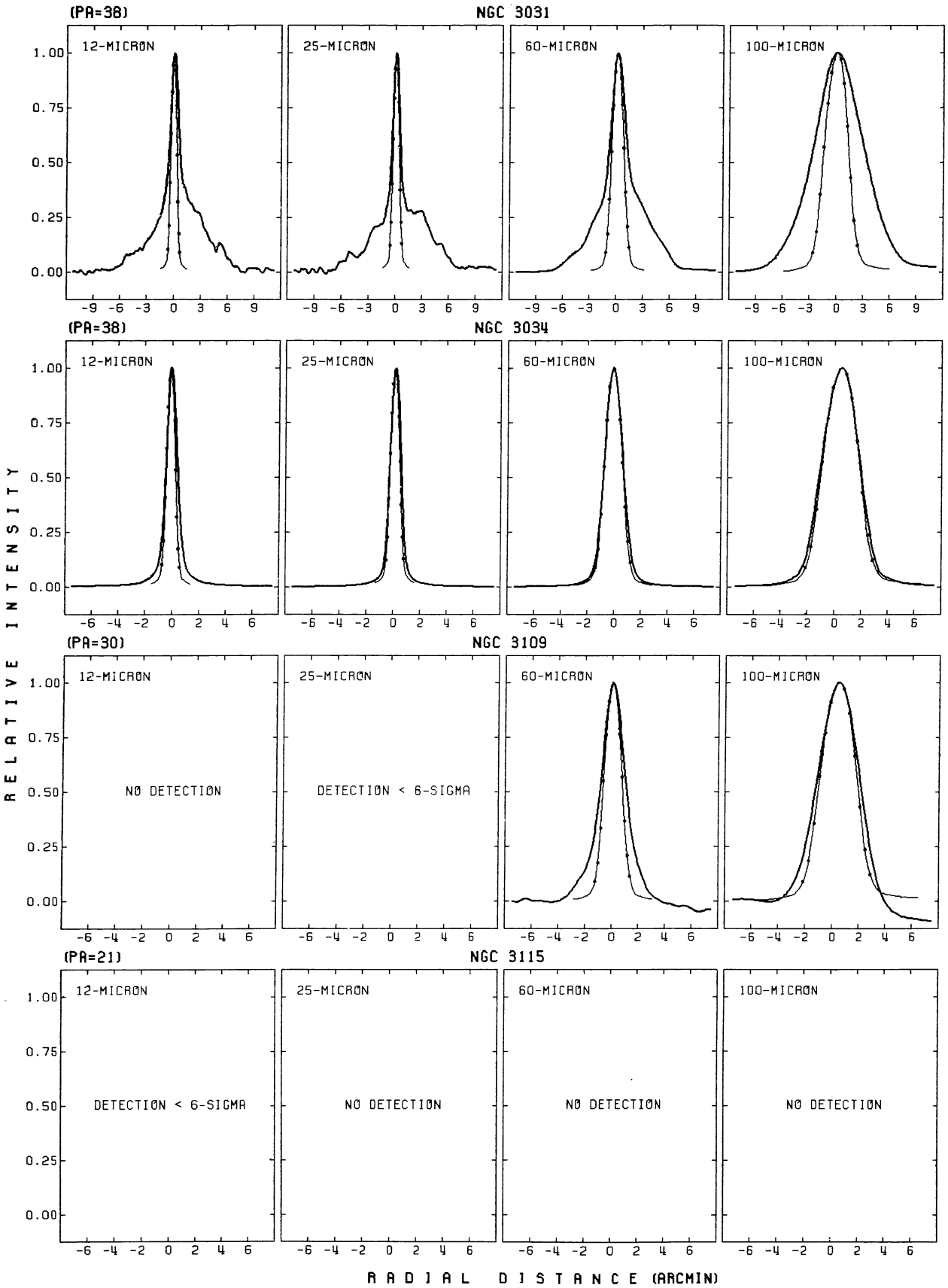

FIG. 1—*Continued*

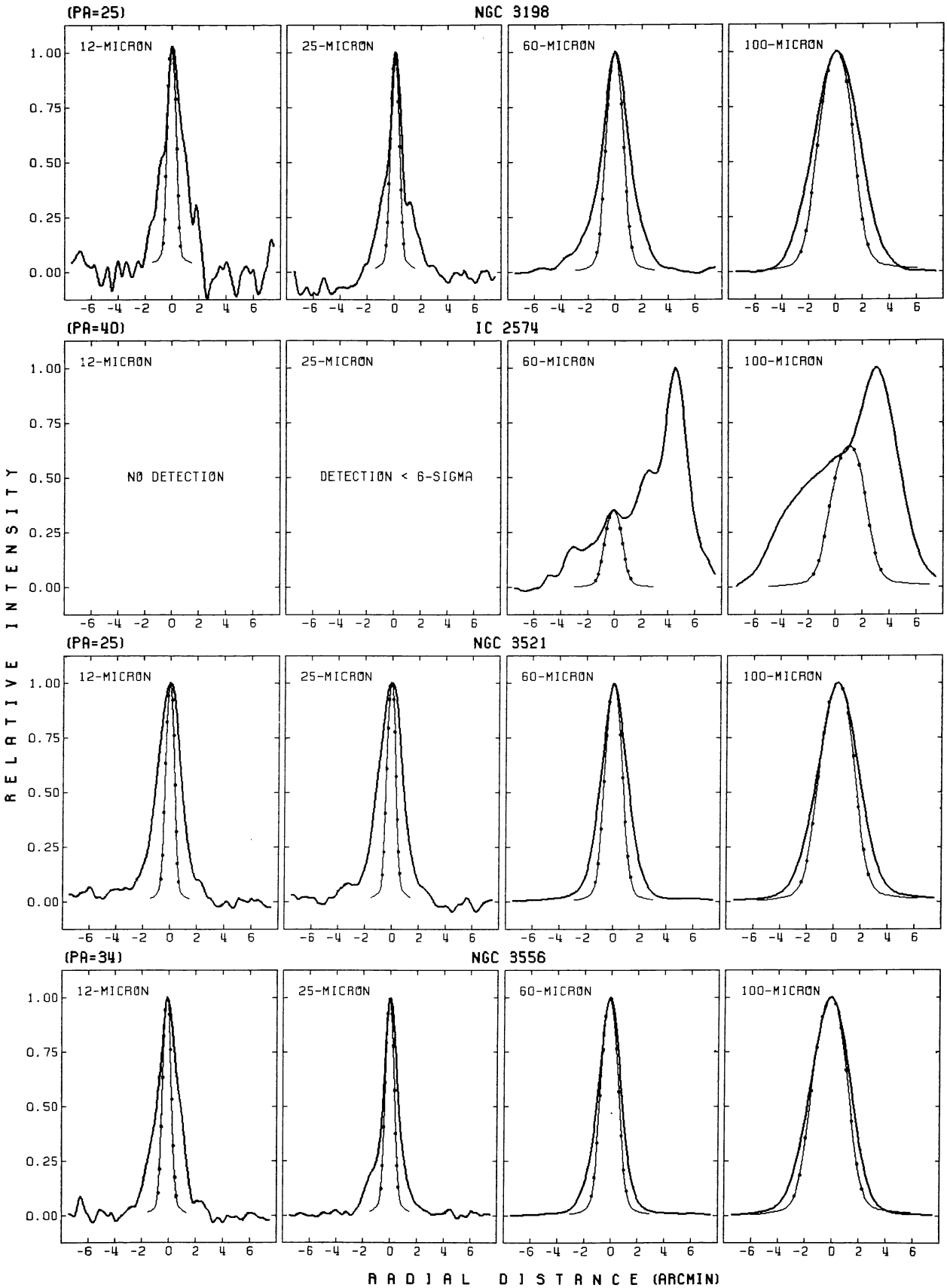

FIG. 1—*Continued*

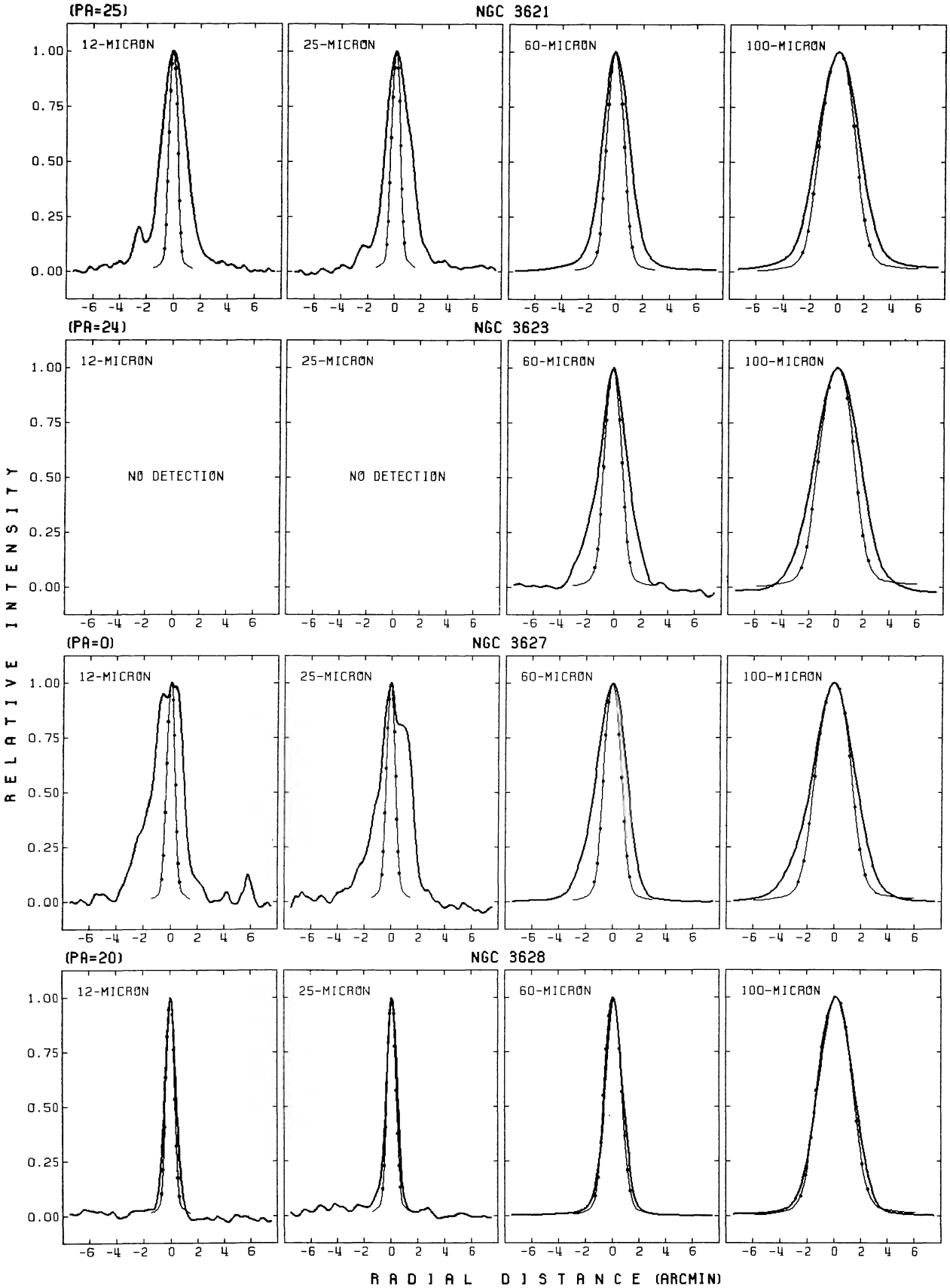

FIG. 1—*Continued*

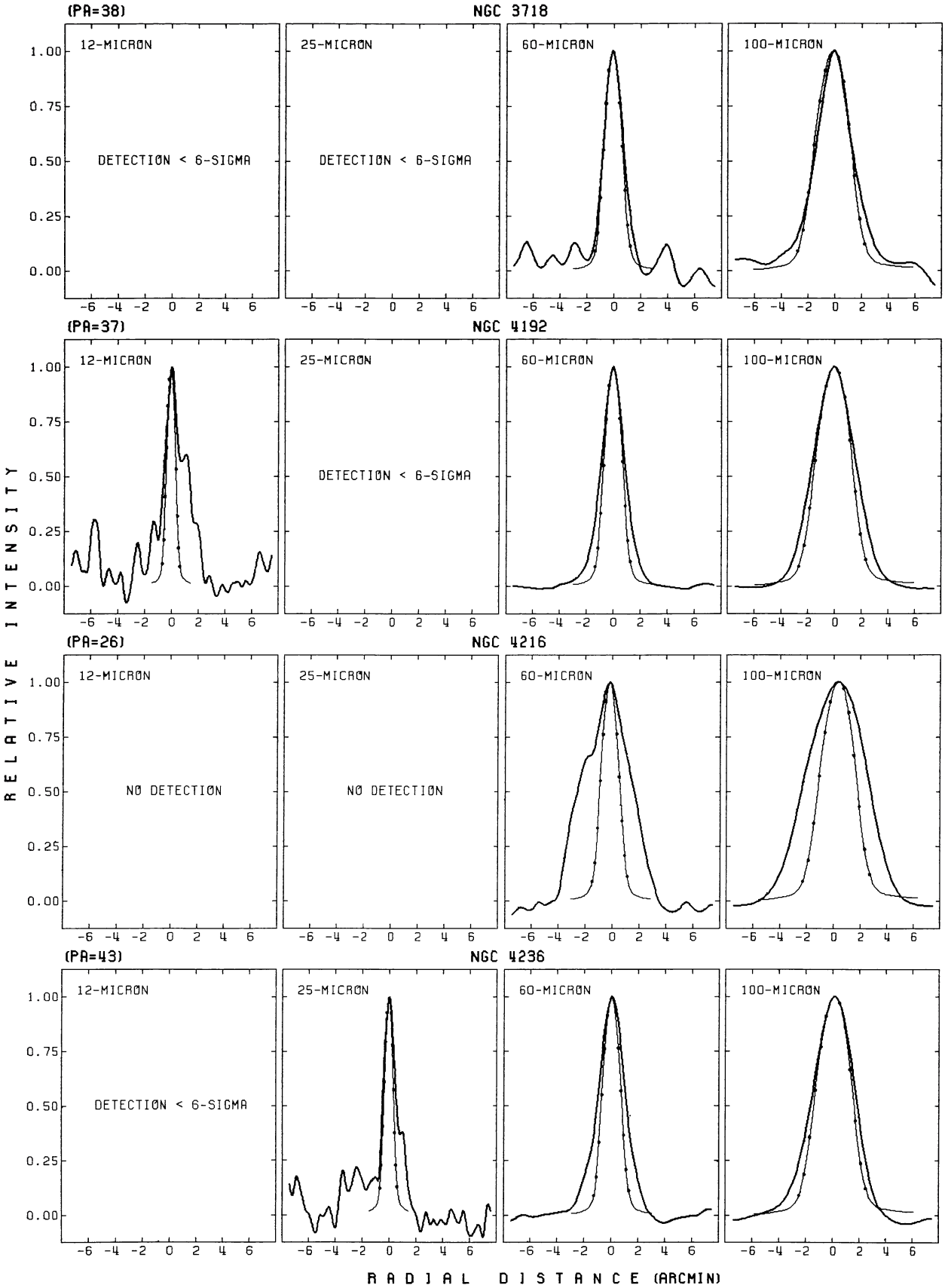

FIG. 1—*Continued*

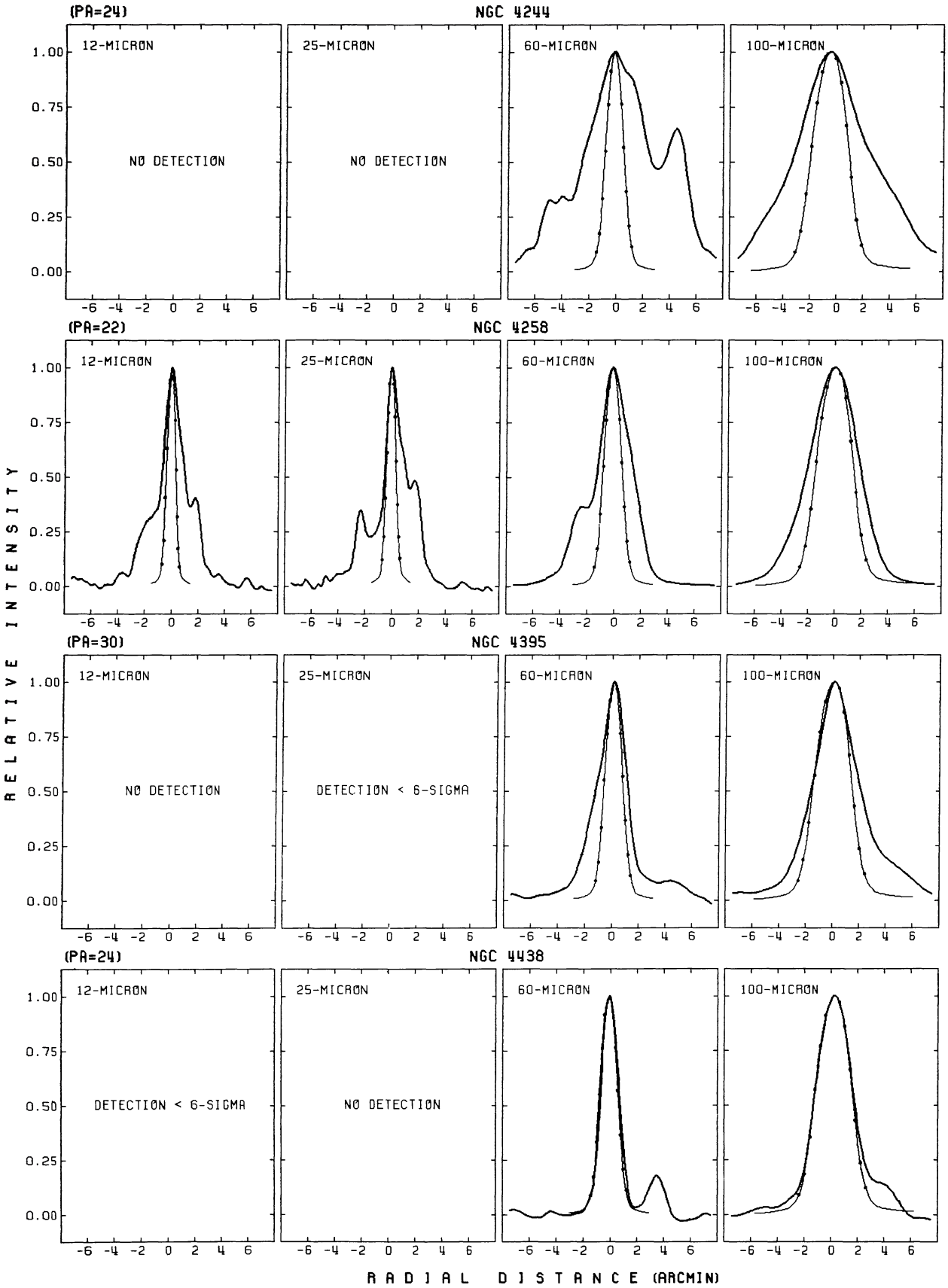

FIG. 1—*Continued*

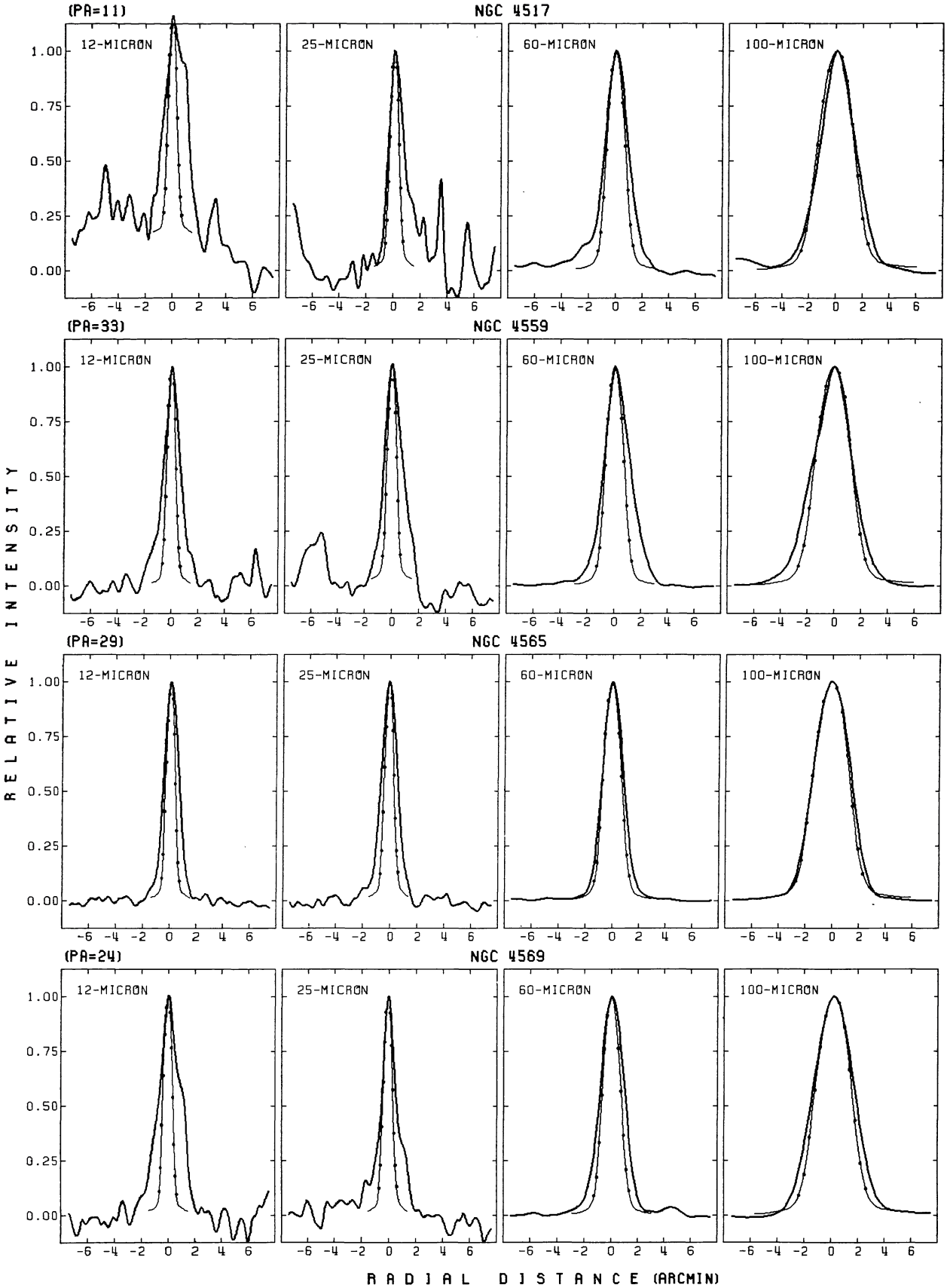

FIG. 1—*Continued*

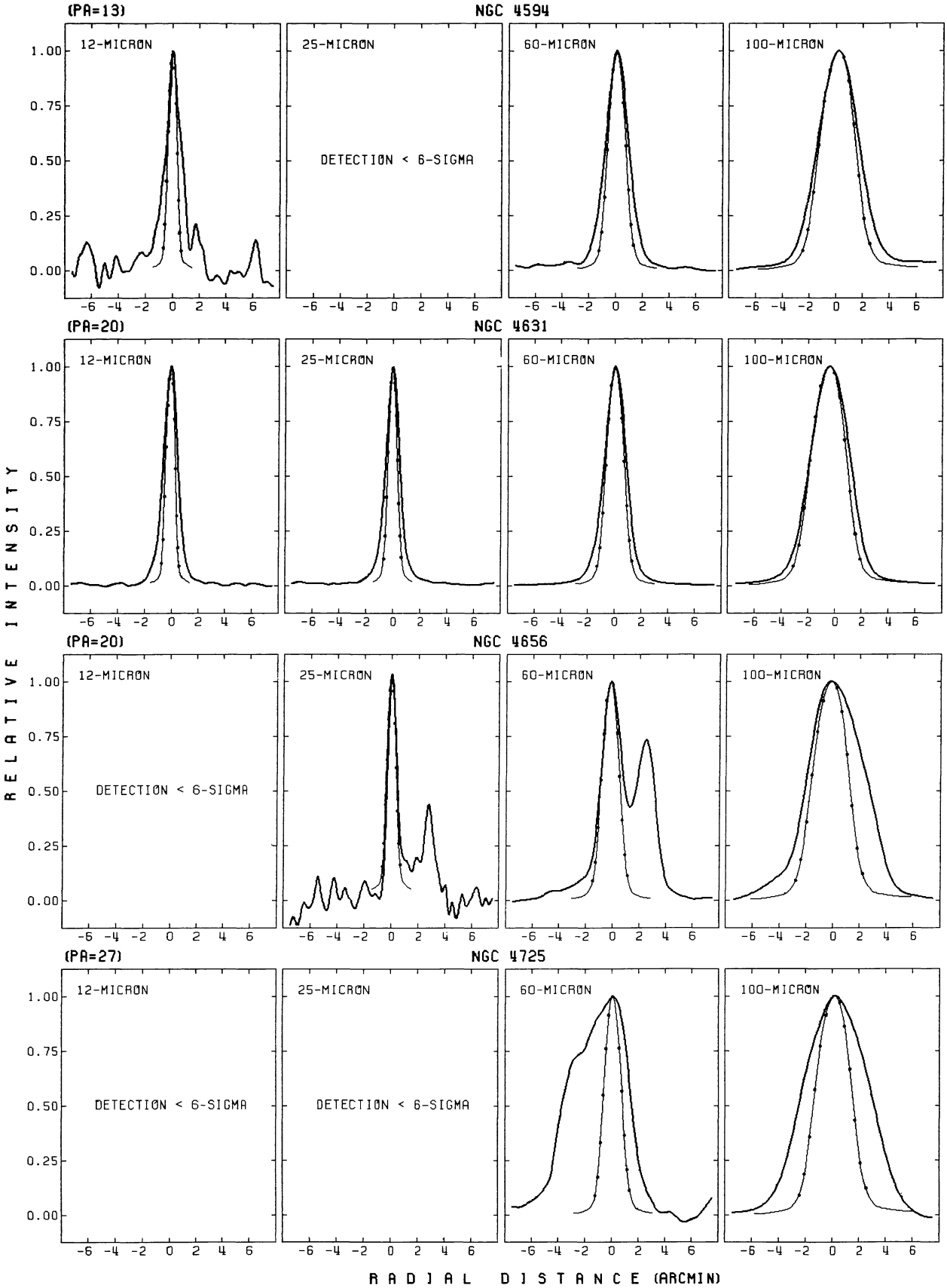

FIG. 1—*Continued*

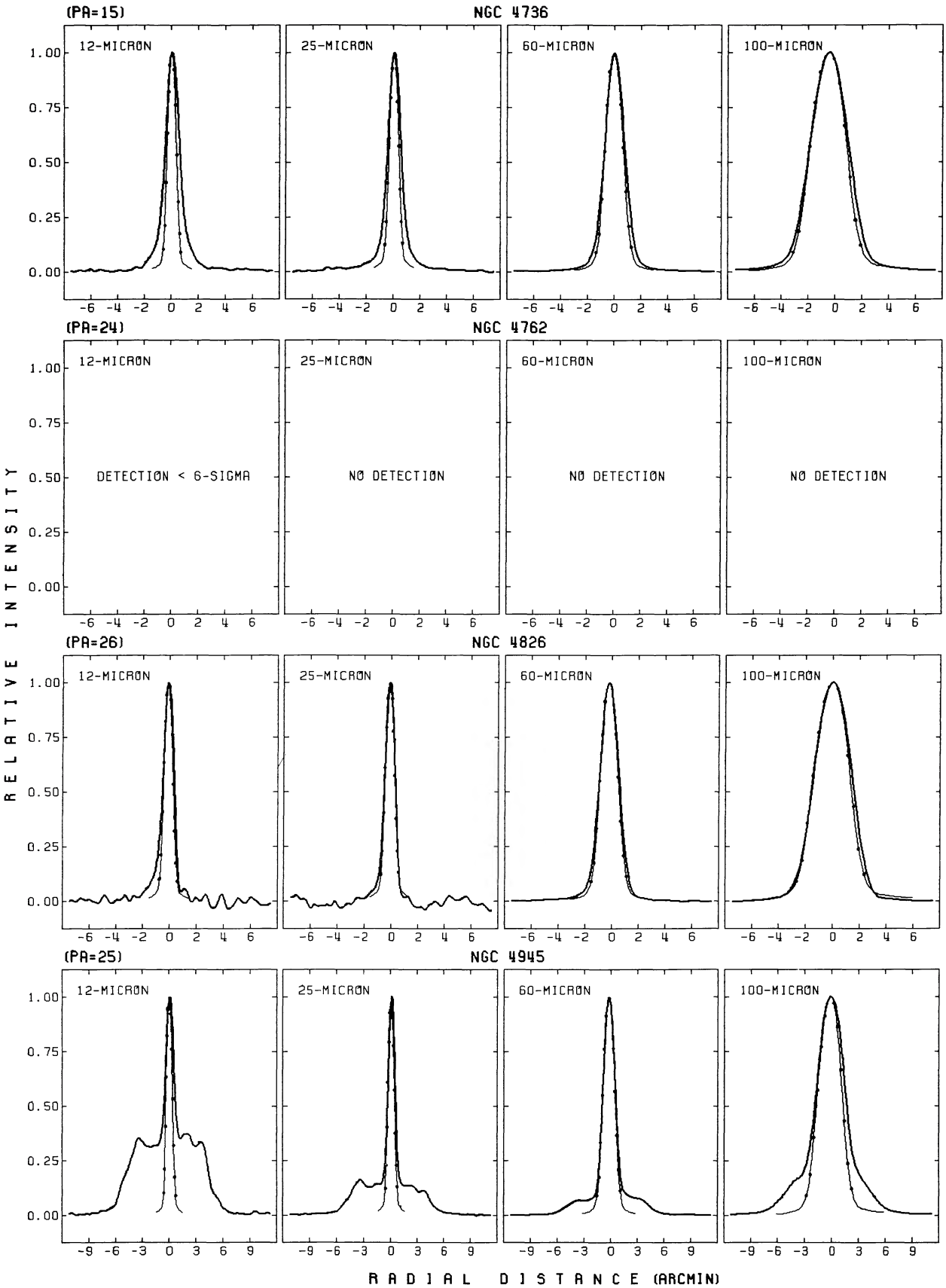

FIG. 1—*Continued*

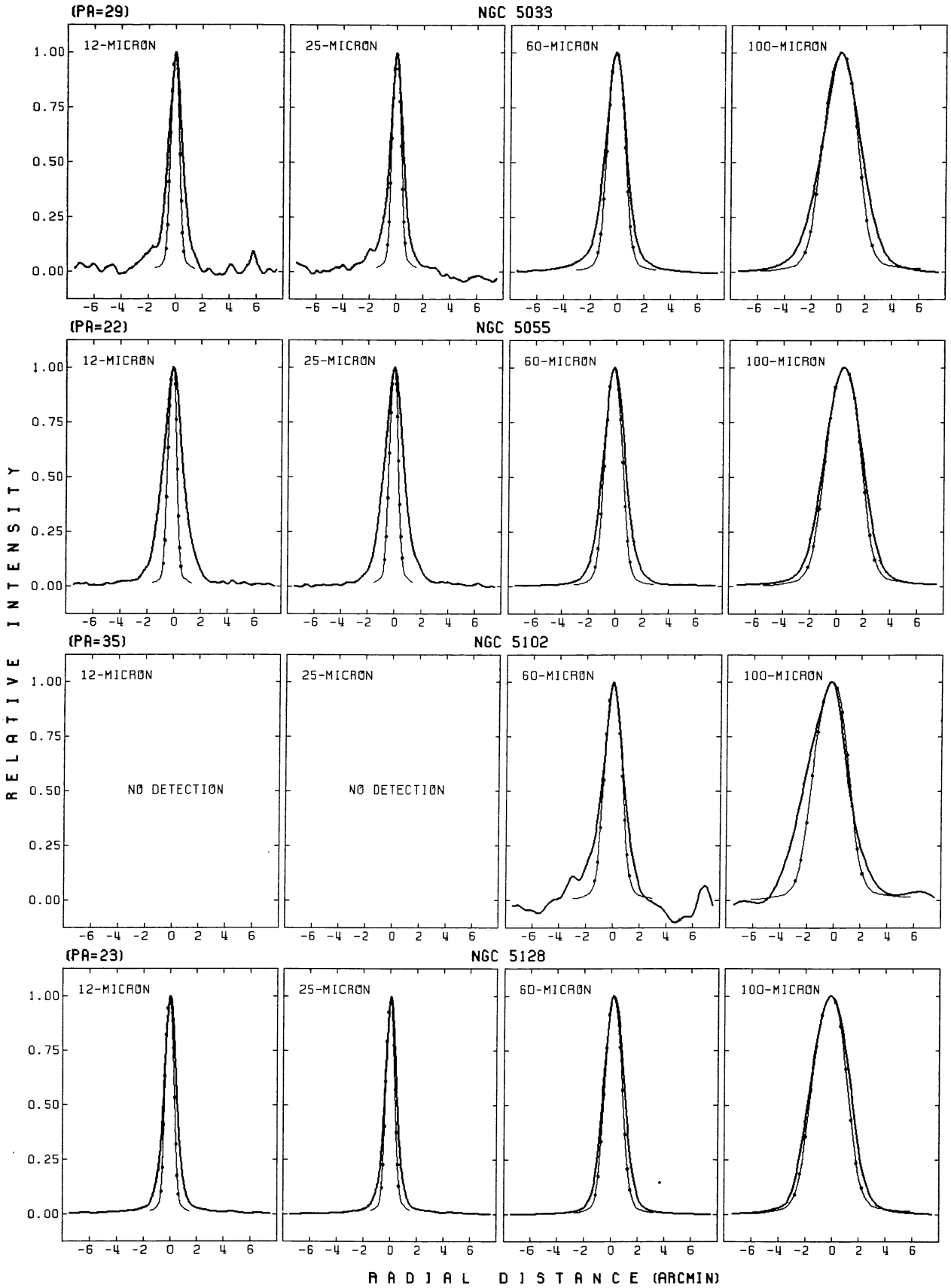

FIG. 1—*Continued*

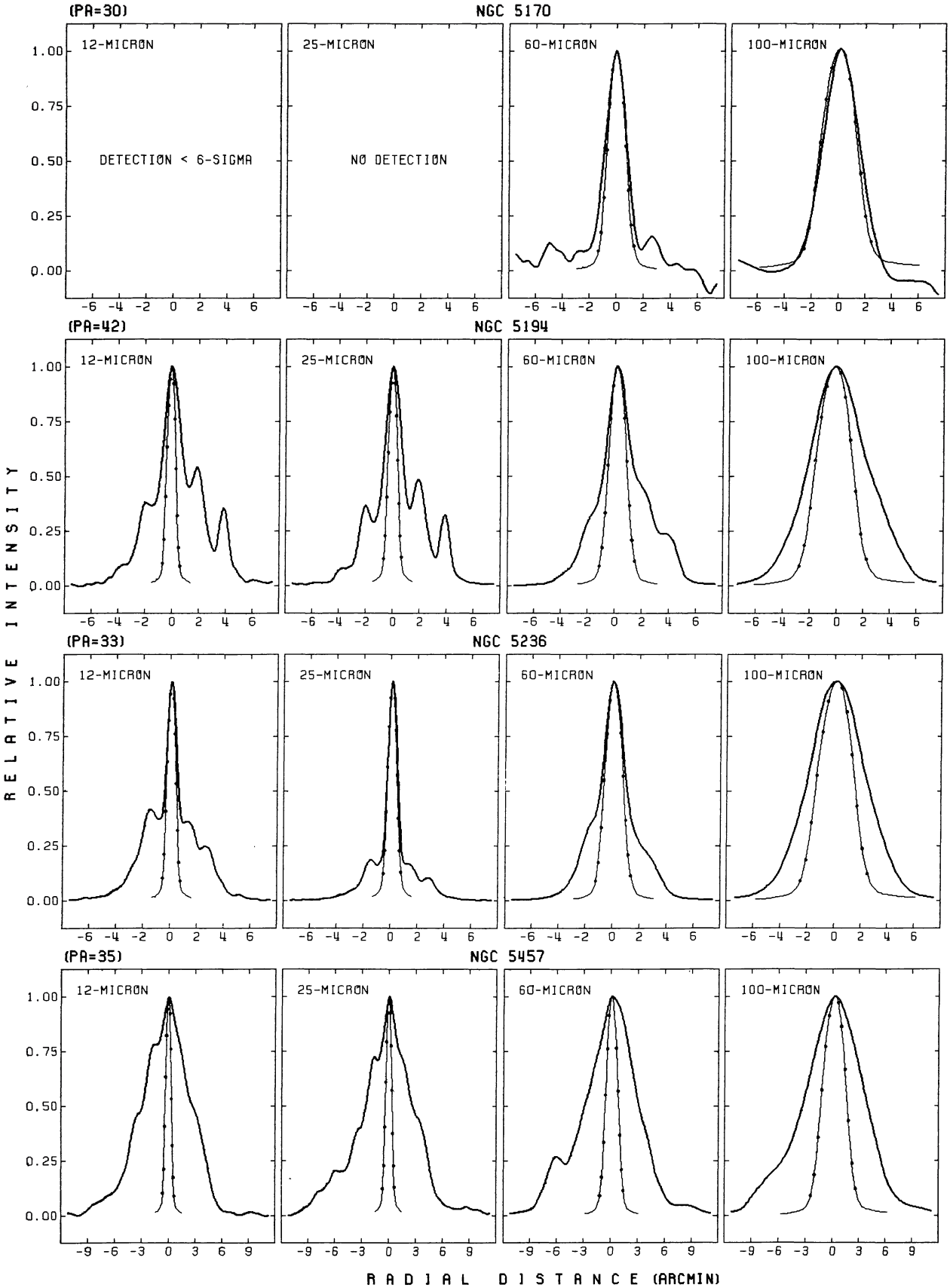

FIG. 1—*Continued*

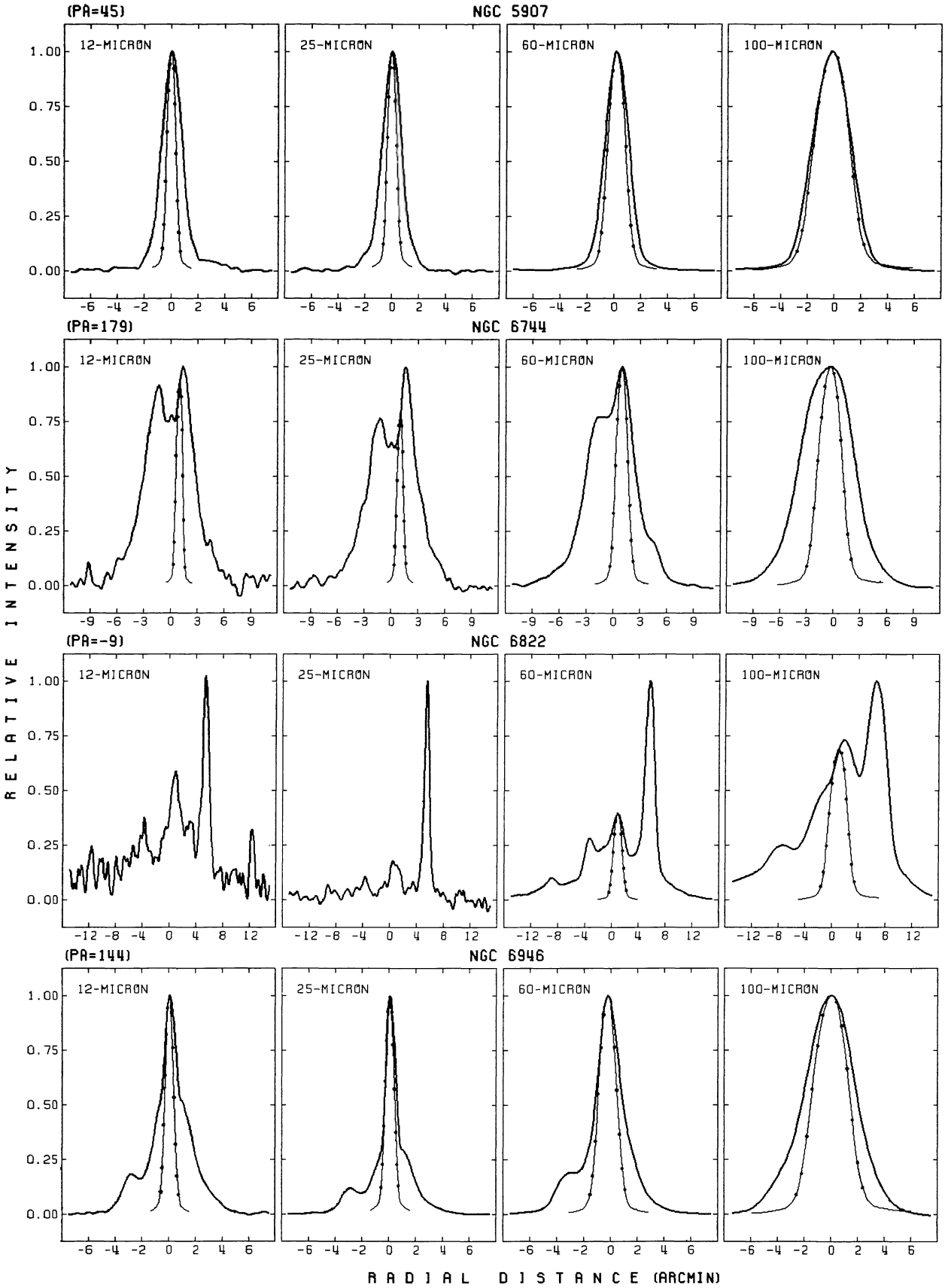

FIG. 1—*Continued*

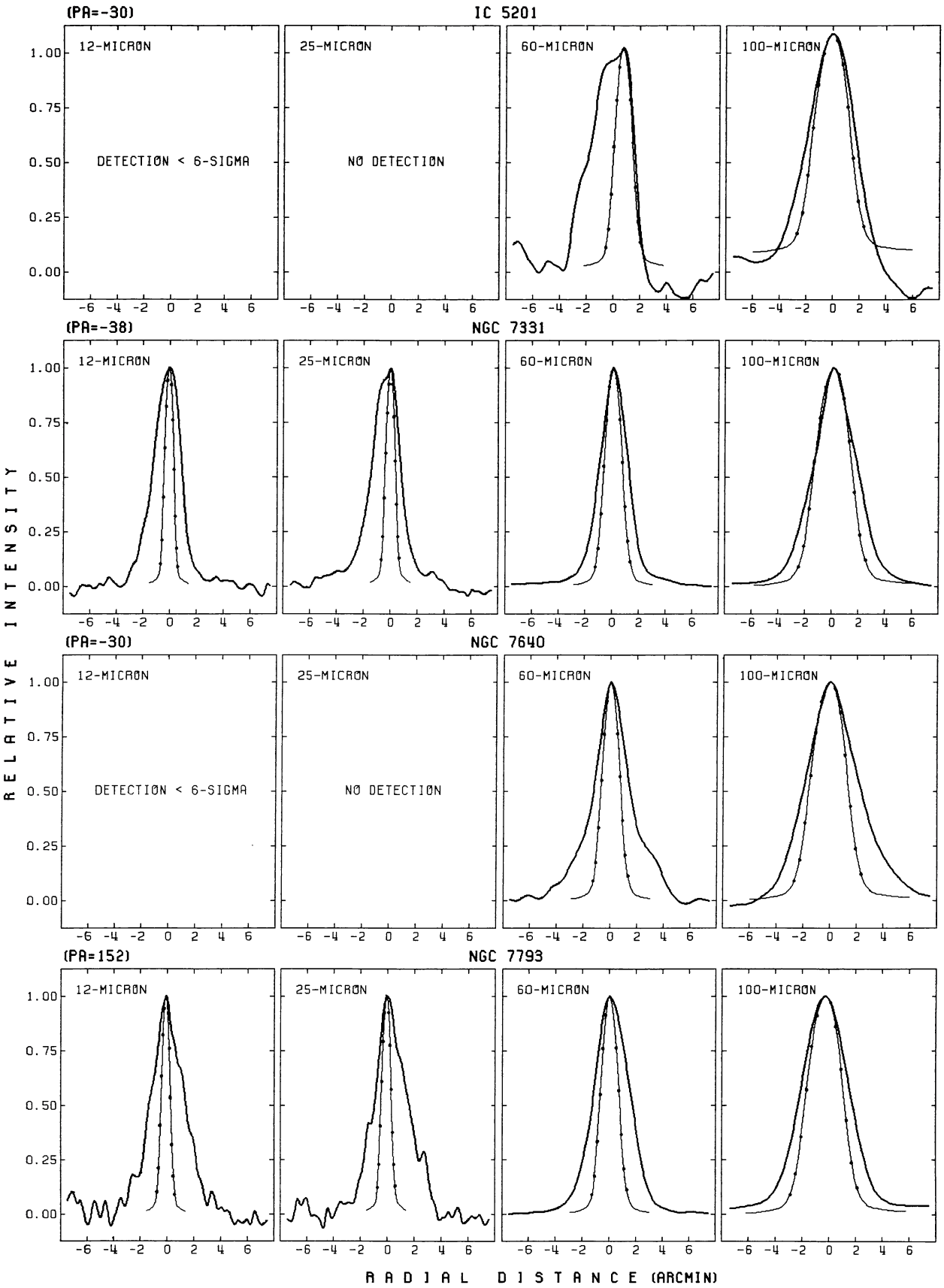

FIG. 1—*Continued*

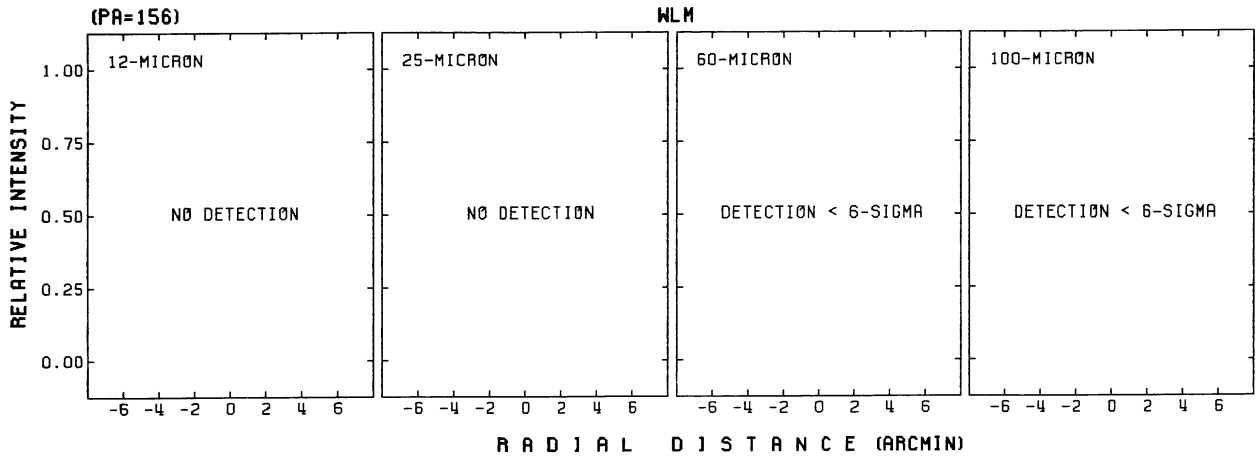

FIG. 1—*Continued*

(i.e., they are the "earliest" type galaxies at 60 μm). Disk emission is seen in each case, but the pointlike nuclear source is very dominant, while the faint "disk" resembles a plateau.

Group 2: NGC 55, NGC 2403, NGC 3031 (M81), NGC 4258, NGC 5194 (M51).—These galaxies are of "later" 60 μm type than group 1 galaxies, exhibiting a less strongly enhanced nuclear source relative to the disk emission. The nuclear source is typically not pointlike, and blends more smoothly into the disk emission. In the larger galaxies spiral arm structure has been resolved.

Group 3: NGC 224 (M31), NGC 247, NGC 300, NGC 598 (M33), NGC 1313, NGC 4244, NGC 4725, NGC 5457 (M101), NGC 6744.—The 60 μm profiles of these nine galaxies are still nucleus-dominated but show less concentration toward the nuclear regions than group 2 galaxies, often having an almost triangular shape. Structure in the outer regions of the galaxies is frequently apparent. The peculiar galaxy NGC 1313 is double-peaked at 12, 25, and 60 μm.

Group 4: SMC, LMC, IC 2574, NGC 4236, NGC 4395, NGC 6822.—These are "late-type" 60 μm galaxies in which the *IRAS* images are dominated by emission from prominent H II region complexes. There is little or no enhanced *IRAS* emission from the nuclear region.

Group 5: NGC 253, NGC 1448, NGC 3109, NGC 3628, NGC 4565, NGC 5055.—For these highly inclined galaxies the *IRAS* scanning direction was very close to the galaxy minor axis. Little information is available on their far-infrared structure.

d) *Comments on the Atlas Maps*

In the following, brief descriptions of the *IRAS* appearance of the atlas galaxies that exhibit particularly interesting infrared structure are given. Caveats in the interpretation of the data are also noted.

NGC 55.—The *IRAS* images of this edge-on galaxy are dominated by three pointlike sources including the nucleus, all of which are seen at both 25 and 60 μm and two of which are seen at 12 μm. The 100 μm beam is too large to resolve either of the off-nuclear point sources. The off-nuclear sources appear to coincide with dust lanes or spiral arms (viewed edge-on) in the optical image.

The orientation of the nuclear point source is affected by the beam scanning direction, and the outer contours of the 60 μm map to the northeast are probably distorted by emission from a small group of background galaxies.

NGC 224 (M31).—The *IRAS* images of M31 have been described previously by Habing *et al.* (1984), Soifer *et al.* (1986), and Walterbos and Schwering (1987). The newly processed data presented here show the same features: the galaxy is well resolved, with a nuclear source and a bright infrared ring that corresponds to prominent dust lanes and the galaxy H I and CO rings.

NGC 205 is seen in the 12, 60, and 100 μm maps, and M32 is seen in the 12 and 25 μm maps.

NGC 253.—The images of this very bright galaxy are very much dominated by reflected emission from the *IRAS* telescope spider. A "hysteresis tail," caused by electronic relaxation effects of the *IRAS* detectors after crossing a bright source (see the *IRAS* Supplement, § IV.A.7), is seen in the forward scanning direction. Because of these effects, useful information is available only along the major axis.

SMC and LMC.—The maps of the SMC and LMC displayed in the atlas were constructed from all-sky survey scans. The 12, 25, and 60 μm maps have been smoothed to the resolution of the 100 μm map ($\sim 3' \times 5'$).

The infrared emission structure of the Magellanic Clouds is typical of group 4 galaxies. Diffuse emission from the galaxy disk is seen, but the infrared images are dominated by localized emission sources coincident with H II regions and optical emission knots seen in the red-light photographs. Diffuse emission at 12 and 25 μm is seen along the optical axial bar of both galaxies.

NGC 598 (M33).—The *IRAS* maps of M33, along with those of the other Local Group members—the Magellanic Clouds and M31—show the most detailed structure of all the galaxies observed. Diffuse emission from the disk and prominent localized sources coincident with the galaxy's brightest H II region complexes are seen in the infrared images. The inner pair of spiral arms is clearly visible in the infrared maps.

IC 342.—IC 342 is one of the most interesting of the galaxies presented here. Although not completely resolved, the main spiral arms can be easily traced in all but the 100

μm image. The arms are superposed on a smooth disk, and a pointlike nucleus is seen in both the optical and the infrared images. The spurs to the east and to the west may be due to background objects.

NGC 1448.—The galaxy is unresolved along the in-scan direction which is near the galaxy minor axis, but may be slightly extended at 60 and 100 μm along the cross-scan (near the galaxy major axis) direction.

NGC 3031 (M81).—Enhanced infrared emission is coincident with the chains of H II regions in the spiral arms to the north and south of the nucleus. The 100 μm image is affected by Galactic cirrus to the north at the lowest contour levels.

IC 2574.—The prominent 60 and 100 μm sources are coincident with the cluster of H II regions to the northeast of the galaxy center. Faint emission from the disk is also seen in these maps. The 100 μm image is affected by Galactic cirrus.

TABLE 8

OPTICALLY LARGE GALAXIES LISTED IN OTHER CATALOGS

Catalog Name (1)	RC2 Name (2)	R.A. (1950) (3)	Dec. (4)	Type (5)	T (6)	D^*_{25} (7)	RC2 D_{25} (8)
U00192	I 10	$0^h17^m36^s$	59°02′ ″	dIrr	10B	8′.7	5′.1
U00452	N0221	0 39 58.0	40 35 33 D	E	−6	13.7	7.6
E411-25	N0289	0 50 17	−31 28 36	Sb	4B	8.6	3.7
E351-30	A0057−33	0 57 47	−33 58 41	dE	−5	65.4	
U00718	N0404	1 06 39.3	35 27 10 D	E/S0	−3A	8.0	4.4
U00864	N0474	1 17 31.7	03 09 17 D	S0	−2A	12.6	7.9
U01249	I1727	1 44 41.6	27 04 55 D		9B	8.7	6.2
U01466	N0772	1 56 35.3	18 45 50 D	Sb	3A	8.7	7.1
U02173	N1055	2 39 10.7	− 0 13 45 D	Sb	3B	8.7	7.6
U02188	N1068	2 40 06.5	− 0 13 32 D	Sb	3A	9.7	6.9
M-02-09-042	N1337[a]	3 25 36.0	− 9 34 00			8.9	
E250-03	N1510	4 01 54	−43 32 11	S...	−6	9.3	1.0
E250-04	N1512	4 02 16	−43 29 11	SB(r:)b	1B	13.7	4.0
E359-27	N1532	4 10 09	−33 00 00	Sc	2B	16.6	5.6
E157-20	N1566	4 18 53	−55 03 23	Sc	4X	10.1	7.6
E486-05	N1744	4 57 56	−26 06 00	SBd	7B	12.3	6.8
E206-20		6 40 24	−50 55 00	dE	−5	29.4	
U03851	N2366	7 23 34.2	69 18 42 D	Irr	10B	9.7	7.6
U04284	N2541	8 11 01.9	49 12 53 D	Sc	6A	8.8	6.6
U04305	A0813+70	8 13 53.5	70 52 13 D	dIrr	10	10.0	7.6
U04821	N2768	9 07 45.2	60 14 40 D	E/S0	−5	8.6	6.3
U04936	N2805	9 16 17.0	64 18 55 D	Sc	7X	8.2	6.3
U05387	N3079	9 58 35.4	55 55 11 D	...	5B	9.4	7.6
U05557	N3184	10 15 17.7	41 40 28 D	Sc	6X	9.2	6.9
U05789	N3319	10 36 15.2	41 56 56 D	SBc	6B	8.2	6.8
U05840	N3344	10 40 46.6	25 11 10 D	Sc	4X	8.2	6.9
U05850	N3351	10 41 19.6	11 58 00 D	SBb	3B	9.2	7.4
U05873	N3359	10 43 21.1	63 29 11 D	SBc	5B	8.7	6.8
U05882	N3368	10 44 06.9	12 05 05 D	Sa/Sb	2X	8.2	7.1
U05986	N3432	10 49 42.7	36 53 05 D	...	9B	8.2	6.2
E572-20	N3981	11 53 34	−19 37 00	Sc	4A	9.3	3.9
U06937	N3992	11 55 01.0	53 39 13 D	SBb	4B	9.0	7.6
E572-47	N4038	11 59 19	−18 35 11	S...	9B	11.5	2.6
E572-48	N4039	11 59 20	−18 36 23	S...	9A	10.1	3.2
U07118	N4125	12 05 37.7	65 27 03 D	E	−5	8.0	5.1
U07183	N4157	12 08 34.6	50 45 51 D	Sb	3X	8.4	6.9
U07278	N4214	12 13 08.8	36 36 19 D	Irr	10X	11.7	7.9
U07377	N4274	12 17 20.2	29 53 33 D	SBa	2B	8.0	6.9
U07508	N4382	12 22 53.2	18 28 03 D	S0	−1A	9.7	7.1
U07532	N4406	12 23 39.7	13 13 25 D	E	−5	14.8	7.4
U07654	N4486	12 28 17.8	12 39 58 D	E	−4	9.2	7.2
U07718	N4526	12 31 30.4	07 58 33 D	S0	−2X	9.2	7.2
U07727	N4535	12 31 47.9	08 28 25 D	Sc/SBc	5X	8.5	6.8
U07878	N4636	12 40 16.6	02 57 43 D	E	−5	9.2	6.2
U07898	N4649	12 41 09.0	11 49 23 D	E	−5	9.2	7.2

TABLE 8—*Continued*

Catalog Name (1)	RC2 Name (2)	R.A. (1950) (3)	Dec. (4)	Type (5)	T (6)	D^*_{25} (7)	RC2 D_{25} (8)
U08286	N5023	$13^h09^m58^s.0$	44°18′13″D	Sc	5	8′.2	6′.5
E508-48	N5078	13 17 05	−27 08 48	SO	1A	43.4	3.2
E576-33	N5084	13 17 34	−21 33 53	SO?	−2	14.5	4.8
E270-17		13 31 39	−45 17 06	S.../I	7	17.5	
U08745	N5322	13 47 35.1	60 26 21 D	E	−5	8.0	5.5
U09499	N5746	14 42 24.2	2 09 53 D	Sb	3X	8.1	7.9
U09631	N5792	14 55 48.2	− 0 53 26 D	SBb	3B	8.7	7.2
U09723	N5866	15 05 07.8	55 57 16 D	S0	−1A	8.6	5.2
E274-01		15 10 47	−46 37 36	Sc:	6	15.6	
U09792		15 13 30	0 03	dE	−5	15.6	
U10359	N6140	16 20 36.0	65 30 30 D	SBc	5B	8.7	6.2
U10642		16 57 18	− 0 28	dE	−5	20.3	
U11012	N6503	17 49 58.7	70 09 26 D	Sc	6A	8.7	6.2
E346-19	N7424	22 54 28	−41 20 11	Sc	6X	12.3	7.6
E291-14		23 14 09	−43 21 53	Sc	6	9.3	
E408-09	I5332	23 31 48	−36 22 41	Sc	7A	10.8	6.6

[a] The RC2 position of NGC 1337 is 0325.66 − 0833.8. The converted diameter of NGC 1337 using the RC2 T index of 6 is less than the 8′ selection limit.

NGC 3628.—The apparent extension to the south of this galaxy in the 60 and 100 μm maps is a "hysteresis tail" in the forward scanning direction.

NGC 4236.—The 60 and 100 μm images appear as two pointlike sources, partially resolved in the cross-scan direction.

NGC 4244.—The 60 μm image is similar to that of NGC 55; two off-nucleus pointlike sources are associated with emission knots in the optical image. The 60 and 100 μm images are affected by Galactic cirrus.

NGC 4395.—The 60 and 100 μm maps are similar to those of IC 2574; enhanced emission is coincident with optical emission knots to the southeast of the galaxy center. The faint optical arm to the north is seen in the 60 μm map.

NGC 4565.—Little detail is visible in the images of this edge-on system. Note that the alignment of the *IRAS* image is rotated slightly from the optical major axis because of the scanning direction.

NGC 4656.—The emission from this galaxy is essentially composed of two point sources, one at the nucleus of NGC 4656 and the other to the northeast of the nucleus at the position of several emission knots seen in the optical image and the small companion irregular galaxy, NGC 4657.

NGC 5055.—The 100 μm image may be affected by "hysteresis" effects on both sides of the galaxy.

NGC 5194 (M51).—The main features visible in the *IRAS* images are a broad plateau centered on M51 and a pointlike source at NGC 5195. There is some evidence for resolution in the in-scan direction of the main spiral arms of M51 at 12 and 25 μm. There is probably residual background emission due to Galactic cirrus in the 60 and 100 μm images.

NGC 5236 (M83).—The images of this galaxy are rectangular, the resolution being inadequate to resolve more than a hint of spiral structure at 12 and 25 μm in the high surface brightness disk. There is a small "hysteresis" problem in the 100 μm image. The low-level spur in the 60 μm image to the east of the nucleus is probably due to emission from a pair of background galaxies.

NGC 5457 (M101).—This is one of the most interesting of the infrared galaxy images presented in the atlas. Several discrete sources associated with H II regions are seen at 25 and 60 μm, superposed on a smooth disk. The optical arm to the northeast is partially resolved in the 60 μm map.

NGC 6822.—This is an intriguing group 4 galaxy. Although the 60 and 100 μm images are somewhat affected by Galactic cirrus, the measured infrared diameter of the galaxy is almost twice its optical diameter, as listed in RC2, corrected for Galactic extinction. Localized infrared sources coincident with H II regions are evident in the 12, 25, and 60 μm maps.

NGC 6946.—The *IRAS* images present a quite centrally concentrated appearance, with some evidence of arm resolution to the northwest. The discrete point source to the southeast is a background object unrelated to the galaxy. The shape of the point source reflects the different scanning angles of the component observations of the maps. A complex background at 100 μm resulted in poor background removal.

The *IRAS* surface brightness maps of the galaxies of this study, written to tape in FITS format, are available as an IPAC product.

This catalog could not have been produced without the able assistance of the staff of the Infrared Processing and Analysis Center (IPAC). In particular, the authors thank Dr. J. Good for developing the two-temperature model, Drs. G. Helou and F. Boulanger for useful comments on this work, E. Barba for preparing the manuscript, and the IPAC Data Management Team members (G. Smith, G. Lairmore, J. Lampley, H.

Hanson, R. Beck, E. Erwin, D. Jackson, L. Lloyd, and R. Urban) for their data processing support. We thank the Palomar Observatory (California Institute of Technology), the European Southern Observatory, and the Mount Wilson and Las Campanas Observatories (Carnegie Institution of Washington) for granting permission to reproduce and display the optical photographs presented in the atlas. This research was supported by The National Aeronautics and Space Administration through the *IRAS* Extended Mission Program.

APPENDIX

ADDITIONAL OPTICALLY LARGE GALAXIES LISTED IN UGC, MCG, AND ESO

As discussed in § I, a major objective of this study is to report global *IRAS* flux densities of all observed galaxies likely to have large enough infrared extents to result in an underestimation of their integrated emission as reported in the PSC and the SSSC. RC2 makes no attempt at completeness, and the RC2 diameters are weighted means of diameters obtained from catalogs which, in some cases, predate more modern compilations of galaxy diameters. For these reasons, the merged catalogs of Nilson (1973, 1974, hereafter UGC and UGCA, respectively), Lauberts (1982, hereafter ESO), and Vorontsov-Velyaminov *et al.* (1962, 1963–1974, hereafter MCG) were searched for possible candidate galaxies not selected from RC2. (The merging of these catalogs to obtain nonredundant all-sky coverage is discussed in the Extragalactic Catalog.)

Diameters listed in these catalogs were converted to the D_{25} scale of RC2 using the transformation equations reported in RC2 and ESO. Five large galaxies not contained in RC2 and one galaxy without a listed diameter in RC2 were found. Fifty-five galaxies listed in RC2 with diameters less than 8′ had converted diameters greater than the selection limit. These additional optically large galaxies are presented in Table 8. Column (1) is the catalog identification of the galaxy—the UGC (U) number, abbreviated ESO (E) designation, or MCG (M) name. Column (2) is the RC2 designation. Columns (3) and (4) give the optical equatorial coordinates (equinox 1950) as listed in the selection catalog or, for the coordinates followed by "D," from Dressel and Condon (1976). Column (5) is the morphological classification as listed in the selection catalog. The morphological classification as coded in RC2 as a T index and bar parameter letter is listed in column (6). For the ESO galaxies not listed in RC2 the T index is from ESO. Column (7) reports D_{25}^{*}, the selection catalog isophotal major diameter converted to the D_{25} scale of RC2. The isophotal diameter as reported in RC2 is listed in column (8).

REFERENCES

Aaronson, M., *et al.* 1982, *Ap. J. Suppl.*, **50**, 241.
Burstein, D., and Heiles, C. 1984, *Ap. J. Suppl.*, **54**, 33.
Cataloged Galaxies and Quasars Observed in the IRAS Survey. 1985, prepared by C. J. Lonsdale, G. Helou, J. Good, and W. Rice (Pasadena: JPL) (Extragalactic Catalog).
Chester, T. 1985, in *Light on Dark Matter*, ed. F. P. Israel (Dordrecht: Reidel), p. 3.
de Jong, T., Clegg, P. E., Soifer, B. T., Rowan-Robinson, M., Habing, H. J., Houck, J. R., Aumann, H. H., and Raimond, E. 1984, *Ap J. (Letters)*, **278**, L67.
de Vaucouleurs, G., de Vaucouleurs, A., and Corwin, H. G., Jr. 1976, *Second Reference Catalogue of Bright Galaxies* (Austin: University of Texas Press) (RC2).
Dressel, L. L., and Condon, J. J. 1976, *Ap. J. Suppl.*, **31**, 187
Gallagher, J. S., and Mould, J. R. 1981, *Ap. J. (Letters)*, **244**, L3.
Habing, H. J., *et al.* 1984, *Ap. J. (Letters)*, **278**, L59.
Helou, G., Khan, I., Malek, L., and Boehmer, L. 1987, *Ap. J. Suppl.*, submitted.
Hodge, P. W. 1963, *A. J.*, **68**, 691.
_____. 1973, *Ap. J.*, **182**, 671.
Huchra, J. A., Davis. D., Latham, D., and Tonry, J. 1983, *Ap. J. Suppl.*, **52**, 89.
Huchtmeier, W. K., Richter, O. G., Bohnenstengel, H. D., and Hauschildt, M. 1983, ESO Preprint No. 250.
Hummel, E. 1980, *Astr. Ap. Suppl.*, **41**, 151.
IRAS Catalogs and Atlases, Explanatory Supplement. 1985, ed. C. A. Beichman, G. Neugebauer, H. J. Habing, P. E. Clegg, and T. J. Chester (Washington, DC: GPO) (*IRAS* Supplement).
IRAS Point Source Catalog. 1985, Joint *IRAS* Science Working Group (Washington, DC: GPO) (PSC).
IRAS Small Scale Structures Catalog. 1986, prepared by G. Helou and D. Walker (Washington, DC: GPO) (SSSC).
Kraan-Korteweg, R. C., and Tammann, G. A. 1979, *Astr. Nach.*, **300**, 181.
Lauberts, A. 1982, *The ESO/Uppsala Survey of the ESO(B) Atlas* (Munich: European Southern Observatory) (ESO).
Low, F. J., *et al.* 1984, *Ap. J. (Letters)*, **278**, L19.
Neugebauer, G., *et al.* 1984, *Ap. J. (Letters)*, **278**, L1.
Nilson, P. 1973, *Uppsala General Catalogue of Galaxies* (*Uppsala Astr. Obs. Ann.*, Vol. **6**) (UGC).
_____. 1974, *Catalog of Selected Non-UGC Galaxies* (Uppsala Obs. Rept., No. 5) (UGCA).
Rice, W. 1988, in preparation (Paper II).
Sandage, A., and Tammann, G. A. 1981, *A Revised Shapley-Ames Catalog of Bright Galaxies* (*Carnegie Inst. Washington Pub.*, No. 635) (RSA).
Sanders, D., and Young, J. 1986, private communication.
Schwering, P. B. W. 1987, *Astr. Ap. Suppl.*, in press.
Schwering, P. B. W., and Israel, F. P. 1987, *Astr. Ap. Suppl.*, in press.
Soifer, B. T., Rice, W., Mould, J. R., Gillet, F. C., Rowan-Robinson, M., and Habing, H. J. 1986, *Ap. J.*, **304**, 651.
Soifer, B. T., *et al.* 1984, *Ap. J. (Letters)*, **278**, L71.
van den Bergh, S. 1959, *Pub. David Dunlap Obs.*, **2**, 147 (No. 5).
_____. 1966, *A. J.*, **71**, 922.
Verter, F. 1985, *Ap. J. Suppl.*, **57**, 261.
Vorontsov-Velyaminov, B. A., and Arhipova, V. P. 1963–1974, *Morphological Catalog of Galaxies*, Vols. 2–5 (Moscow: Moscow State University) (MCG).
Vorontsov-Velyaminov, B. A., and Krasnogorskaja, A. A. 1962, *Morphological Catalog of Galaxies*, Vol. **1** (Moscow: Moscow State University) (MCG).
Walterbos, R. A. M., and Schwering, P. B. W. 1987, *Astr. Ap.*, in press.
Young, E. T., Neugebauer, G., Kopan, E. L., Benson, R. D., Conrow, T. P., Rice, W., and Gregorich, D. T. 1985, *A User's Guide to the IRAS Pointed Observation Products*, IPAC Preprint Pre-0008N (POG).

T. DE JONG: Universiteit Amsterdam, Sterrenkundig Instituut, Roetersstraat 15, 1018 WB, Amsterdam, The Netherlands

H. J. HABING: Sterrewacht Leiden, P.O. Box 9513, 2300 RA, Leiden, The Netherlands

E. L. KOPAN, CAROL J. LONSDALE, L. A. LLOYD, and W. RICE: IPAC, Mail Code 100-22, California Institute of Technology, Pasadena, CA 91125

G. NEUGEBAUER and B. T. Soifer: California Institute of Technology, Downs 320-47, Pasadena, CA 91125